AN ABSTRACT OF THE THESIS OF

Jeffrey T. Loats for the degree of Doctor of Philosophy in Physics presented on July 27, 2004.

Title: Angular Correlation Measurements from the β Decay of ^{166m}Ho and ^{166}Tm and the Properties of the Gamma Vibrational Band in ^{166}Er

Abstract approved:

Redacted for Privacy

Angular correlations of gamma rays from excited states of ^{166}Er have been measured following the β decays of ^{166m}Ho ($J^{\pi} = 7^{-}$, $t_{1/2} = 1200$ y, $Q = 1854$ keV) and ^{166}Tm ($J^{\pi} = 2^{+}$, $t_{1/2} = 7.7$ h, $Q = 3040$ keV). Data was collected using the 8π spectrometer, an array of 20 Compton-suppressed Ge detectors. Basic theory of gamma-ray spectroscopy and deformed nuclei is presented along with experimental methods and results. The δ(E2/M1) mixing ratios have been measured for ten mixed-multipolarity transitions between the gamma and ground rotational bands, as well as for three of the intra-gamma-band transitions, two of which have not previously been measured. Comparison with previous experiments shows favorable results, with generally smaller limits of uncertainty. Results are compared with basic and modern theories about the collective behavior of these rotational bands.

Angular Correlation Measurements from the β Decay of ^{166m}Ho and ^{166}Tm and the Properties of the Gamma Vibrational Band in ^{166}Er

by

Jeffrey T. Loats

A THESIS

submitted to

Oregon State University

in partial fulfillment of

the requirements for the

degree of

Doctor of Philosophy

Presented July 27, 2004

Commencement June 2005

Doctor of Philosophy thesis of Jeffrey T. Loats presented on July 27, 2004.

APPROVED:

Redacted for Privacy

Major Professor, representing Physics

Redacted for Privacy

Chair of the Department of Physics

Redacted for Privacy

Dean of the Graduate School

I understand that my thesis will become part of the permanent collection of Oregon State University libraries. My signature below authorizes release of my thesis to any reader upon request.

Redacted for privacy

Jeffrey T. Loats, Author

ACKNOWLEGEMENTS

From Mr. Briggs, my high-school physics teacher, to the many mentors I have met in graduate school, I have consistently found those who wanted to share their love of physics with the world. Their enthusiasm was infectious and molded by these examples I have chosen the same path for my career. What a treat it is to share the wonders of the world with each other.

My immense thanks to Ken Krane for being exactly the kind of professor I hope to be. Your example will be a guide for all my years as a physicist and I thank you for taking the time and energy to help me through this. My thanks also to John Wood for consistent and thoughtful assistance in all aspects of this work.

The other graduate students in my research group, Paul Schmelzenbach and CJ Staples, were wonderful partners in juggling, racquetball, hearts and sometimes even the occasional physics discussion. W. David Kulp and James Mitchell Allmond of Georgia Tech were extremely helpful and a pleasure to work. I wish you all continued success and joy as you go forward with your careers.

In the middle of all this I managed to find a woman willing to marry me, and for that I am eternally grateful. Melissa Lyn Jenkins Loats, thank you for your understanding, your humor, your love and your tireless belief in me.

None of this would have even gotten started without the influence of my parents. There is little mystery in why I turned out be a curiosity driven scientist, but that doesn't make me any less grateful. All of four of you have influenced my struggle for this degree and have provided the best support a son and graduate student could ask for.

Thanks to Eric Olson for discussions about chocolate spin and islands of stability.

There were also many others that helped with this work directly and indirectly. Thanks to those at LBNL who helped this experiment happen and those at OSU who helped to forward my career in physics and make it a great place to have been for these years of my life.

This investigation was supported in part by US Department of Energy Grant FG03-98ER41060.

TABLE OF CONTENTS

Page

TABLE OF CONTENTS (Continued)

Page

TABLE OF CONTENTS (Continued)

Page

TABLE OF CONTENTS (Continued)

Page

LIST OF FIGURES

Figure Page

LIST OF FIGURES (Continued)

Figure Page

LIST OF TABLES

LIST OF TABLES (Continued)

LIST OF TABLES (Continued)

Angular Correlation Measurements from the β Decay of ^{166m}Ho and ^{166}Tm and the Properties of the Gamma Vibrational Band in ^{166}Er

1. Introduction

1.1. Motivation

The nucleus, shrouded by a cloud of electrons, remains in many ways somewhat mysterious to scientists. After years of study, with great successes along the way, many of the theories about the behavior of the nucleus remain highly phenomenological in nature. As radioactive elements become a common part of modern medicine, cosmological questions probe the first moments of the universe and humanity's scientific curiosity leads us to explore other worlds, a complete understanding of the interaction between many protons and neutrons in a nucleus still eludes us. Thus, despite the highly abstracted and seemingly detached nature of nuclear structure studies, understanding these basic building blocks of nature remains a key to our scientific development.

A particular group of nuclei that holds special interest for nuclear physicists is that in which the nucleus is non-spherical. In this region the excitations of the nucleus take on a different character, exhibiting collective excitations in which the nucleus as a whole expresses its energy in rotations and vibrations. The study of these nuclei informs our basic understanding of the structure of the nucleus and the interactions present there.

In this study we examined the radioactive β decays of both ^{166m}Ho ($J^{\pi} = 7^-$, $t_{1/2} = 1200$ y, $Q = 1854$ keV) and ^{166}Tm ($J^{\pi} = 2^+$, $t_{1/2} = 7.7$ h, $Q = 3040$ keV) to the stable nucleus ^{166}Er. The ^{166}Er nucleus sits at the center of the so-called deformed region and is the best of a few examples of nuclei with even numbers of both protons and neutrons in which the collective excitations of the nucleus dominate its behavior in a clear manner. The two decays explored here feed the states of ^{166}Er in very different ways, populating many of the excited states of the ground and gamma-vibrational bands. The gamma rays emitted by the de-excitation of these levels offer numerous opportunities to study the interactions between the two rotational bands. For these reasons ^{166}Er has long stood as a favorite test for theories hoping to explain these interactions.

This work was motivated by the need for a study that uses both decays to investigate the properties of ^{166}Er in a comprehensive and coherent manner. Such a study, using both decays in the same work, has not been undertaken since the late 1960s, in which time great strides have been made in detector technology. The recent availability of large detector arrays, such as the 8π array used in this study, offers an opportunity to perform gamma-ray spectroscopy experiments with unprecedented accuracy. The electronics of such an array allow us to do specific coincidence gating with software after the data has been collected, allowing for much more flexibility than the older method of using hardware coincidence gates.

The primary focus of this work is the measurement of the δ(E2/M1) mixing ratios for the gamma-to-ground transitions in ^{166}Er. These quantities represent sensitive

tests for the various theories that apply to this nucleus. With only a couple of exceptions previous measurements of these mixing ratios in ^{166}Er were based on only a few gamma rays and used methods that leave doubts about the best values for these quantities.

1.2. Summary

In this work we present the basic theories behind angular correlation measurements of deformed nuclei. As this work is primarily experimental in nature, a comprehensive treatment is not presented. We start with a description of the multipole theory of electromagnetic radiation and its connection to selection rules and angular correlation theory in nuclear decay. This is followed by a discussion of collective motion in deformed nuclei, including predictions of mixing ratios that can be done using the basic rotational model. We then describe band-mixing theory and its effects on the mixing ratio predictions. Finally a brief description of the interacting boson approximation (IBA), which is the leading microscopic model for deformed nuclei, is given. No IBA model calculations are presented in this work, but it bears mentioning as the leading competing theory for description of these nuclei.

After this theoretical groundwork has been laid we turn to a discussion of the previous work that has been done regarding these decays and their daughter, ^{166}Er. This discussion is broken down into several sections based on the type of experiment and the goals of the measurements.

Next we offer a detailed explanation of the experimental equipment, radioactive sources, and data processing and analysis methods used in this experiment. In particular

we offer a discussion of the ways in which δ(E2/M1) mixing ratios were extracted in this work. It is our opinion that this discussion could promote a more effective method for extracting these values in future experiments.

Experimental results for ten mixed-multipolarity gamma-to-ground transitions are presented, as well as three intra-gamma-band mixing ratios, two of which have not been previously measured. We also present the results of band-mixing analyses being carried out by other members of this group, as they have some bearing on our discussion.

Finally, these results are compared with previous experiments as well as with both simple and complex theoretical calculations. The systematics of our measurements are explored within the structure of the basic models.

2. Gamma-Ray Spectroscopy in Nuclear Physics

In the study of the nucleus perhaps the most common method is the study of the gamma rays emitted when a nucleus transitions from one state to another state of lower energy. When this energy is released in the form of a gamma-ray photon we are given a direct glimpse into the structure of the nucleus.

Each nuclear state can be described by the good quantum numbers J and π. Here we use J to represent the total of the intrinsic and orbital angular momentum of all the nucleons. We will refer to J as the "spin" of the nuclear state. As with any quantum mechanical angular momentum, the total spin J has a projection quantum number M, representing the projection of J on some arbitrary lab axis. The parity of the state, π, is also a good quantum number, and can be either positive or negative. In a nuclear transition both the initial state J_i^π and the final state J_f^π have definite angular momentum and parity, therefore it is useful to represent the gamma ray that connects in a manner that also has definite angular momentum and parity.

2.1. Multipole expansion of electromagnetic radiation

In general a photon, and the electromagnetic field that it represents, does not have a definite angular momentum. In order to describe photons for which angular momentum is a good quantum number we must use the multipole expansion of electromagnetic radiation.

Following the method of Jackson [1] we assume the electric and magnetic fields have a sinusoidal time dependence and start with Maxwell's equations in a source-free region

$$\begin{aligned} \vec{\nabla}\times\vec{E} &= ik\vec{B} & \vec{\nabla}\times\vec{B} &= -ik\vec{E} \\ \vec{\nabla}\bullet\vec{E} &= 0 & \vec{\nabla}\bullet\vec{B} &= 0 \end{aligned} \tag{2-1}$$

By eliminating $\vec{B}$ from these equations we can see that the scalar quantity $\vec{r}\bullet\vec{E}$ must satisfy the Helmholtz wave equation

$$(\vec{\nabla}^2 + k^2)(\vec{r}\bullet\vec{E}) = 0 \tag{2-2}$$

The general solutions to this equation are given by

$$\psi(\vec{x}) = \sum_{L,m}[A_{Lm}^{(1)}h_L^{(1)}(kr) + A_{Lm}^{(2)}h_L^{(2)}(kr)]Y_{Lm}(\theta,\phi) \tag{2-3}$$

where the coefficients $A_{Lm}^{(1)}$ and $A_{Lm}^{(2)}$ are given by boundary conditions, the $h(kr)$ are the Hankel functions and the $Y_{Lm}(\theta,\phi)$ are the spherical harmonics. Using this solution for $\vec{r}\bullet\vec{E}$ in Equation (2-2) we then follow a similar path for $\vec{B}$. The general solution to Maxwell's equations in term of a multipole expansion is then given by

$$\begin{aligned} \vec{B} &= \sum_{L,m}\left[a_E(L,m)f_L(kr)\vec{X}_{Lm} - \tfrac{i}{k}a_M(L,m)\nabla\times g_L(kr)\vec{X}_{Lm}\right] \\ \vec{E} &= \sum_{L,m}\left[\tfrac{i}{k}a_E(L,m)\nabla\times f_L(kr)\vec{X}_{Lm} + a_M(L,m)g_L(kr)\vec{X}_{Lm}\right] \end{aligned} \tag{2-4}$$

where $a_E(L,m)$ and $a_M(L,m)$ give the contributions of electric-type and magnetic-type multipole radiation (also known as transverse magnetic and transverse electric fields respectively). The radial functions $f_L(kr)$ and $g_L(kr)$ are linear combinations of the Hankel functions and the $\vec{X}_{Lm}$ are the normalized vector spherical harmonics

$$\vec{X}_{Lm}(\theta,\phi) = \frac{1}{\sqrt{L(L+1)}} \vec{L} Y_{Lm}(\theta,\phi) \tag{2-5}$$

The importance of this expansion is that it offers a way to describe electromagnetic fields that have definite angular momentum. Separating the electric-type and magnetic-type fields offers the further refinement of an electromagnetic field with good angular momentum and good parity. It can be shown that the two types of radiation have opposite parities for the same multipole order L, with the parity calculated as $(-1)^L$ for electric type radiation and as $(-1)^{L+1}$ for magnetic type. Since $L=1$ radiation comes from a fluctuating dipole moment we refer to $L=1$ as "dipole radiation". Similarly $L=2$ is called quadrupole radiation, etc. As a short hand notation we refer to the type of the radiation and the angular momentum; e.g. E2 is electric quadrupole radiation, ML refers to magnetic radiation of angular momentum L, etc.

Now that we can describe a gamma ray with a definite angular momentum, we can state that the angular momentum of the gamma ray must be able to connect the total angular momentum of the initial and final nuclear states. In other words $\vec{J}_i = \vec{L} + \vec{J}_f$ must be a valid vector equation. This can be stated as one of the basic "selection rules" for nuclear transitions; only multipoles that are greater than or equal to the spin difference between the states can be emitted for a certain nuclear transition, i.e. $L \geq \left|J_f - J_i\right|$. Note that monopole-type (L = 0) radiation is not possible in gamma rays because photons are spin 1 particles, restricting them to dipole or greater multipole orders.

This selection rule can be combined with the parity properties of the multipole orders to generate the basic multipole selection rules, summarized in Table 2-1.

Table 2-1: Selection rules for gamma ray transitions in the nucleus.

Parity Change	Allowed radiation types (as permitted by $L \geq \left\|J_f - J_i\right\|$)
$\Delta\pi$ = yes	E1, M2, E3, ...
$\Delta\pi$ = no	M1, E2, M3, ...

2.2. Emission probabilities of multipole orders

A useful way of predicting the relative probability of emission for different radiation types and multipole orders in nuclear transitions comes from the Weisskopf estimates [2]. These estimates are not intended to predict experimental results directly, but rather to give us an estimation tool for relating multipole orders in nuclear transitions. To arrive at these general estimates we must make simplifying assumptions about the matrix elements that describe the transition between the initial and final nuclear states. Starting from Fermi's Golden Rule we can derive an expression for the probability of emission of a gamma ray of type σL where σ is E or M and L is the angular momentum of the gamma ray.

$$\lambda(\sigma L) = \frac{2(L+1)}{\varepsilon_0 \hbar[(2L+1)!!]^2}\left(\frac{E}{\hbar c}\right)^{2L+1}\left|\left\langle J_f M_f \left| M(\sigma L) \right| J_i M_i \right\rangle\right|^2 \qquad (2\text{-}6)$$

Here $M(\sigma L)$ is the operator that connects the initial and final states and creates a gamma ray of the appropriate angular momentum and parity. In this equation the factors in front of the matrix element stem from the density of states considerations in Fermi's Golden Rule. Note that the probability of emission is often referred to as the "intensity" in nuclear physics.

Since our knowledge of specific nuclear wave functions is extremely limited we first assume that the initial and final nuclear wave functions are those of a single proton, transitioning between shell model states (the shell model is discussed in Section 3.1). To treat the electric-type radiation we assume that the electric moments of the nucleus come solely from the single orbiting proton. Additional simplifying assumptions, such as assuming the radial portion of the wave function is constant inside the nuclear radius and zero outside, and that the angular portion of the matrix element integral is approximately unity, lead us to the following transition probability for electric radiation of multipole order L.

$$\lambda(EL) \cong \frac{8\pi(L+1)}{L[(2L+1)!!]^2} \frac{e^2}{4\pi\varepsilon_0 \hbar c} \left(\frac{E}{\hbar c}\right)^{2L+1} \left(\frac{3}{L+3}\right)^2 cR^{2L} \tag{2-7}$$

where E is the energy of the emitted photon in MeV, R is the mean radius of the nucleus, and the other quantities are familiar physical constants. Similar assumptions and approximations for the magnetic-type transition probability of multipole order L yield

$$\lambda(ML) \cong \frac{8\pi(L+1)}{L[(2L+1)!!]^2} \left(\mu_p - \frac{1}{L+1}\right)^2 \frac{e^2}{4\pi\varepsilon_0 \hbar c} \left(\frac{E}{\hbar c}\right)^{2L+1} \left(\frac{3}{L+3}\right)^2 cR^{2L-2} \tag{2-8}$$

where μ_p is the magnetic moment of the proton in units of nuclear magnetons.

We can then use $R \approx R_0 A^{1/3}$ to calculate these transition probabilities for the lowest multipole orders of radiation in terms of the mass of the nucleus in question and the energy of the photon emitted. The results of these calculations can be summed up with a few general guidelines.

- For a given type of radiation (E or M) increasing the multipole order by one decreases the probability of emission by a factor of roughly 10^{-5}.
- In medium and heavy nuclei electric-type radiation will be emitted more often than magnetic-type radiation of the same multipole order by a factor of about 100.

From these basic estimates we can calculate the amount of competition between different multipole orders in medium and heavy nuclei:

$$\frac{\lambda(\mathrm{M2})}{\lambda(\mathrm{E1})} = \frac{\lambda(\mathrm{M2})}{\lambda(\mathrm{M1})}\frac{\lambda(\mathrm{M1})}{\lambda(\mathrm{E1})} = 10^{-5}10^{-2} = 10^{-7} \quad \text{for} \quad \Delta\pi = \text{yes}$$

$$\frac{\lambda(\mathrm{E2})}{\lambda(\mathrm{M1})} = \frac{\lambda(\mathrm{E2})}{\lambda(\mathrm{E1})}\frac{\lambda(\mathrm{E1})}{\lambda(\mathrm{M1})} = 10^{-5}10^{+2} = 10^{-3} \quad \text{for} \quad \Delta\pi = \text{no}$$

From these calculations we can see that the lower multipole orders dominate easily under most circumstances and that M2 radiation is fairly rare. Similar calculations for octupole (L = 3) radiation shows that this multipole order competes with lower orders only under extremely rare circumstances. Thus, in medium and heavy nuclei most observed gamma rays will have characteristics of E1, M1 or E2 radiation.

In addition to these basic estimates it is known that the emission of electric quadrupole radiation, E2, is often enhanced by nuclear structure effects, such as

collective motion of the nucleus. Thus, the 10^{-3} ratio calculated for E2/M1 competition above can be increased by many orders of magnitude. We will discuss in the following sections the ways in which we can experimentally discriminate between different multipole orders and measure the competition that occurs in actual nuclei.

When we are interested in comparing theoretical transition probabilities with experiment the Weisskopf estimates are too simplified to suffice. Without making the simplifying assumptions inherent in the Weisskopf estimates we can instead define the reduced transition probability [3]

$$B(\sigma L, J_i \to J_f) = \frac{1}{2J_i+1} \sum_{M_i,M_f} \left| \left\langle J_f M_f \left| M(\sigma L) \right| J_i M_i \right\rangle \right|^2 \tag{2-9}$$

Using the Wigner-Eckart theorem to remove the dependence on M we can also write the $B(\sigma L, J_i \to J_f)$ in terms of the reduced matrix element.

$$B(\sigma L, J_i \to J_f) = \frac{1}{2J_i+1} \left| \left\langle J_f \left\| M(\sigma L) \right\| J_i \right\rangle \right|^2 \tag{2-10}$$

The usefulness of the reduced transition probability, $B(\sigma L)$, as opposed the total transition probability, Equation (2-6), is that it allows us to compare transition strengths between two gamma rays without the influence of the E^{2L+1} or the M dependent geometrical factors. Thus $B(\sigma L)$ gives us a direct glimpse at the nuclear wave functions that are connected by the radiation in question. When comparing theoretical models to experiment the $B(\sigma L)$ can be a valuable tool. The total transition probability is now given by

$$\lambda(\sigma L) = \frac{2(L+1)}{\varepsilon_0 \hbar L[(2L+1)!!]^2}\left(\frac{E}{\hbar c}\right)^{2L+1} B(\sigma L) \qquad (2\text{-}11)$$

Note that this transition probability is now summed over the possible initial and final M substates, unlike that given in Equation (2-6).

2.3. Internal conversion

Instead of emitting a gamma ray to get rid of its excess energy, the nucleus may instead interact with an electron in one of the lowest electronic shells. In this interaction (sometimes described by a virtual photon) the electron is ejected from the atom with a kinetic energy equal to the energy difference between the nuclear levels minus the binding energy of the electron. This interaction is the only way for electric monopole (E0) radiation to occur and is therefore the only mechanism allowed for transitions between $J^\pi = 0^+$ levels in the nucleus. Internal conversion also competes with gamma-ray emission in all other transitions but the probability for internal conversion drops off very quickly at higher energies [2].

The degree to which internal conversion competes with gamma-ray emission is characterized by the internal conversion coefficient

$$\alpha = \frac{\lambda_e}{\lambda_\gamma} \qquad (2\text{-}12)$$

where λ_e is called the partial decay probability and represents the probability that a particular level will decay by internal conversion of an electron. Similarly, λ_γ is the partial decay probability for emission of a gamma ray (which is a sum of expressions like

Equation (2-6)). Combining the partial decay probabilities gives the total decay probability, $\lambda_t = \lambda_\gamma + \lambda_e$, which is related to the half-life, $t_{1/2}$, of that particular nuclear level by

$$\lambda_t = \frac{0.693}{t_{1/2}} \tag{2-13}$$

The relative transition probability for internal conversion processes can be calculated with high accuracy based on the well understood electronic wave functions. Thus, the internal conversion coefficient for competition with a particular multipole order of gamma emission can be calculated and compared with experiment. This is one of the methods for experimentally determining the multipole order of a particular gamma ray, which in turn is one of the methods for determining the spin and parity of the nuclear energy levels.

2.4. Angular correlation of gamma-rays

For the purposes of this study the most important consequence of the multipole representation of the electromagnetic field is the angular distribution that occurs for different multipole orders.

Electromagnetic transitions take place between specific *M* substates of the initial and final spin states of the nucleus. For a given change in *M* the emission probability for each multipole order of radiation has a specific angular dependence. The dipole and quadrupole dependence is summarized in Table 2-2 [1].

Table 2-2: Angular dependence of emission probability for different multipole orders of gamma radiation.

Multipole Order	$\Delta M = 0$	$\Delta M = \pm 1$	$\Delta M = \pm 2$
Dipole (L=1)	$\sin^2\theta$	$\frac{1}{2}(1+\cos^2\theta)$	N.A.
Quadrupole (L=2)	$6\sin^2\theta\cos^2\theta$	$(1-3\cos^2\theta+4\cos^4\theta)$	$(1-\cos^4\theta)$

However, the energy splitting between different M substates is observable in nuclei only under very special circumstances. In particular, in gamma-ray spectroscopy we generally work with detectors that have an energy resolution on the order of keV, while the energy splitting of the M substates is at most on the order of μeV. Thus we cannot distinguish between M substates in observing gamma rays and so we end up observing a sum over all possible initial and final M substates. As an illustrative example let us consider a dipole transition from an initial state of spin one to a final state of spin zero. If we cannot distinguish between the three M substates of the initial state we will have to sum up their angular dependence functions to describe the angular dependence of the observed gamma ray. Given that thermal excitations are generally on the order of meV we expect that the three initial substates will be approximately equally populated. We can now see that summing the three contributions to the angular distribution with equal magnitudes removes the angular dependence entirely:

$$W(\theta) \propto \sin^2\theta + \tfrac{1}{2}(1+\cos^2\theta) + \tfrac{1}{2}(1+\cos^2\theta) = \text{const.}$$

This is a general result that can be easily shown for other multipole orders. If the M substates of an initial state are equally populated, radiation emitted from that state will be isotropic.

Therefore we can see that what we require is a method of creating unequal population in the various M substates. This can be accomplished in a very direct manner by cooling the radioactive sample to extremely low temperature and then applying a powerful magnetic field. This large magnetic field creates a larger degree of splitting between the M substates and the low temperature means that the lower energy M substates will be more populous than those of higher energy. This method is known as low temperature nuclear orientation (LTNO) and offers an alternate way of measuring the angular dependence of emitted gamma rays.

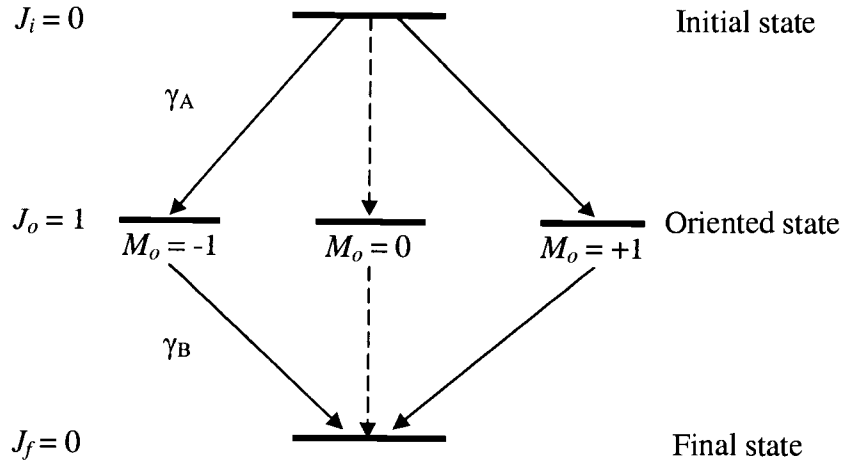

Figure 2-1: Example 0-1-0 cascade. Dotted transitions are not observed if we orient the laboratory z axis on the direction of γ_A. The unequal population of the M_o substates allows the directional distribution of γ_B to be observed.

Another method of creating unequal population in the M substates is called angular correlation. Let us extend our previous example by imagining a state of spin zero that feeds the spin-one state by emission of a gamma ray, γ_A, as depicted in Figure 2-1. For reasons that will become clear we will now call the spin-one state the oriented state. Once again we can imagine three transitions between the $M_i = 0$ state of the initial spin-zero state and the three M_o substates of the spin-one oriented state. Recall that $\Delta M = 0$ transitions have a $\sin^2\theta$ angular distribution, meaning their probability of being emitted along the z axis is zero. Thus, if we orient our laboratory z axis so that it lines up with the direction of emission of this first gamma ray, we remove the possibility of observing the $M_i = 0$ to $M_o = 0$ transition. Therefore the oriented state now has no population in its $M_o = 0$ substate. The subsequently emitted γ_B will have an anisotropic angular distribution due to the lack of the $\Delta M = 0$ term in the angular correlation function:

$$W(\theta) \propto \tfrac{1}{2}(1+\cos^2\theta) + \tfrac{1}{2}(1+\cos^2\theta) = 1+\cos^2\theta$$

By correlating the direction of emission of the second gamma ray relative to the direction of the first we can observe this angular dependence.

Generalizing to all multipoles and spin states leads to the angular correlation function [4].

$$W(\theta) = \sum_{k=even} B_k U_k A_k P_k(\cos\theta)\,. \qquad (2\text{-}14)$$

The B_k are called the *orientation parameters* and depend on the properties of the first observed gamma ray as well as the spins of the levels that it connects. The U_k are called the *deorientation coefficients* and depend on properties of any unobserved radiation

between the first and second observed gamma rays as well as the spins of the levels they connect. Note that if the orienting gamma ray and the observed gamma ray connect directly, with no intervening radiations, the U_k coefficient is equal to one. The A_k are called the *angular distribution coefficients* and depend on the properties of the final observed gamma ray as well as the spins of the levels that it connects. Lastly, the P_k are simply Legendre polynomials of k^{th} order. B_k, U_k and A_k are described in detail in the next section.

Only even terms appear in this sum due to the fact that we are not observing the polarization of the emitted gamma rays. Summing over the unobserved polarization states causes the odd terms in this sum to vanish [5]. The highest order term in this sum is determined by the spins of the nuclear levels in the cascade as well as the multipole orders of the radiations connecting them. Whichever is smaller of $2J_{max}$ or $2L_{max}$ (where J_{max} is the highest spin in the cascade and L_{max} is the highest multipole order involved) determines the highest term that will appear in Equation (2-14). Generally this means only $k = 0$, 2 and 4 appear and we will assume this form from here on.

2.5. Mixing ratios and angular correlation coefficients

In general, gamma rays connecting levels in a nucleus do not consist of a single pure multipolarity. Rather, except in cases where selection rules prohibit it, the radiation field of a gamma ray may have a mixture of multipolarities. To describe this mixture the

parameter δ is defined as the ratio of reduced matrix elements of radiation of multipole orders L and L', where $L' = L + 1$.

$$\delta = \frac{\langle J_2 \| L' \| J_1 \rangle}{\langle J_2 \| L \| J_1 \rangle} \tag{2-15}$$

For example, δ is often used to represent the mixture of E2 and M1 radiation types. Given this definition, the actual percentage of E2 or M1 radiation present in a given gamma ray is given by

$$\%E2 = \frac{\delta^2}{1+\delta^2} \cdot 100\% \tag{2-16}$$

$$\%M1 = \frac{1}{1+\delta^2} \cdot 100\% \tag{2-17}$$

If a transition is purely E2 this δ is considered to be infinite. If the transition is purely M1 δ is zero. The mixing ratio δ can be directly related to the reduced transition probabilities B(E2) and B(M1) (see Section 3.5).

Given this notation we can now turn to the functional form of the angular correlation coefficients that appear in Equation (2-14). Consider a cascade that goes sequentially from J_4 to J_1 by emitting gamma rays γ_A, γ_B and γ_C as shown in Figure 2-2.

First, the B_k orientation parameters, which describe the orientation of J_3 by γ_A, are given by the form

$$B_k = \frac{F_k(L_A, L_A, J_4, J_3) + (-1)^{L_A + L_A'} 2\delta(\gamma_A) F_k(L_A, L'_A, J_4, J_3) + \delta(\gamma_A)^2 F_k(L'_A, L'_A, J_4, J_3)}{1+\delta(\gamma_A)^2} \tag{2-18}$$

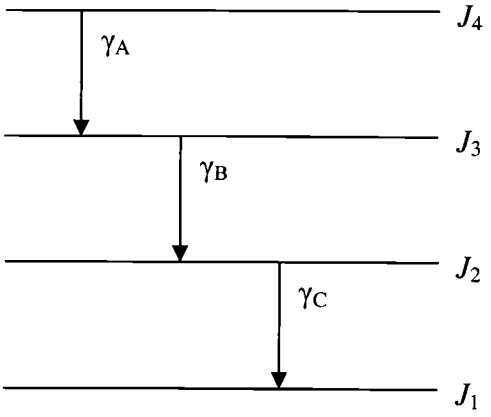

Figure 2-2: Example gamma-ray cascade. Nuclear levels of spins $J_1 - J_4$ are connected by gamma rays γ_A, γ_B and γ_C.

The F_k coefficients depend only on the angular momenta involved and are essentially ratios of Clebsch-Gordan coefficients. Values for F_k coefficients have been previously tabulated [4] for easy reference. $\delta(\gamma_A)$ is the L'/L mixing ratio of the gamma ray γ_A and again L_A is the lowest multipole order of radiation in γ_A (usually 1) and $L'_A = L_A + 1$. Except in the rare case when we are considering E3/E1 mixing, the phase factor $(-1)^{L+L'}$ is always simply (-1).

Next, one U_k deorientation coefficient will appear in Equation (2-14) for each unobserved radiation that takes place between γ_A and γ_C. Each U_k coefficient is given by the form

$$U_k(J_3, J_2) = \frac{U_k(J_3, J_2, L_B) + \delta(\gamma_B)^2 U_k(J_3, J_2, L'_B)}{1 + \delta(\gamma_B)^2} \qquad (2\text{-}19)$$

Here the notation can get confusing, but the $U_k(J,J,L)$ are again an angular momenta dependent factor [4] used in with $\delta(\gamma_B)$ to calculate the total $U_k(J,J)$ coefficient.

Lastly, the A_k angular distribution coefficients have a very similar form to the B_k coefficients:

$$A_k = \frac{F_k(L_C, L_C, J_1, J_2) + 2\delta(\gamma_C)F_k(L_C, L'_C, J_1, J_2) + \delta(\gamma_C)^2 F_k(L'_C, L'_C, J_1, J_2)}{1+\delta(\gamma_C)^2} \quad (2\text{-}20)$$

Note the change of the sign of the middle term in the numerator as well as the change in order of the spins of the nuclear levels. To conform to the notation in the literature the nuclear spins are always listed with the intermediate spin last.

Note that for each of these coefficients in the limit of an infinite or zero mixing ratios they reduce to a single F_k or U_k factor. Thus, if any of the transitions in the cascade have pure multipolarity, the form of the overall expression is much simplified. If all the transitions are of pure multipolarity the angular correlation function $W(\theta)$ is calculable directly. This offers a very useful check during experiment and can aid in the calculation of any correction factors that may arise.

Additionally, it is a property of the $F_k(L_1, L_2, J_a, J_b)$ coefficients that if $L_1 + L_2 < k$, the coefficient will be identically zero. For this reason, in the A_4 and B_4 coefficients the terms in the numerator that are constant or linear in δ nearly always vanish, leaving only the term that is quadratic in δ.

As previously mentioned it is the δ mixing ratios of various gamma rays that were the main focus of this study. The equations described in this section form the critical connection between the δs and the experimental data. In an experiment where both A_2 and A_4 are measured (for example) each will give two possible values for the mixing ratio δ. Ideally two of these four values will overlap, and may be averaged to produce a value for

δ. This is the predominant method for finding δ in most previous experiments. Other, sometimes-preferable methods for deducing δ from experimental angular correlation data are described in Section 5.6.

2.6. Angular correlation correction factors

There are two additional factors that must appear in Equation (2-14) when the equation is applied to actual experiment.

First, the angle θ represents an exact measure of the angle between the direction of emission of the two gamma rays involved. In reality gamma-ray detectors have a finite size and thus subtend a small range of angles. A correction factor Q_{kk} must be introduced into Equation (2-14) to correct for this small uncertainty in the correlation angle for each gamma ray. This correction is generally on the order of 2% for the k=2 term and 5% for the k=4 term (there is no correction to the k=0 term). A description of how these correction factors were calculated has been previously published [6].

Second, during the lifetime of a nuclear state the orientation of that state (caused by the gamma ray that fed the level) may be altered due to its environment. Electric and magnetic fields surrounding the nucleus can cause the populations of the M substates to lose their unequal populations, thus diminishing the directional correlation effect. The degree to which this occurs is affected primarily by the lifetime of the nuclear state and the environment of the nucleus. The lifetime of a nuclear state is a direct consequence of the total probability that it will decay in some way in a given amount of time. In turn these probabilities are strongly influenced by the energy available for such decay. Thus

with very rare exception the lower a state is in total energy, the longer its lifetime will be. In general most nuclear states have lifetimes on the order of picoseconds which is short enough that the surrounding environment has a negligible effect on the orientation of the state. In the case of a longer lifetime a correction factor G_k must be measured to account for this effect. This G_k then appears as a factor in Equation (2-14), giving us the fully corrected form

$$W(\theta) = \sum_{k=even} B_k U_k A_k Q_{kk} G_k P_k(\cos\theta) \tag{2-21}$$

When using this form in experiment we will use the more explicit form

$$W(\theta) = N(1 + A_{22} Q_{22} G_2 P_2(\cos\theta) + A_{44} Q_{44} G_4 P_4(\cos\theta)) \tag{2-22}$$

where N is an arbitrary normalization factor determined by experimental conditions and $A_{kk} = B_k U_k A_k$. Note that in the literature for this type of experiment the G_k and Q_{kk} factors are sometimes included in the A_{kk} coefficient (or this combination is sometimes referred to as A'_{kk}. We will use the above definitions throughout the rest of this work, having paid careful attention to the formats used by other authors.

3. The Structure of Deformed Nuclei

The behavior of highly deformed nuclei can be understood with great success using a few important models. Single-particle nuclear shell models offer a natural starting point as well as useful approximation tools. The collective behavior of the nucleus can be treated effectively using the quantum mechanical rigid rotor and harmonic oscillator.

In those instances where the basic collective models begin to fail, theories such as band mixing and the interacting boson approximation can bring theory back into agreement with experimental results.

3.1. The nuclear shell model

Early experiments in nuclear physics were soon able to show that the nucleus had properties, such as binding energies, neutron-capture cross sections and changes in the nuclear charge radius, that change smoothly as a few more nucleons were added but would then abruptly change at a certain point and then begin smooth variation again [2]. This behavior had been seen before in atoms and had been explained with phenomenal success using the electronic shell model. Thus a similar nuclear shell model was applied to the nucleus.

The successful nuclear shell model [7] reproduces the "magic numbers" of 2, 8, 20, 28, 50, 82 and 126. These magic numbers are the total number of either protons or neutrons (which each have their own shells) that are present in the nucleus just before a

large jump in various properties of the nucleus. In other words, these are the numbers which must represent closed shells.

In this model of the nucleus all excited states are understood as excitations of one or more nucleons from one shell to another higher-lying shell. These single-particle excitations offer a good first glimpse at the transitions of the nucleus and can be used to create simple but powerful approximations about the properties of gamma-ray de-excitation. The Weisskopf estimates mentioned earlier are built from a single-particle excitation model and offer very useful descriptions of gamma-ray emission, though they are based on a nucleus with spherical symmetry.

In addition to the energy required to move a nucleon from one shell state to another, there is clear evidence for a pairing force in the nucleus. Nucleons tend to pair up with other nucleons of the same type (protons with protons, for example). In a spherical nucleus the pairing force expresses itself in a reduction in energy when the angular momenta of two particles in the same shell-model state are coupled together. In particular, the arrangement in which the two nucleons couple to produce a spin zero pair is the most energetically favored state. This is the reason that a nucleus with hundreds of nucleons will have a ground state that has at most a few units of angular momentum. In particular, so-called "even-even" deformed nuclei, in which there is an even number of protons and neutrons, always have a ground state with $J = 0$ due to the grouping of all their nucleons into pairs of zero angular momentum.

Thus, as in the electronic shell model, the nuclear shell model predicts that near a closed shell the behavior of the nucleus should be dominated by the properties of the few

extra (or missing) protons or neutrons. Only when the nuclear shells are far from being filled would we expect to see excitations of the nucleus as a whole. This region, far from closed shells, is also the region in which we see the greatest deformation in nuclei. Further evidence for "collective excitation" in deformed nuclei is given by their exceptionally low-lying excited states. In medium and heavy nuclei a single-particle excitation will generally require on the order of 2 MeV of energy. However, in highly deformed nuclei excited states of a few hundred keV or less are common, implying that the single-particle excitation model is not capable of explaining the low-lying energy levels of these nuclei. In this region we must examine collective models such as rotation and vibration of the nucleus as a whole.

3.2. Rotational excitations of the deformed nucleus

The deformation of the nucleus can be expressed by describing the shape of the nuclear surface. This shape can, of course, be expanded as a combination of spherical harmonics [2]. The 0^{th}-order term in such an expansion, representing a non-deformed spherical nucleus, would simply be the average radius of the nucleus R_{avg}. However, adding higher order terms would increase the total volume of the nucleus, so an additional 0^{th}-order term is included to conserve the nuclear volume. A 1^{st}-order term in this expansion would correspond to a shift of the nuclear center of mass, which cannot occur due only to internal forces between nucleons. Thus, the lowest order of interest is the second-order term, called a quadrupole deformation.

$$R(\theta,\phi) = R_{avg}(1 + a_{00}Y_{00}(\theta,\phi) + \sum_{\mu=-2}^{\mu=2} a_{2\mu}Y_{2\mu}(\theta,\phi) + \ldots) \quad (3\text{-}1)$$

Symmetry requirements restrict the values of the coefficients $a_{\lambda\mu}$, and positive values for a_{20} correspond to a prolate (elongated) nuclear shape, while negative values correspond to a oblate (flattened) shape. The static shape of most deformed nuclei is a prolate shape, though rotations of this shape, described in the next section, can make the nucleus appear oblate.

The most common mode of collective excitation for a deformed nucleus is a simple rotation. There is strong evidence that at low spins this rotation does not alter the shape of the nucleus by more than a few percent [3]. Thus, treating the nucleus as a quantum mechanical rigid rotor gives an excellent first approximation. The classical kinetic energy of such a rotation is given by $E = J^2/2\Im$ where J is the angular momentum of the rotation and $\Im$ is the moment of inertia. If we assume a deformed shape with cylindrical symmetry we have three moments of inertia $\Im_1 = \Im_2 \neq \Im_3$ where the subscripts refer to the intrinsic coordinate system of the nucleus and the 3 axis is the nuclear symmetry axis (see Figure 3-1).

We can now rewrite the total angular momentum as a vector sum of its three components J_1, J_3 and J_3, which allows us to write the rotational energy of the nucleus as

$$E = \frac{J^2}{2\Im} + \left(\frac{1}{2\Im_3} - \frac{1}{2\Im}\right)J_3^2 \quad (3\text{-}2)$$

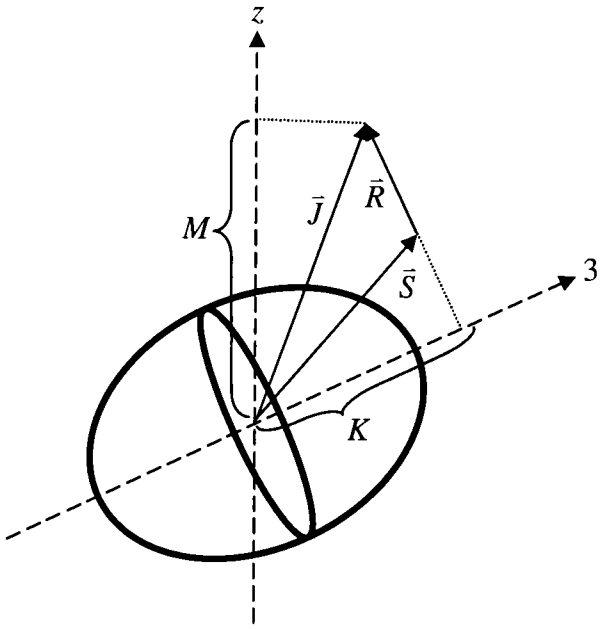

Figure 3-1: Diagram of angular momentum components for an axially symmetric deformed nucleus. The total angular momentum, $\vec{J}$, is the sum of the intrinsic angular momentum $\vec{S}$ and the rotational angular momentum $\vec{R}$ (which must be perpendicular to the nuclear symmetry axis in an axially symmetric nucleus). The projection of $\vec{J}$ on the nuclear symmetry axis is K and the projection of $\vec{J}$ on the laboratory z axis is given by M.

where $\Im_1 = \Im_2 = \Im$. In making the transition to quantum mechanics we replace the angular momentum operator J_{op}^2 with its eigenvalue $\hbar^2 J(J+1)$ and the angular momentum projection operator J_3^2 with the projection quantum number $\hbar^2 K^2$

$$E = \hbar^2 \left(\frac{J(J+1)}{2\Im} + \left(\frac{1}{2\Im_3} - \frac{1}{2\Im} \right) K^2 \right) \tag{3-3}$$

Note that K represents the projection of the total angular momentum J onto the symmetry axis of the nucleus.

The importance of this expression for the energy of a rotating deformed nucleus is that it predicts the energy spacing we should expect to see in rotational excitations of the nucleus. As mentioned before, the ground state of an even-even nucleus has a spin $J^{\pi} = 0^{+}$ and therefore a projection $K = 0$ as well. Due to the reflection symmetry of the nucleus this $K = 0$ state can have only even spin states built on it [3]. Therefore as we add rotational excitations to this ground state we expect to see energy levels that follow the $J(J+1)$ spacing of a pure quantum mechanical rotor (see Figure 3-2).

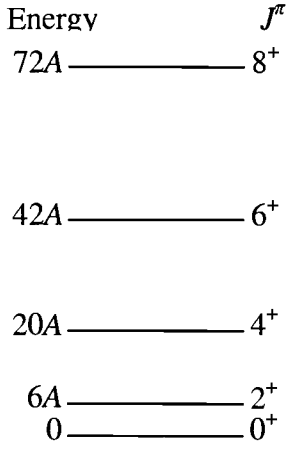

Figure 3-2: Diagram showing $J(J+1)$ spacing of rotational excitations of a deformed nucleus. The energy scaling factor A is arbitrary but is used here to show the energy spacing.

^{166}Er is one of the best examples of this ground state rotational "band"; the ratio of the energy of the 4^{+} state to the energy of the 2^{+} state is 3.29 which compares well with the $J(J+1)$ value of 3.33. This was one of the earliest pieces of evidence for the idea that ^{166}Er and nearby nuclei were strongly deformed.

3.3. Vibrational excitations of the deformed nucleus

The other primary collective excitation is the vibration of the nuclear shape. This process can be described as adding a sinusoidal time dependence to the $a_{\lambda\mu}$ coefficients in Equation (3-1). Adding time dependence to the a_{00} coefficient would cause an expansion and contraction of the nucleus, requiring enough energy to stretch the strong force holding the nucleus together. Thus we expect to see this kind of vibration only at extremely high excitation energies and we won't concern ourselves with it further. We are thus concerned with quadrupole ($\lambda = 2$) or higher vibrations of the nucleus.

A quadrupole vibration adds an angular dependence corresponding to a 2^{nd}-order spherical harmonic to the nuclear shape, and thus we expect it to add 2 units of angular momentum in the process. Therefore the energy of a quadrupole vibration is given by

$$E = \hbar\omega(N + \tfrac{5}{2}) \tag{3-4}$$

where N is the number of vibrational quanta, called phonons, and we have a zero point energy of $\frac{5}{2}\hbar\omega$ because the spin-2 quadrupole vibration has five possible M substates (M = -2, -1 ... 2), and thus five degrees of freedom. We can see from this description that adding successive vibrational quanta will increase the energy by the same amount each time.

The spins of the vibrational levels are less obvious than those of the rotational levels. For a spherical nucleus we start with the $J^{\pi} = 0^{+}$ ground state of an even-even nucleus. Adding a single quadrupole phonon yields a 2^{+} state. Adding an additional

quadrupole phonon means coupling together the $J = 2$ of the first phonon with another $J = 2$ for the second phonon, with no restrictions about the direction of either. Starting with the five M substates of the first phonon we can add or subtract the M substates of the second phonon to construct a set of possible M substates for the combined states. This method, called an "M-scheme", yields the result that only three states can be created by this coupling; one with spin 0, one with spin 2, and one with spin 4. Thus, when adding a second quadrupole phonon we expect to create a triplet of states, all with twice the energy of the first quadrupole vibration state (barring any perturbations for the moment). Following a similar method we can deduce the result of adding additional quadrupole phonons.

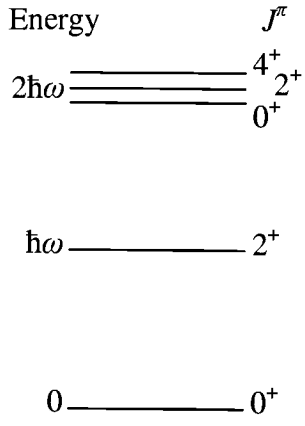

Figure 3-3: Diagram showing the energy levels of the states created by the first two quadrupole vibration phonons. Compare the spacing here with that found in Figure 3-2.

Finally, experiments show that the energy of a quadrupole phonon is on the order of 1 MeV, generally quite a bit larger than the energy spacing between the rotational levels. Figure 3-3 shows a schematic of the energy levels of vibrational excitations.

When we turn our attention to a deformed nucleus we must adjust our discussion a bit. The lack of spherical symmetry in the nucleus gives an intrinsic axis of reference for the angular momenta involved in vibrations. In this case we can categorize quadrupole vibrations by the projection of the total angular momentum on the symmetry axis of the nucleus. As described earlier, this is projection is called the K quantum number and is shown in Figure 3-1.

Specifically we break up our quadrupole vibrations into gamma vibrations and beta vibrations. A beta vibration corresponds to a fluctuation in the degree of deformation of the nucleus, which is equivalent to adding a sinusoidal time dependence to the coefficient of the Y_{20} term in Equation (3-1). For a prolate (elongated) nucleus, this can be imagined as a pushing and pulling on the ends of the elongated shape. Since the nucleus retains its axial symmetry (and because of the 0 projection quantum number of the spherical harmonic) we can see that the angular momentum of this vibration will have no projection on the nuclear symmetry axis and will form a $J^{\pi} = 0^{+}$ state with $K = 0$.

Gamma vibrations can be imagined as pushing and pulling on the sides (rather than the ends) of the elongated deformed nucleus. This vibration is equivalent to adding a sinusoidal time dependence to the $Y_{2,2}$ and $Y_{2,-2}$ terms in Equation (3-1). This type of vibration obviously breaks axial symmetry and from its connection to the spherical

harmonics we can tell that it will carry two units of angular momentum along the symmetry axis of the nucleus. Thus it will create a $J^{\pi} = 2^{+}$ state with $K = 2$.

3.4. Combining collective excitations: Band structure

In a real deformed nucleus vibrational and rotational excitations occur together to create excited states. Generally speaking, a series of rotational states, called a "band", can be built on any vibrationally excited state, or even on a pair-breaking single-particle excited state. Building a rotational band on a beta vibration results in a "band head" with $J^{\pi} = 0^{+}$ and successive rotational states of even spin above that, much like the ground state band.

A gamma vibrational band starts with a $J^{\pi} = 2^{+}$ band head with $K = 2$ upon which we build rotational states of $J^{\pi} = 2^{+}, 3^{+}, 4^{+}, 5^{+}$, etc. Figure 3-4 shows how the ten lowest excited state of ^{166}Er display this band structure very well. We can clearly see the ground state and gamma bands, with increased energy spacing as the rotational excitations are added.

The presence of a well-defined gamma band has been established in many deformed nuclei [8]. However, the same cannot be said for beta bands. Frequently several states with $J^{\pi} = 0^{+}$ are found at roughly the same energy with each level showing some of the signs of a beta vibration. Decades after its theoretical introduction, the beta vibration and the $J^{\pi} = 0^{+}$ level that it predicts continue to be a roundly debated subject [8].

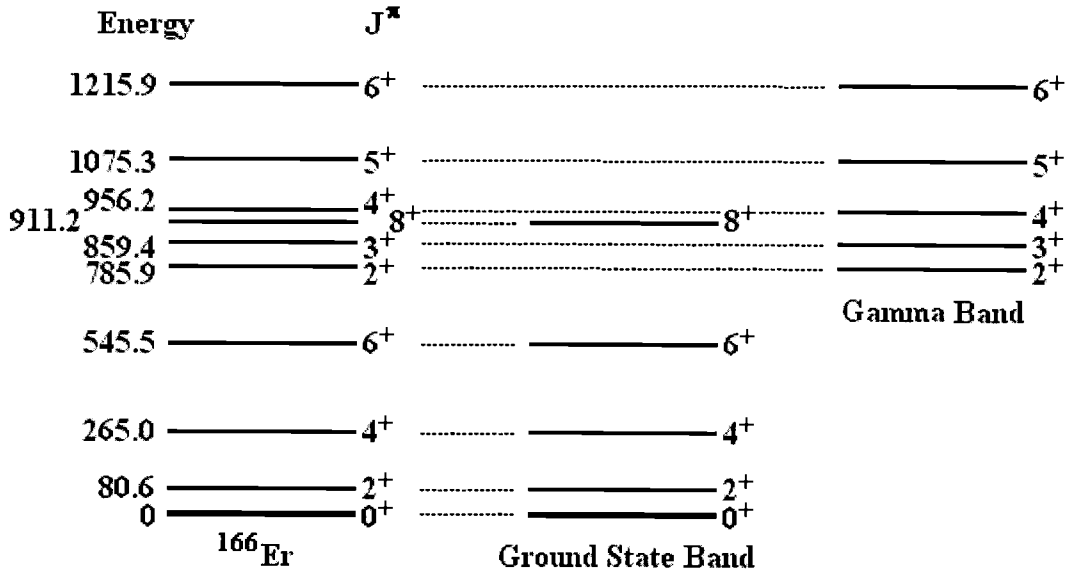

Figure 3-4: Band structure of the low lying levels in ^{166}Er.

3.5. Intra-band transition probabilities

In this work we will be particularly interested in B(E2) and B(M1) values for transitions that take place between bands and inside bands. Given a few reasonable assumptions, these quantities can be calculated from theory.

The electric quadrupole operator is defined as [9]

$$eQ_{op} = \int \rho_e(\vec{r}) r^2 (3\cos(\theta) - 1) dv \tag{3-5}$$

The diagonal matrix elements of this operator give the intrinsic electric quadrupole moment, Q_0, of the nucleus in the state $|J, K, M\rangle$.

$$Q_0 = \langle J, K, M | Q_{op} | J, K, M \rangle \tag{3-6}$$

Q_0 is a measure of how much the nuclear charge distribution deviates from spherical symmetry and can be directly related to the deformation of the nucleus. Note that this is not the same as the observed electric quadrupole moment, but rather represents the electric quadrupole moment of the nucleus in its own rest frame.

The non-diagonal matrix elements of the electric quadrupole operator $\langle J_f, K_f, M_f | Q_{op} | J_i, K_i, M_i \rangle$ represent transitions between different states by E2 radiation. As mentioned in Section 3.2, there is good evidence that the shape of the nucleus, and therefore its intrinsic quadrupole moment, does not change appreciably as rotational excitations are added to a band-head state. Thus, if we assume that the initial and final states are part of the same rotational band, and employ the Wigner-Eckart theorem, we can calculate the reduced transition matrix element [10]

$$\langle J_f, K \| M(\mathrm{E2}) \| J_i, K \rangle = \frac{1}{\sqrt{2J_i + 1}} \langle J_i, K, 2, 0 | J_f K \rangle \left(\frac{5}{16\pi} \right)^{1/2} eQ_0 \qquad (3\text{-}7)$$

where $M(\mathrm{E2})$ is the electric quadrupole tensor, $\langle J_i, K, 2, 0 | J_f K \rangle$ is a Clebsch-Gordan coefficient and $|J_f - J_i| \leq 2$. Using Equation (2-10) we can now calculate the reduced transition probability $B(\mathrm{E2})$ for transitions within a band

$$B(\mathrm{E2}; J_i K \rightarrow J_f K) = \frac{5}{16\pi} \langle J_i, K, 2, 0 | J_f K \rangle^2 e^2 Q_0^2 \qquad (3\text{-}8)$$

A similar analysis may be performed for the M1 reduced transition probabilities within a rotational band. However we can ignore the case of $K = 0$ bands because all

states have even spin, and thus M1 transitions are not allowed. For bands with $K > \frac{1}{2}$ and $|J_f - J_i| \leq 1$ we have [10]

$$B(\mathrm{M1}; J_i K \rightarrow J_f K) = \frac{3}{4\pi} \mu_N^2 \left(g_K - g_R\right)^2 K^2 \left\langle J_i, K, 1, 0 \middle| J_f K \right\rangle^2 \tag{3-9}$$

where g_K and g_R are the intrinsic and rotational gyromagnetic ratios and μ_N is the nuclear magneton. An important consequence of Equation (3-9) is to note that this theory forbids M1 transitions between states of a band of $K = 0$.

With these expressions in hand, we can now use Equation (2-11) to take the ratio of the transition probabilities for E2 and M1 for a single gamma ray.

$$\frac{\lambda(\mathrm{E2})}{\lambda(\mathrm{M1})} = \frac{3}{100}\left(\frac{E}{\hbar c}\right)^2 \frac{B(\mathrm{E2})}{B(\mathrm{M1})} \tag{3-10}$$

This expression is actually simply the square of the mixing ratio $\delta(\mathrm{E2/M1})$ for the gamma ray in question. Substituting for the Bs and taking a square root using the convention of Krane and Steffen [11] we can calculate a theoretical value for $\delta(\mathrm{E2/M1})$

$$\delta = \frac{\sqrt{3}}{10} \frac{E}{\hbar c} \frac{\left\langle J_f, K \middle\| M(\mathrm{E2}) \middle\| J_i, K \right\rangle}{\left\langle J_f, K \middle\| M(\mathrm{M1}) \middle\| J_i, K \right\rangle} \tag{3-11}$$

where the E2 matrix element is in units of electron barns, the M1 matrix element is in units of nuclear magnetons, and E is in MeV. It should be noted that in most theories it is the ratio of reduced matrix elements that is calculated. This ratio, which is not unitless, must then be used in Equation (3-11), producing the unitless $\delta(\mathrm{E2/M1})$ mixing ratio which is the quantity actually measured in the laboratory.

From Equation (3-11) we use Equations (3-8) and (3-9) to express $\delta(\mathrm{E2/M1})$ in terms of Q_0 and $(g_K - g_R)$ for transitions within a band.

$$\delta = \sqrt{\frac{3}{5}} \frac{e}{4\mu_N \hbar c} E \frac{1}{\sqrt{(J_i+1)(J_i-1)}} \frac{Q_0}{(g_K - g_R)} \tag{3-12}$$

This expression allows us to predict values for the mixing ratio $\delta(\mathrm{E2/M1})$ based solely upon the spin of the level in question and intrinsic properties of the nucleus for that band. It can also be reversed, allowing us to examine the electric and magnetic properties of a band by measuring the mixing ratio of transitions between states in the band.

3.6. Interband E2 transition probabilities

The formalism developed in the previous section can also be used to predict some aspects of transitions between bands. Specifically, if we make the assumption that the intrinsic quadrupole moment is the same for the gamma and ground bands, we can calculate the ratio of the E2 transition probabilities for selected gamma rays. As an example we will consider the 2^+ to 2^+ gamma-to-ground transition and the 2^+ to 0^+ gamma-to-ground transition as shown in Figure 3-5.

Both transitions are assumed to be pure-E2 multipolarity due to the $\Delta K = 2$ nature of the transitions (not to mention the $\Delta J = 2$ of γ_2). Using Equation (2-11) we can write the ratio of the transition probabilities for these two gamma rays.

$$\frac{\lambda(\gamma_1)}{\lambda(\gamma_2)} = \frac{E(\gamma_1)^5}{E(\gamma_2)^5} \frac{B(\mathrm{E2},\gamma_1)}{B(\mathrm{E2},\gamma_2)} \tag{3-13}$$

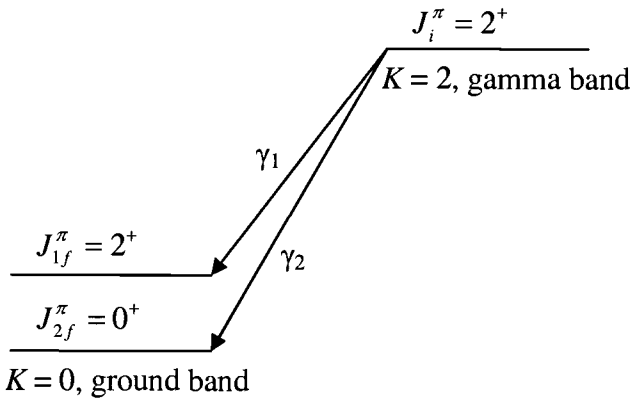

Figure 3-5: Gamma rays whose intensity ratio can be predicted from basic theory. Due to the $\Delta K = 2$ nature of γ_1 it is assumed to be a pure-E2 gamma ray.

where all the other constants have cancelled out in this ratio. We can now employ Equation (2-10) to give

$$\frac{\lambda(\gamma_1)}{\lambda(\gamma_2)} = \frac{E(\gamma_1)^5}{E(\gamma_2)^5} \frac{\left|\left\langle J_{1f}, K_f \| M(\mathrm{E2}) \| J_i, K_i \right\rangle\right|^2}{\left|\left\langle J_{2f}, K_f \| M(\mathrm{E2}) \| J_i, K_i \right\rangle\right|^2} \tag{3-14}$$

where $K_i = 2$ and $K_f = 0$. Finally, in much the same way that the Wigner-Eckart theorem removes the M dependence of a matrix element to produce a reduced matrix element we can use a similar relation to remove the J dependence of the reduced matrix element [10]

$$\left\langle J_f, K_f = 0 \| M(\sigma L) \| J_i, K_i \right\rangle = \sqrt{2J_i + 1}(-1)^{J_i + J_f + K_i} \left\langle J_i, K_i, L, \Delta K \middle| J_f, 0 \right\rangle \left\langle K_f \middle| M(\mathrm{E2}) \middle| K_i \right\rangle X \tag{3-15}$$

where $X = \sqrt{2}$ for $K_i \neq 0$ and $X = 1$ for $K_i = 0$. The J dependence is now expressed in the Clebsch-Gordan coefficient and the remaining "intrinsic" matrix element depends only on K. Using Equation (3-15) we can now write Equation (3-14) as

$$\frac{\lambda(\gamma_1)}{\lambda(\gamma_2)} = \frac{E(\gamma_1)^5}{E(\gamma_2)^5} \frac{\langle J_i, K_i, 2, 2 | J_{1f}, K_f \rangle^2 \left| \langle K_f | M(\mathrm{E2}) | K_i \rangle \right|^2}{\langle J_i, K_i, 2, 2 | J_{2f}, K_f \rangle^2 \left| \langle K_f | M(\mathrm{E2}) | K_i \rangle \right|^2} \tag{3-16}$$

in which the intrinsic matrix elements in the numerator and denominator are equal and will therefore cancel out. Thus, the ratio of transition probabilities reduces to the fifth power of the energy ratio times the square of the ratio of Clebsch-Gordan coefficients. Using the example of ^{166}Er the energies for these transitions are $E(\gamma_1) = 705$ keV and $E(\gamma_1) = 785$ keV. With the readily looked up Clebsch-Gordan coefficients we can calculate this ratio as

$$\frac{\lambda(\gamma_1)}{\lambda(\gamma_2)} = 0.835 \tag{3-17}$$

Similar calculations can be made for gamma rays emitted from all other gamma band states. These calculated ratios can then be compared with experimental values to evaluate the applicability of this nuclear model (see Section 3.8).

3.7. Intra-band cascade to crossover ratios

Another calculation that can be done easily for this model is known as a cascade-to-crossover ratio. One of the characteristics of band structure in deformed nuclei is the high relative probability that a state will decay "within band." In the gamma band these strengths can be compared by looking at two transitions from the same level, one of which is a transition to the next lower state in the band (called the cascade transition) and

the other of which skips over that level to land two levels lower (called the crossover transition). This situation is diagramed in Figure 3-6.

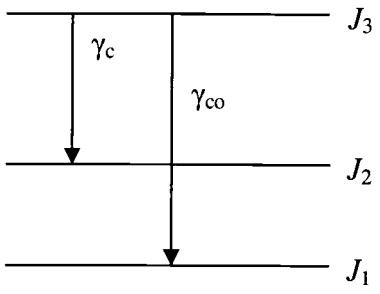

Figure 3-6: Diagram showing the "cascade" and "crossover" transitions, γ_c and γ_{co}.

For a gamma band cascade-to-crossover analysis we know that all the parities of the nuclear states will be positive and that the spins of the levels will grow by one as we go up the band. This means that the cascade transition can have both E2 and M1 character. Thus, we can write the ratio of intensities for the two transitions as

$$\frac{\lambda(\gamma_c)}{\lambda(\gamma_{co})} = \frac{\lambda(\gamma_c;\mathrm{E2}) + \lambda(\gamma_c;\mathrm{M1})}{\lambda(\gamma_{co};\mathrm{E2})} \tag{3-18}$$

where we have split the intensity of the cascade transition into its multipole components. Using equations (2-16) and (2-17) we can rewrite the numerator so that

$$\frac{\lambda(\gamma_c)}{\lambda(\gamma_{co})} = \frac{\lambda(\gamma_c;\mathrm{E2})\left(1+\frac{1}{\delta(\gamma_c)^2}\right)}{\lambda(\gamma_{co};\mathrm{E2})} = \frac{\lambda(\gamma_c;\mathrm{E2})}{\lambda(\gamma_{co};\mathrm{E2})}\left(1+\frac{1}{\delta(\gamma_c)^2}\right) \tag{3-19}$$

Now, as we have done before, we can rewrite the ratio of intensities in terms of a ratio of B(E2) values (Equation (2-11)), which can then be expressed as reduced matrix elements (Equation (2-10)) to produce

$$\frac{\lambda(\gamma_c)}{\lambda(\gamma_{co})} = \frac{E_c^5}{E_{co}^5} \frac{\left|\left\langle J_2, K \left\| M(\mathrm{E2}) \right\| J_3, K \right\rangle\right|^2}{\left|\left\langle J_1, K \left\| M(\mathrm{E2}) \right\| J_3, K \right\rangle\right|^2} \left(1 + \frac{1}{\delta(\gamma_c)^2}\right) \tag{3-20}$$

We now employ a version of Equation (3-15) to remove the J dependence of the reduced matrix elements, leaving only the intrinsic matrix elements

$$\frac{\lambda(\gamma_c)}{\lambda(\gamma_{co})} = \frac{E_c^5}{E_{co}^5} \frac{\left\langle J_3, K, 2, 0 \middle| J_2, K \right\rangle^2 \left|\left\langle K \left| M(\mathrm{E2}) \right| K \right\rangle\right|^2}{\left\langle J_3, K, 2, 0 \middle| J_1, K \right\rangle^2 \left|\left\langle K \left| M(\mathrm{E2}) \right| K \right\rangle\right|^2} \left(1 + \frac{1}{\delta(\gamma_c)^2}\right) \tag{3-21}$$

The intrinsic matrix elements will cancel out leaving a ratio of Clebsch-Gordan coefficients

$$\frac{\lambda(\gamma_c)}{\lambda(\gamma_{co})} = \frac{E_c^5}{E_{co}^5} \frac{\left\langle J_3, K, 2, 0 \middle| J_2, K \right\rangle^2}{\left\langle J_3, K, 2, 0 \middle| J_1, K \right\rangle^2} \left(1 + \frac{1}{\delta(\gamma_c)^2}\right) \tag{3-22}$$

Thus, the δ(E2/M1) mixing ratio can be calculated from the relative intensities and energies of the intra-band transitions, offering a simple test of this theoretical model.

3.8. Band mixing and E2 intensities

From nearly the first comprehensive study of nuclei with clearly defined gamma bands it was discovered that the theoretical calculation of the transition probability ratios between bands based on this model (see Section 3.6) did not match the experimental data well at all. For example, the current accepted intensities [12] would give a value of 1.1

(with a relative uncertainty of less than 5%) for the quantity in Equation (3-17) which we calculated as 0.835. Other transitions in many nuclei give similarly poor agreement with the predictions of Section 3.6.

One method of bringing this theory back into agreement with the experimental transition intensities is to assume that there is some mechanism for mixing states with $\Delta K = 2$. The mechanism for such mixing is not stated as part of this theory, but the effect is assumed to be small and can therefore be treated using first-order perturbation theory. We assume that the wave functions for each state in the bands is actually a linear combination of the state from that band, plus a small admixture of the state from the other band with the same spin [10]

$$\begin{aligned} \left|J_g\right\rangle &= \left|J, K=0\right\rangle - c(J)\left|J, K=2\right\rangle \\ \left|J_\gamma\right\rangle &= \left|J, K=2\right\rangle + \tfrac{1}{2}c(J)\left(1+(-1)^J\right)\left|J, K=0\right\rangle \end{aligned} \tag{3-23}$$

The mixing obviously vanishes for odd J since there are no odd J states in the ground band. The admixture amplitude $c(J)$ is given by

$$c(J) = \varepsilon_2 \left(2(J-1)J(J+1)(J+2)\right)^{\frac{1}{2}} \tag{3-24}$$

where ε_2 is a spin independent strength parameter.

The effect of this mixing is that the E2 operator can now connect the gamma and ground band states both through the original $\left\langle J, K=0\left|M(\mathrm{E2})\right|J, K=2\right\rangle$ matrix element as well as through the diagonal matrix elements $\left\langle J, K=0\left|M(\mathrm{E2})\right|J, K=0\right\rangle$ and $\left\langle J, K=2\left|M(\mathrm{E2})\right|J, K=2\right\rangle$. These last two matrix elements will be modified by the

admixture amplitude $c(J)$, but will still contribute to the overall E2 strength. The term that is quadratic in $c(J)$ is neglected under the assumption that $c(J)$ is small. These diagonal matrix elements can be reduced with the Wigner-Eckart theorem and then related to the intrinsic electric quadrupole moments of the gamma and ground band as given in Equation (3-7). Therefore if we make the common assumption that the intrinsic electric quadrupole moments of the two bands are the same, we can use these mixed states to come up with a reduced transition probability

$$B(\mathrm{E2}; J_i, K=2 \rightarrow J_f, K=0) = 2\left\langle J_i, 2, 2, -2 \middle| J_f, 0 \right\rangle^2 \left| M_1 + M_2 \left(X_f - X_i \right) \right|^2 \quad (3\text{-}25)$$

where the parameters M_1 and M_2 are spin-independent parameters and $X = J(J+1)$. The implication is that the square-root of the reduced transition probabilities can be expressed as a *linear* function of the parameter $\left(X_f - X_i \right)$ with a slope and intercept determined by M_1 and M_2. A parameter often measured in experiment is z_2 where

$$z_2 = \frac{2M_2}{M_1 - 4M_2} \quad (3\text{-}26)$$

and M_2 is related to our original admixture strength parameter ε_2 by

$$M_2 = \varepsilon_2 \left(\frac{15}{8\pi} \right)^{\frac{1}{2}} eQ_0 \quad (3\text{-}27)$$

This formalism, first developed by Mikhailov, can be used to produce a "Mikhailov" plot (see Section 6.4) which plots the square-root of the experimental $B(\mathrm{E2})$ values vs. $\left(X_f - X_i \right)$, as in Equation (3-25), to determine the efficacy of the

band-mixing model. Experimental results for ^{166}Er have agreed very well with the band-mixing model ever since it was first applied.

Additional evidence for the band-mixing model is given by the deflections in energy of the even members of the gamma band. As we would expect from basic perturbation theory, a mixing of states from the gamma and ground bands will cause a repulsive effect in the two energies, i.e. we expect the ground-state energies to be pushed down and the even-spin states of the gamma band to be pushed up (the odd-spin states have no counterparts to mix with). Recall that we expect the energy spacing of the gamma band to follow the $J(J+1)$ rotational model. Experiments have shown that there is an odd-even staggering of the energies, relative to the expected $J(J+1)$ spacing [13]. This offers further evidence for some form of mixing between the two bands.

The calculations performed in Section 3.7 are relatively insensitive to the addition of first-order band mixing. This insensitivity comes from the inherently small value of the cross-band off-diagonal matrix elements and from the small value of the mixing parameter that describes ^{166}Er. Thus, even with evidence of band mixing between the gamma and ground bands, the cascade-to-crossover ratios from Section 3.7 should remain a valid prediction.

3.9. M1 strengths in the band-mixing model

The band-mixing model allows diagonal matrix elements to appear in transition probabilities for gamma rays connecting the gamma and ground bands. This not only

affects the E2 strengths, as shown, but also allows M1 transitions to appear for the first time. Up to now, M1 transitions had been forbidden by the K selection rule, but of course that rule holds only to the extent that K is a good quantum number.

These M1 admixtures can also be analyzed from the basic first order band-mixing theory. Doing so allows us to calculate the mixing ratio $\delta(\mathrm{E2/M1})$

$$\delta \cong E\frac{-AQ_0}{z_2(g_K - g_R)} \tag{3-28}$$

This expression bears an obvious relationship to Equation (3-12), and the constant A contains a ratio of Clebsch-Gordan coefficients, some other spin-dependent factors and some physical constants. This expression is arrived at by several approximations: we have neglected terms that are quadratic or higher in the band-mixing strength parameter ε_2, we have assumed the contributions to the E2 strength from the cross terms in the matrix elements are negligible compared to the un-mixed terms, and we have neglected a term of the order $4z_2$, which is on the order of 16% for ^{166}Er. Further discussion and calculations using this expression are carried out in Section 7.2.

3.10. The interacting boson approximation

The issues addressed by the rotational model and band-mixing theory can also be addressed by other theoretical constructions. In particular two versions of the interaction boson approximation (IBA) have been developed as alternate ways to treat the structure of deformed nuclei. We do not develop this model in any detail in this work, but rather mention it as an alternative to the theories we have developed so far.

It can be argued that in many ways the rotational model is too oversimplified. In particular, the effects of valence nucleons are completely ignored in this model, treating the nucleus as a collective entity regardless of partially filled shells. In contrast, the IBA model ignores only fully closed shells. For the remaining nucleons it applies two known effects: the pairing force, which pushes the nucleus towards spherical symmetry, and the so called "quadrupole force", which causes the quadrupole deformations in nuclei that are far from closed shells. However, as its name implies, the IBA model does not treat each nucleon separately. Instead, each pair of nucleons is coupled together to create a boson. If the total angular momentum of the individual nucleons is coupled to a total of zero, this is called an "s boson." Likewise a total coupled angular momentum of two is called a "d boson." It is the behavior of these s and d bosons that are treated by a quantum-mechanical Hamiltonian. From these basic assumptions a complex algebra is developed, describing the usual quantum mechanical players such as creation and annihilation operators.

In the basic IBA model, known as IBA-1, protons and neutrons are treated as indistinguishable components of the nucleus. An important consequence of this is the total lack of M1 transitions. In analogy with the basic rotational model, IBA-1 has no mechanism to explain the presence of M1 transitions in deformed nuclei.

However, any mechanism, regardless of the specific model, that allows mixing between bands that differ by $\Delta K = 1$ offers a path for M1 transitions to occur between states in a rotational band. Much like the $\Delta K = 2$ band mixing described previously, $\Delta K = 1$ mixing would mean that each ground and gamma-band state could actually be a

linear combination of states from the original band and states from some $K=1$ band. Thus, M1 transitions could occur between the portions of the gamma and ground states that differed by $\Delta K=1$.

IBA-2, which no longer treats protons and neutrons identically, opens up the possibility that the two groups of nucleons could be undergoing different motions. This model has had success in proposing a specific form for the $K=1^+$ band which could mix with the gamma and ground bands. The specific $K=1^+$ example is called a "scissors mode" because it involves the protons and neutrons oscillating out of phase with each other. This mode of excitation is the subject of much study and calculation and is predicted to occur between 2 and 3 MeV above the ground state.

Several papers have compared the IBA-2 model with band-mixing models in terms of their success in explaining experimentally measured M1 strengths [24,33].

4. Previous Work

4.1. Understanding β decay experiments

The nuclear energy levels discussed in Chapter 3 can be excited in a number of ways, offering many methods for their experimental investigation. In particular, the radioactive decay of a "parent" nucleus often leaves the newly formed "daughter" nucleus in an excited state. The daughter then sheds this excess energy through processes including gamma ray emission and internal conversion, as mentioned previously. Beta decay, perhaps the most common form of radioactive decay, is a process in that converts a neutron to a proton, or vice-versa. This process changes the elemental character of the nucleus but does not change the nuclear mass number A. The process of turning a neutron into a proton is called β^- decay because a negatively charged electron is also emitted as described by

$$\mathrm{n} \rightarrow \mathrm{p} + \beta^- + \bar{\nu}_e$$

Here β represents the electron and $\bar{\nu}_e$ is an anti-neutrino which must be present to conserve momentum and lepton number, but does not interest us in these experiments. The process of turning a proton into a neutron is called β^+ decay and can be similarly described by

$$\mathrm{p} \rightarrow \mathrm{n} + \beta^+ + \nu_e$$

where β^+ is an anti-electron (positron). A process known as electron-capture competes with β^+ decay but instead of ejecting a positron an inner atomic electron is absorbed.

These processes must follow certain "selection rules" that govern the degree to which a certain excited state of the daughter will be populated in the β decay process. A general overview of these selection rules is as follows [2].

- "Allowed" decays are those in which the difference in total angular momentum between decaying state in the parent and the populated state in the daughter is zero or one ($\Delta J = 0$ or 1), and in which there is no parity change ($\Delta\pi = \text{no}$).
- "First forbidden" decays are those for which $\Delta J = 0,1,2$ and $\Delta\pi = \text{yes}$. Due to the nature of β decay, these processes are less likely to occur than allowed decays, but not actually forbidden as the name implies.
- "Second forbidden" decays are those in which $\Delta J = 1,2$ or 3 and $\Delta\pi = \text{no}$. However, since the $\Delta J = 1$, $\Delta\pi = \text{no}$ case is covered by the allowed decays, second forbidden decays are seen only for $\Delta J = 2$ or 3.

Higher forbidden decays can be described, but these selection rules are enough to serve this discussion. The key is that each step up in forbiddenness causes sharp decrease in the probability of decay, usually on the order of 10^{-4} [2]. Thus, if a given state may β decay to several different states in the daughter nucleus, those for which the transition is allowed will be populated strongly, first forbidden transitions will happen less often and second forbidden or higher decays will be observed only in rare circumstances.

The nucleus ^{166}Er can be created through the β decays of two different parent nuclei. Two different states of ^{166m}Ho decay to ^{166}Er through β^- decay while ^{166}Tm decays

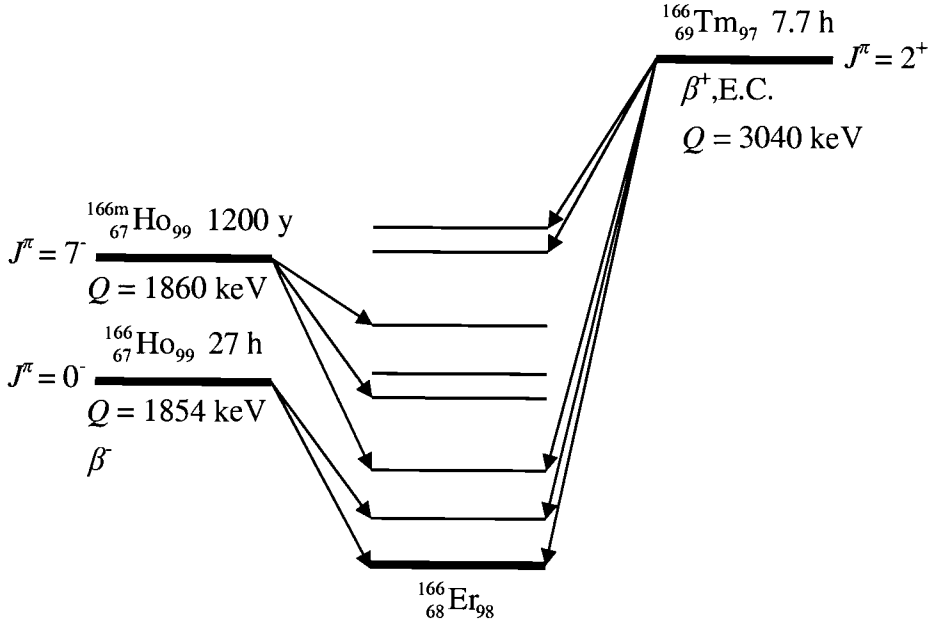

Figure 4-1: Schematic of β decays leading to excited states of ^{166}Er.

to the same daughter through β^+ decay and electron capture. The higher of the two ^{166}Ho states is a long lived excited state (called a meta-stable state or an isomer and denoted by ^{166m}Ho) that cannot decay to the ground state due to the large difference in spin. A schematic of these three decays is shown in Figure 4-1. Note that the three parents start from very different spin and parity states. ^{166m}Ho decays from a spin 7 state and thus, according to the β decay selection rules, will populate similarly high-spin states in the daughter nucleus. The energy difference between the ^{166m}Ho parent and the ground state of the ^{166}Er daughter is 1860 keV, and thus this energy must be released in the process of going from one to the other. This is known as the Q-value of the decay and represents the total energy available to the β decay and potential subsequent gamma-ray decays. This decay has a half-life of approximately 1200 years and can thus be studied at great leisure.

Due to the very long half-life of ^{166m}Ho and the wide range of gamma-ray energies emitted in this decay, ^{166m}Ho has been extensively studied and has become a widely used calibration source.

The lower-spin ground state of ^{166}Ho has a spin of 0 and decays with a half life of 27 hours with a Q-value of 1854 keV. This activity has not been studied as extensively and was not examined in this study at all.

The ^{166}Tm parent decays from a $J^{\pi} = 2^{+}$ ground state with a Q-value of 3040 keV and thus populates low- and middle-spin states in the ^{166}Er daughter, giving a very different glimpse of its nuclear structure.

These radioactive decays can be studied by simply placing a sample in front of one or more gamma-ray detectors. Experiments like this may use multiple detectors to collect coincidence and angular correlation data. Alternatively, low temperature nuclear orientation (LTNO) experiments can be used to collect angular distribution information with only a single detector, though usually several are used.

4.2. Other experiment types

Beta decay of an unstable parent is not the only way to investigate the properties of a nucleus of interest. Many different types of projectiles, from neutrons to medium-weight atoms, can be used in scattering experiments that leave the target nucleus in an excited state.

Transfer reactions, also called "in-beam" experiments, create the nucleus of interest by impacting a target with a projectile in a carefully crafted manner to produce

the appropriate nucleus. An example of such an experiment would be firing α particles at a sample containing ^{164}Dy with a carefully chosen energy so that the α particle will be absorbed and two neutrons will be ejected, leaving behind a ^{166}Er nucleus in an excited state. This reaction is described in short-hand by ^{164}Dy(α,2n)^{166}Er.

Coulomb-excitation experiments are those in which the target and projectile do not "touch", meaning there is no exchange of nucleons. These experiments rely on the Coulomb interaction of the projectile and target to excite the target. Coulomb-excitation experiments tend to excite the nucleus as a whole, and are thus a very useful tool for examining collective excitations.

The previous work described in the following sections is broken down into categories for easy comparison. However, some experiments and publications are applicable to more than one category and may therefore appear in more than one section.

4.3. Previous examinations of the decay of ^{166m}Ho

Studies of the decay of the ^{166m}Ho isomer have been done in several ways. Early studies used sodium-iodide (NaI) detectors, which are more efficient, but have much poorer resolution than the germanium (Ge) detectors developed around the middle of the 20th century.

4.3.1. Spectroscopic studies

As mentioned, ^{166m}Ho has become a calibration standard used to test gamma-ray detection equipment before use in other experiments. ^{166m}Ho is good for these purposes

because of the consistent and precise results from experiments done to determine the spectroscopic details of the decay (i.e. the exact gamma-ray energies and intensities that it emits). Once it was proposed as a calibration standard further experiments were done to improve on the spectroscopic information about the decay, and now ^{166m}Ho can be considered once of the most carefully studied radioactive decays on the chart of the nuclides.

The first comprehensive experimental studies of the ^{166m}Ho decay were performed by Reich and Cline in 1963 [14] and 1965 [15]. Their first experiment was performed using NaI detectors which have a significantly poorer resolution than the Ge detectors used in later experiments. Despite this difficulty the experiment was able to effectively explain much of the structure of the populated levels of ^{166}Er. Their 1965 experiment was conducted using both NaI and Ge detectors and allowed them to clarify their earlier experiment and expand on it quite a bit. 33 gamma-rays were observed in these experiments and 14 nuclear levels were proposed.

Since these early experiments several experiments have been done to extend and improve the work of Reich and Cline, notably the works by Kato [16], Sampson [17] and Danilenkov [18]. Comparisons between the measured intensities of the gamma-to-ground transitions and those expected from the band-mixing model are also performed in these papers, generally with favorable results. The most recent comprehensive spectroscopic work on ^{166m}Ho was done by J. Morel in 1995 [19] and the results of all these measurements have been compiled by Shurshikova and Timofeeva in the Nuclear Data Sheets [12].

4.3.2. Nuclear structure studies

Interpretations of the level scheme were also performed by Reich and Cline in their 1965 experiment [15]. In this study angular correlation experiments were used to assist in assigning spins to the nuclear levels. Calculations of $\delta(\mathrm{E2/M1})$ mixing ratios were presented and both band-mixing and asymmetric rotor models were compared with the experimental results. Investigations of the negative parity bands in ^{166}Er were also performed here along with possible theoretical interpretations. These experiments also solidified the Q-value of this decay and firmly established the existence of the gamma-vibrational band. The mixing ratios in this paper were deduced from the quadratic forms of the angular correlation coefficients.

A 1967 experiment by Gunther and Parsignault [20] confirmed much of the work by Reich and Cline and added a few transitions to their decay scheme. In addition this work presented band-mixing analysis and claimed that the intrinsic quadrupole values of the gamma and ground bands were in fact different by a factor of 1.38 (a claim later disputed by another Reich and Cline paper).

A short time later in 1967 Burson [21] performed a spectroscopic study of the ^{166}Er nucleus using all three β-decay parents. This study contributes a small amount of new spectroscopic information to the decay scheme and offers analysis of the observed intensities in terms of band-mixing theory.

In 1969 Sunyar [22] published a paper describing the cascade-to-crossover intensity measurement, and the mixing ratios of the cascade transitions predicted by the

basic rotational model. This paper did not present new experimental data but used the currently available experimental intensities. It should be noted that Sunyar uses an intrinsic electric quadrupole moment for the gamma band that is 1.38 times that of the ground band (as per the work by Gunther and Parsignault above). Mixing ratios for three cascade intra-gamma band transitions are presented based on intensities and simple rotational model calculations.

Reich and Cline published another treatment of the ^{166m}Ho decay in 1970 [13] addressing the question of whether the gamma and ground bands have differing intrinsic electric quadrupole moments. They conclude that the two bands do indeed have the same intrinsic electric quadrupole moment (within their uncertainty limits) and give some convincing arguments regarding why previous studies have concluded otherwise. In this paper Reich and Cline observe and quantify the odd-even energy shift of the gamma band. They also observe evidence for considerable M1 transition strength inside the gamma band and use a cascade-to-crossover analysis to predict the mixing ratios of three of the intra-gamma band cascade transitions (using equal Q_0 values for both bands). This analysis concludes with the deduction that the quantity $|g_K - g_R|$ is constant within the gamma band.

In 1972 Carlsson [23] used a perturbed angular correlation experiment to determine the gyromagnetic ratio, g_R, of the 6^+ ground-band state which agreed with previously determined values for the $g_R(4^+)$ and $g_R(2^+)$ ground-band states well enough

that the authors concluded that this ratio stays constant throughout the band, as predicted by theory if there is no centrifugal stretching of the nucleus at higher spins.

In 1975 Baker [24] used both Ge-NaI and Ge-Ge coincidence systems to investigate this decay. Their measurements of angular correlations involving nine gamma-to-ground band transitions represents the first attempt to comprehensively study the $\delta(\mathrm{E2/M1})$ mixing ratios of all the gamma-to-ground transitions observable in this decay (the 2^+ gamma to 2^+ ground transition is not present in the ^{166m}Ho decay with enough strength to be measured). Their results were compared with what they call the dynamic deformation model (DDM), in which the g-factors of the excited states depend on intrinsic properties like the quadrupole deformation parameters. While the authors do not compare their work with that of previous measurements, they generally agree with the order of magnitude and sign found by Reich & Cline [15]. The mixing ratios in this paper were deduced from the quadratic forms of the angular correlation coefficients.

In 1981 Krane and Moses [25] performed an LTNO experiment on ^{166m}Ho allowing a slightly different view of the angular distribution measurements. LTNO experiments measure the A_k angular distribution coefficients, whereas angular correlation experiments can measure either the A_k angular distribution coefficients or B_k orientation parameters. From this experiment Krane and Moses extract angular distribution coefficients for 24 gamma rays and E2/M1 mixing ratios for nine of the gamma-to-ground transitions. They measured these mixing ratios from two different oriented sources and published two sets of values for the mixing ratios. Investigations of the mixing ratios emitted by the negative parity states fed in the ^{166m}Ho decay were also

presented, allowing further interpretation of these negative parity bands. The mixing ratios in this paper were deduced from the quadratic forms of the angular correlation coefficients.

As mentioned previously, in 1981 Kato [16] performed precision measurements of the relative intensities of gamma rays in the ^{166m}Ho decay. Mixing ratios were also measured for six of the gamma-to-ground transitions, however, the signs of the mixing ratios were not presented. Kato's values are generally in poor agreement with other measurements done around the same time. The mixing ratios in this paper were deduced from the quadratic forms of the angular correlation coefficients.

Also in 1981 Lange [26], who is part of the same group as Baker [24], added to their previous measurements of the ^{166m}Ho decay. This study measured the angular correlations and mixing ratios of nine gamma-to-ground transitions, improving over previous measurements. Measurements of transitions from the negative parity bands were also performed and compared with the measurements performed by Reich and Cline. A possible hindrance of these experiments is that while most gamma rays were detected using high resolution Ge detectors, a NaI detector was used to gate on the 184 keV 4^+ to 2^+ ground band transition. Thus coincidence measurements with the 184-keV transition could be susceptible to Compton backscattering processes (see Section 5.5.2). This would affect only a few measurements, but the poor resolution of the NaI detector leaves open the possibility that this effect was unaccounted for. The mixing ratios in this paper were deduced from the quadratic forms of the angular correlation coefficients.

In 1984 Marshak [27] published a paper describing a method for finding the mixing ratios by chi-squared minimization using a new set of LTNO data. The authors compare this method to the previously dominant method of solving for δ using the angular correlation coefficients. The authors noted that while the previous method often produces satisfactory values of δ, it tends to underestimate the uncertainty in the result. Comparisons of the two methods are presented for five cases, including three gamma-to-ground transitions.

In another 1985 paper, Alzner [28] used the integral perturbed angular correlation method to measure the gyromagnetic ratios of the 4^+, 6^+ and 8^+ ground band states and of the 6^+ gamma band state. In contrast with the work done by Carlsson [23] they concluded that there is evidence that the g-factor is being reduced at higher spins. Measurements of the angular correlation coefficients and mixing ratios were also presented for three gamma-to-ground transitions.

A 1988 paper by Adam [29] takes on the question of whether the intrinsic electric quadrupole moments of the gamma band and ground band are equal. Their chi-squared minimization analysis argues strongly for the two bands having equal intrinsic electric quadrupole moments. They then use this assumption to calculate the band mixing parameter z_2.

In 1990 Hamilton [30], who collaborates with Marshak [27], published a paper discussing the inconsistency of the signs of the mixing ratios being produced by experimentalists. Their results for nine gamma-to-ground mixing ratios are presented in comparison with other recent experiments. These mixing ratios are extracted using the

chi-squared minimization of Marshak's LTNO data, rather than the quadratic method used by most previous studies. Results are also compared with the dynamic deformation model introduced in the paper by Baker in 1975. They find that this model has some success in predicting the signs and relative magnitudes of the mixing ratios. They conclude that experiment and theory predict that most of the $\Delta J = 0$ transitions between the gamma and ground bands will have the opposite sign compared to the other gamma-to-ground transitions.

A 1992 paper by Wagner [31] uses high accuracy intensity measurements of the intra-gamma band transitions to calculate the mixing ratios for four cascade transitions. These measurements follow from the paper by Adam [29] (who works in the same research group as Wagner), and use their assumption of equal intrinsic electric quadrupole moments in the gamma and ground bands.

Also in 1992 a paper by Ardisson [32] calculated band-mixing values which compare favorably with previous measurements, though are not as precise as those of Adam [29].

Finally, in 1996 Alfter [33], a collaborator of Alzner [28], was the first to directly measure a mixing ratio of one of the intra-gamma band mixing ratios in the ^{166}Er nucleus. They arrived at a value of $1.94^{+0.23}_{-0.21}$ for the mixing ratio of the 119 keV 5^+ to 4^+ gamma to gamma transition. However, they measured this mixing ratio using the coincident 875 keV 4^+ to 2^+ gamma-to-ground transition, which is also in coincidence with another gamma ray of energy 121 keV. It appears from the partial spectrum displayed in their

article that they did not take into account the effects of this nearby peak. This paper also presents analysis of the intra-gamma band transitions in terms of the IBA-2 model.

4.4. Previous examinations of the decay of ^{166}Tm

4.4.1. Spectroscopic studies

The decay of ^{166}Tm is significantly more difficult to study than ^{166m}Ho. The half-life is only 7.7 hours, offering a narrow window for experimental counting. In addition a Q-value of just over 3 MeV means that many states are populated by the β^+ and E.C. decay; resulting in a spectrum of more than 350 gamma rays spread from 74 to 2860 keV.

One of the early comprehensive studies of this decay was performed by Żylicz [34] in 1965. In this work the authors were able to place 70 of the 90 gamma rays they observed into a consistent level scheme and solidified the observed levels not populated in the ^{166m}Ho decay. Internal conversion measurements are used to determine the parities and likely spins of the observed levels. Some analysis of the levels, given in terms of single-particle states, is presented here as well.

Considerable improvements to the spectroscopic information for this decay were introduced by Adam in 1979 [35]. This study used γ-γ coincidences and internal conversion electrons to identify over 301 gamma rays, most of which were successfully placed into their proposed level scheme. This same group updated their study in 1989 [36] using refined coincidence techniques and an anti-Compton spectrometer.

The data from this later experiment by Adam remains by far the most comprehensive and precise spectroscopic information on the ^{166}Tm decay, and the Nuclear Data Sheets summary of this decay is almost entirely built from the data produced by Adam.

4.4.2. Nuclear structure studies

The 1979 paper by Adam [35] was primarily focused on the spectroscopy information for the ^{166}Tm decay but also included some analysis of their measured intensities in terms of band mixing and intrinsic properties of the bands. Their values are compared with those found by Reich and Cline in 1970 [13].

In 1980 Budzynski [37] performed a set of measurements of angular correlations following the decay of ^{166}Tm. Much like the experiment by Lange [26] this experiment could be susceptible to backscatter problems arising from using a NaI detector as a coincidence gate (see Section 5.5.2). Given the difficulty of measuring gamma-to-ground mixing ratios from the ^{166}Tm decay this paper gives a decent set of values for the lowest-spin transitions and is in good agreement with an earlier similar study by West [40]. However, in comparison with contemporary measurements from the ^{166m}Ho decay there is very poor agreement with Budzynski's results.

In 1987 Kracíková [38] performed an LTNO measurement on the ^{166}Tm decay in which they measured the angular correlations and mixing ratios of many gamma rays including four gamma-to-ground transitions. No analysis of the data was presented.

4.5. Previous examinations of the properties of ^{166}Er

In 1972 Domingos [39] performed a Coulomb excitation experiment to study the lower-spin transitions between the gamma and ground bands in several even-even nuclei, including ^{166}Er. Values are presented for the mixing ratios of the 2^+ to 2^+ and 4^+ to 4^+ gamma-to-ground transitions as well as analysis based on first order band mixing theory.

In 1976 West [40] used the reaction ^{160,162,164}Dy(α,2n)^{162,164,166}Er to produce gamma rays for which they measured angular distributions (relative to the projectile beam). These data were used to explore the properties of rotational bands in ^{162}Er, ^{164}Er and ^{166}Er. Previously unidentified $J^\pi = 9^+$ and 10^+ members of the gamma band in ^{166}Er were presented along with mixing ratios from a few of the lower-spin gamma-to-ground transitions. A graphical version of the quadratic method for deducing the mixing ratios was used in this paper.

In 1991 and 1992 Berendakov and Demidov [41,42] published a two papers on neutron scattering with three different Er nuclei, A = 166, 168 and 170. They present mixing ratios for the lower spin members of the gamma-to-ground transitions. Generally speaking their numbers agree with other previous and concurrent measurements and they agree with Hamilton [30] in their signs, but their error bars are larger and thus don't contribute much to the values themselves. This group did adopt the chi-squared minimization method for finding values of the mixing ratio, as proposed by Marshak [27].

In 1996 Brandolini [43] performed Coulomb excitations on ^{164}Er, ^{166}Er and ^{168}Er. The g-factors for the ground band were measured for states up to spin 10^+ as well as for the 2^+ gamma-band head. They conclude, in contrast with the work by Alzner [28], that the g-factors of the ground band do not change appreciably as the spin increases.

4.6. Previous relevant theoretical work

In 1987 Lipas [44] published a comprehensive calculation of the gamma-to-ground mixing ratios using a second-order IBA-1 model (the inclusion of the second order allows M1 transitions between the bands to occur). They attempt to model the mixing ratios of a wide grouping of nuclei in an attempt to find a consistent parameterization. Their results are compared with the experimental results by Lange [26] as well as to the DDM calculations done by Baker [24].

A paper by Binarh in 1989 [45] examines the properties of the intra-gamma-band transitions in deformed even-even nuclei. They deduce mixing ratios for these transitions based on intensity measurements (from contemporary works) and compare these with basic IBA-1 models. They conclude that the mixing ratios for cascade transitions in the gamma band are systematically close to 2 using several different theories.

4.7. Summary of previous work

Previous investigations of the properties of ^{166}Er have been extensive and productive. We summarize this work as follows:

- The "spectroscopy" (meaning energies and intensities of gamma rays, and energies, spins and parities of excited levels) of the ^{166m}Ho decay to ^{166}Er are very well understood. ^{166m}Ho is used as a calibration standard in many gamma-ray experiments.
- The spectroscopy of the ^{166}Tm decay to ^{166}Er is less well-understood, with uncertainty about the placement of several gamma rays as well as doubt about the spins of the excited states fed in this decay.
- In both decays, the gamma-vibrational band is well-defined and has been solidly established by experiment. In the ^{166m}Ho decay states up to spin 8 in the gamma band are fed, while the ^{166}Tm decay feeds gamma band states up to spin 5.
- Band-mixing analysis, following the model proposed by Bohr & Mottelson [10] and using the Mikhailov plot, has been very successful in describing the E2 transition probabilities of the gamma-to-ground transitions.
- Methods for deducing $\delta(\mathrm{E2/M1})$ mixing ratios have been examined and chi-squared minimization has been proposed as the preferred procedure.
- Mixing ratios have been measured for many gamma-to-ground transitions on several occasions, though the agreement between different experiments is not always good. In particular, early experiments left much doubt about the signs of the mixing ratios. Such measurements are much rarer for the ^{166}Tm decay.
- Several models have been proposed to explain the observed gamma-to-ground mixing ratios, with varying degrees of success.

- Analyses of the mixing ratios of intra-gamma-band transitions using model-dependent calculations have been presented on several occasions, but only one of these values has been measured directly.
- There have been some conflicting results regarding whether the ground and gamma bands have the same intrinsic electric quadrupole moment. Current consensus indicates that if the two values are different it is by less than ~5%.
- There have also been conflicting reports about whether the gyromagnetic ratios of states in the rotational bands are constant or changing with increasing spin. The most comprehensive of these studies concludes that they are constant as the spin increases.

5. Experimental Method

5.1. Radioactive sources

5.1.1. Holmium decay source

The ^{166m}Ho source ($t_{½} = 1200$ y) was purchased in June 1999 from Isotope Product Laboratories. 10 microcuries were purchased in the form of $HoCl_3$ in 0.1M HCl with a concentration of 2μCi/mL, i.e. there was a total of 5 mL. The activity was created by neutron bombardment of chemically separated stable Ho and contained no other radioactive contaminants. Approximately 1 μCi of this source was removed and kept at Oregon State University, while the remaining 9 μCi sample was transported to the LBNL facility.

This source was counted in the 8π for a total of 107 hours during the period October 15th to 24th, 1999. In this time approximately 3.5×10^8 multiplicity-one and 1.7×10^8 coincidence events were collected.

5.1.2. Thulium decay source

The ^{166}Tm source was prepared by the reaction ^{166}Er(α,4n)^{166}Yb. The ^{166}Yb then decays to ^{166}Tm with a half life of 56.7 hours, emitting a single gamma ray of energy 82.3 keV in the process. By producing ^{166}Yb rather than the ^{166}Tm, we have the advantage of working with a source with a much longer half life. The ^{166}Er-oxide powder, which was enriched to 96.3%, was purchased from Oak Ridge National Laboratory. The powder was

contained within folded aluminum foils which were then bombarded by 50 MeV alpha particles on the 88" Cyclotron at LBNL. No degrader foils were used to reduce the beam energy. The samples were allowed to cool for at least 24 hours allowing any activated aluminum to decay away. The powder was then dissolved into a solution of water and HCl, creating a source with an activity of approximately 20 μCi. Other similar samples were created with the purpose of combining samples on a regular basis to bolster the source activity. After approximately one half life of counting a given sample, a 2nd sample would be added, creating a sample of approximately the same strength as the original.

The ^{166}Tm activity was counted in the 8π for a total of 265 hours during the period October 30th to November 10th, 1999. In this time approximately 5.5×10^{8} multiplicity-one and 5.5×10^{8} coincidence events were collected.

5.1.3. Thulium source contaminants

Due to the reaction used to create ^{166}Yb, some amounts of ^{167}Yb and ^{165}Yb were also created by (α,3n) and (α,5n) reactions. See Figure 5-1 for a schematic of the contaminant decays. These two parents β decay to Tm daughters with corresponding masses, ^{167}Tm and ^{165}Tm, with half lives of 17.5 minutes and 9.9 minutes respectively. The gamma rays associated with these decays were not observed, which make sense due to the many hours between the source coming out of the beam and being placed into the 8π apparatus for counting.

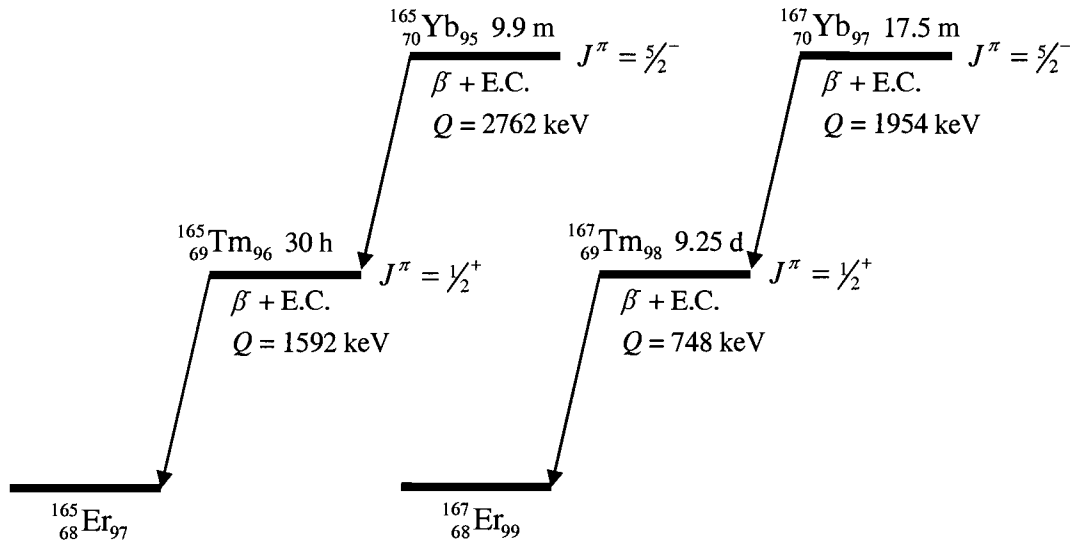

Figure 5-1: Beta decays of the contaminants in the ^{166}Tm source.

The ^{167}Tm and ^{165}Tm daughters also β decay to Er daughters of the same mass. The decay of ^{167}Tm to ^{167}Er has a half-life of 9.25 days, and produces only 11 gamma rays, out of which only one could possibly interfere with the measurement of the ^{166}Tm decay. This one gamma has an energy of 531.54 keV and occurs only 1.6 times per 100 decays. This contaminant was determined to have an activity approximately 0.37 times that of the activity of ^{166}Tm, indicating that the bombarding energy in the reaction used to create the sample was a bit lower than it should have been. The effects of these contaminants were mostly avoided using coincidence gating methods, though they were carefully considered when dealing with singles spectra (such as during the calculation of detector efficiencies).

The decay of ^{165}Tm ($t_{1/2} = 30$ h) is associated with many gamma rays across a wide range of energies. However, this contaminant was determined to have an activity of

no more than 0.007 times that of ^{166}Tm. This small contribution was carefully checked for overlaps with important peaks in the ^{166}Tm decay, but was mostly avoided through the use of coincidence measurements, which make up the bulk of this work.

5.2. The 8π spectrometer

The 8π spectrometer was constructed in 1984 at the Chalk River Nuclear Laboratories in Chalk River, Ontario. It was originally designed for the study of nuclear structure and reaction dynamics through gamma-ray spectroscopy [46] and was used primarily for "in-beam" work while at Chalk River. The 8π was moved to the 88" cyclotron at LBNL in 1996 which is where the present work was done.

5.2.1. Physical apparatus

The core of the 8π spectrometer consists of twenty high-purity germanium detectors arranged in a spherical array facing inward. The face of each detector was 22 cm from the center of the sphere, where the radioactive source was placed for counting. The twenty detectors, numbered 0-19, were arranged on four rings, with five detectors on each ring. The rings are centered on a horizontal axis (which is the beam line when this instrument is used online). Imagining the beam line as a z axis, the four rings have polar angles of approximately 37°, 79°, 101°, and 143°, relative to the center of the array. A schematic representation is shown in Figure 5-2.

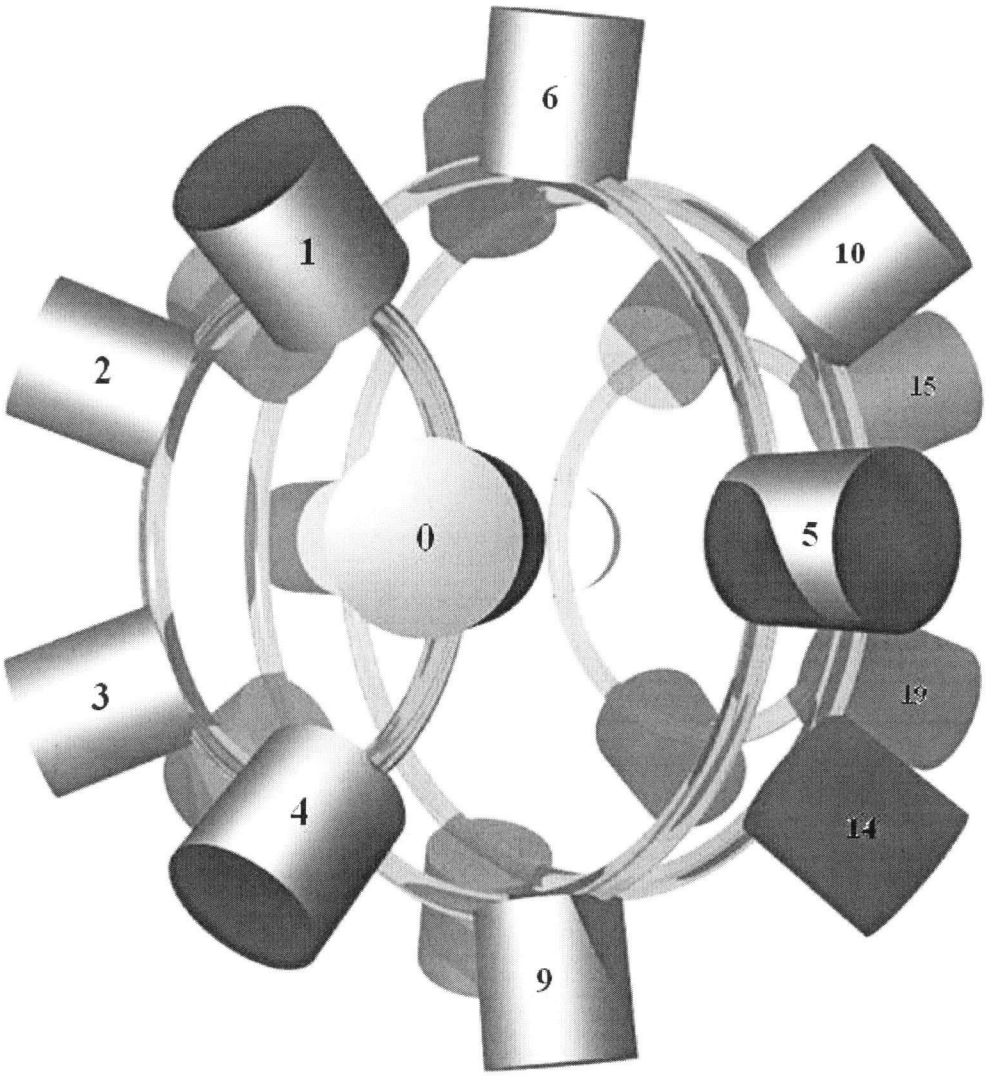

Figure 5-2: Schematic showing the geometry of the 8π spectrometer. Four rings of five detectors each are shown. The horizontal axis about which the four rings are centered would be the beam line in an online experiment. Selected detector numbers are shown. The diagram shows the sizes of the germanium crystals relative to a source to detector distance of only 14 cm, rather than the 22 cm actually used in these experiments.

5.2.2. Germanium detectors

The germanium semiconducting crystal in the detectors absorbs a gamma ray through three competing processes: the photoelectric effect, Compton scattering and electron-positron pair production. In all three cases the end result is that many electrons absorb enough energy to move out of the valence band of the Ge semiconductor crystal and move up into the conduction band. These electrons are then collected by the high voltage applied to the crystal. If the gamma ray is entirely absorbed inside the crystal the amplitude of the resulting electrical signal is proportional to the energy of the gamma ray. However, it is possible for a gamma ray to Compton scatter inside the crystal and then escape, leaving behind only part of its total energy. This results in a "Compton background" in the spectrum of a gamma ray detector that occurs at a lower energy than the gamma ray in question. A typical spectrum is shown in Figure 5-3. Here we can see that each gamma ray in the spectrum sits on top of the Compton background generated by gamma rays of higher energy.

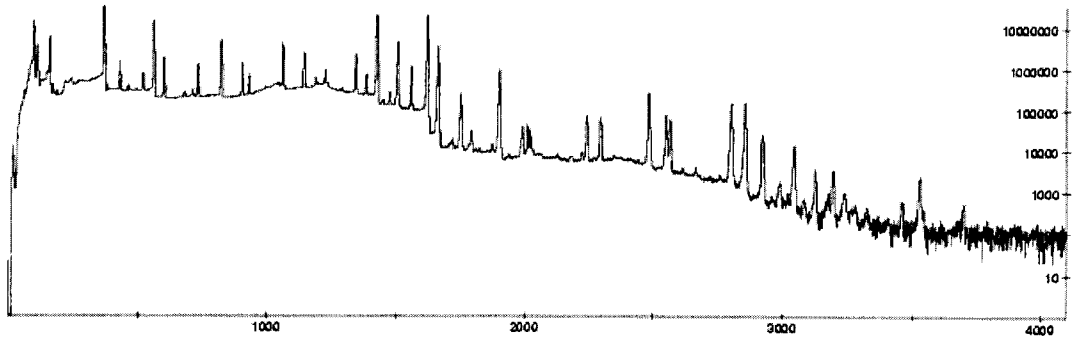

Figure 5-3: ^{166m}Ho sample spectrum showing the Compton background present underneath nearly all gamma-ray peaks. The horizontal scale is in channels (2 chn = 1 keV) and the vertical is a log scale of counts.

5.2.3. Compton suppression

Due to the experimental difficulty presented by the Compton background, the 8π spectrometer was built so that each Ge detector is enclosed on its back (furthest from the source) and sides by a Bismuth Germanium Oxide (BGO) detector. The BGO detector serves to partially suppress the Compton background in the main detector. If the BGO detector detects a gamma ray, any signal coming from the main detector at that moment is ignored. Since the BGO detector is shielded from the source itself, we can assume that when it fires it is detecting a gamma ray that has escaped the Ge detector that the BGO detector surrounds. As we can see in Figure 5-3 this process does not entirely suppress the Compton background. This is because the BGO detector does not cover the entire germanium detector and the BGO detector is not perfectly efficient. However, the presence of this "Compton suppression" significantly improved the quality of the data and increased the sensitivity of the experiment.

5.2.4. Scaled-down singles mode

Once the signal left the germanium detector it went through a series of electronics and was eventually delivered to a computer that recorded the data on tape. Several noteworthy processes happened to the data on its way to being recorded. First, a time window of approximately 100 ns is applied to the detector as a whole. This window discriminates between multiplicity-one events, in which only one gamma ray is detected in the entire array within the time window, and higher-multiplicity events, in which two or more gamma ray signals are received within the time window. An ideal experiment

would have roughly equal quantities of multiplicity-one and multiplicity-two events. Since multiplicity-two events allow for more sensitive measurements of weak gamma rays, we generally want to collect as much multiplicity–two data as possible. However, given that the 8π array had an overall efficiency on the order of 1%, a multiplicity-two event was roughly 100 times less likely to be recorded than a multiplicity-one event. With the source strength we used, the resulting multiplicity-one events would overload the array, making it nearly impossible for the coincidence events to be counted. For this reason, the 8π array was run in "scaled-down singles" mode. First, when a signal from the entire detector was processed it was "labeled" as being either a multiplicity-one event or a multiplicity-two or greater event. Multiplicity-one events were then "scaled-down" by an adjustable factor. For example, if the scale-down factor was 24, then only every 24^{th} multiplicity-one event was actually processed by the electronics and recorded, all others being immediately rejected. This reduced the processing load of the system significantly and allowed the counting of stronger sources than the system could otherwise handle.

Events with a multiplicity greater than one were not "scaled down" in this manner. Instead they were sent through slightly different timing circuitry so that their time stamp would be noticeably different from that of a multiplicity-one event. This created an additional way to discriminate between events of different multiplicity.

5.2.5. Timing

The timing information served two purposes in this experiment. First, it allowed us to separate actual multiplicity-one events from pile-up events. A pile-up event is when

a second gamma ray enters a detector while the scattered electrons from the first are still being collected (modern detectors are able to tell when this happens if the timing between the two gamma rays is larger than a certain minimum value). When this occurred, the electronics of the system allowed the event through, marking it as a multiplicity-one event, but giving it the time delay associated with events of multiplicity two or greater. Thus, in the timing spectrum of the multiplicity-one events there is a sharp peak full of actual multiplicity-one events, and a wider background of pile-up events. By setting a narrow gate of only about 4 ns on this multiplicity-one event "peak" we were able to exclude the pile-up data from our analysis.

The second purpose of the time stamp information was to allow timing gates to be used to separate actual cascade coincidences, in which the two gamma rays come from the same nucleus, from "accidental" coincidences, in which the two gamma rays come from different nuclei that happen to emit at almost the same moment. Ideally, when viewing the time-difference spectrum of all coincidences there would be a sharp peak near zero and a low background extending to infinity. The low background would stem from the "accidental" coincidences that occur when two different nuclei happen to emit the gamma rays in question at nearly the same moment in time. Since these events are uncorrelated, they are equally likely to occur with any given time difference. The experimenter can then set a time-difference window on this spectrum, selecting the "real" coincidences in the sharp peak and excluding most of the accidental coincidences in the low background. To account for the few remaining accidental coincidences a gate of the

same size can be set on the background away from the peak and then the resulting spectrum can be subtracted from the spectrum of real coincidences.

However, the design of the electronics in the 8π was such that the entire time-difference spectrum was only 100 ns wide (coincidences outside this limit were not recorded as such). In addition, each detector in the array had a different inherent timing offset, causing the time-difference spectrum to deviate quite a bit from the ideal. A timing gate of 35 ns was set on the time-difference spectrum with the safe assumption that nearly all real coincidences would be well within this window. However, the shape of the time-difference spectrum lead us to conclude that a background timing gate could not be subtracted to account for accidental coincidences. A method for accounting for accidentals was developed later in the analysis (see Section 5.5.3).

5.3. Experimental data stream

5.3.1. Raw data format

The data from this experiment were recorded on 8 mm magnetic tape as a sequence of double integers (integers written using two bytes instead of one, allowing values up to 65535). Each signal coming from the detector electronics, which can be of any multiplicity, is recorded as an "event". In the resulting data stream, each event has the same structure. First there are three numbers representing information from the inner BGO ball, which was not used in this experiment. These numbers are ignored. Then comes a number representing the multiplicity of the event (GeMu) followed by signals

from the individual detectors involved in the event. The number of the detector is recorded (GeID), followed by the energy of the gamma ray (GeE), followed by the time stamp for that gamma ray (GeT). Finally, the end of the event is signified by the number 65535 (FFFF in hexadecimal notation) called the End Of Event flag. Thus, a multiplicity-2 event would have 11 numbers: 3 BGO numbers, GeMu, GeID, GeE, GeT, GeID, GeE, GeT, EOE.

The data stream for this experiment contained a small proportion of "bad" events. These are events in which some part of the event format is incorrect. This includes events with a multiplicity of zero, events without an EOE flag, or events in which any of the values were not possible, such as a GeID of 30, or an energy above 8095. As part of the first step of analysis these bad events were catalogued and removed from the data.

5.3.2. Dropped bits

When viewing a gamma ray spectrum from the data it was noted that sometimes there was a distinct pattern of odd-even staggering in the data. Figure 5-4 shows an example of this pattern. Combining this with the observation that on many occasions the EOE flag was written as 65534 instead of 65535, we concluded that sometimes the last bit of a particular number was being dropped from the data. In binary the last bit determines whether the number is odd (last bit = 1) or even (last bit = 0). Thus, if the last bit were occasionally dropped, the counts from the odd channels in a spectrum would be

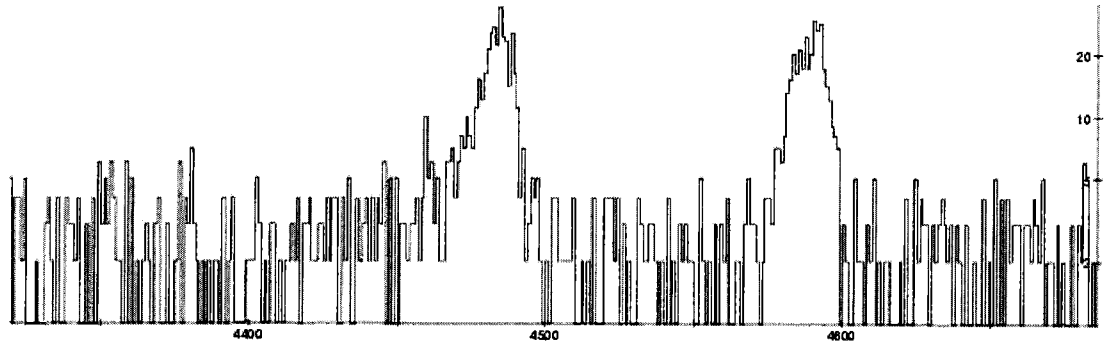

Figure 5-4: Section of a spectrum showing the odd-even staggering present in the original spectrum. This effect was eliminated by compressing the spectrum so that the original odd-even pairs would be combined into a single channel.

deposited on the even channel immediately below, resulting in the observed pattern. This evidence suggested the disturbing possibility that bits were being dropped from other numbers in the data stream, with potentially disastrous affects on the validity of the data.

In analyzing this possibility we considered each number in the data stream and the consequences to the data if it the last bit were dropped for that number.

Dropping the last bit would have very limited consequences in the time stamp (GeT) of each gamma ray because the timing gates used are all much wider than 1 channel. Thus, dropping the last bit of the time stamp was not a major concern.

If the multiplicity number (GeMu) were affected by dropped bits, we would expect to see many events listed as multiplicity-two, but with the structure of a multiplicity-three event. There is very little evidence of this, and this would not compromise the data since it would be an obviously wrong multiplicity.

Most disturbing was the possibility that the last bit of the detector number (GeID) was being dropped. If this had occurred, incorrect identification of the detector would lead to the incorrect angle being used to calculate angular correlations. However, several observable situations should arise if bits were being dropped in the GeID number. First, a similar odd-even staggering in the detector-hit patterns should be apparent, i.e. if we look at how often a gamma ray was detected in each detector, dropped bits from the GeID would cause the even detectors to seem to be triggered more often than the odd detectors. Some detectors were indeed triggered more often than others, but the pattern was consistent with efficiency measurements and did not exhibit any odd-even staggering. Second, we would expect to see many "self-coincidences" in which a multiplicity-two event has the same detector listed for both of its gamma rays. This would happen if detector 16 was in coincidence with detector 17, but detector 17 was recorded as 16 due to a dropped bit. Real self-coincidences are not possible given the electronics configuration, so they would be strong evidence of dropped bits in the GeID number. There are instances of self-coincidences in the data, though they are very rare, comprising less than 1 per every 100,000 events recorded. However, they occur just as often with odd detectors as with even detectors, which would not be true if they were caused by dropped bits. Given the lack of an odd-even staggering in the detector hit pattern, and the extreme rarity of even detector self-coincidences, we feel secure in concluding that bits were not dropped from the detector number.

Therefore the only remaining consequence of dropped bits is the odd-even staggering in the energy spectrum. To correct for this the spectrum was compressed from

an 8191-channel spectrum to a 4095-channel spectrum. In the process each even channel and the odd channel immediately above it were combined into a single channel. This eliminates the odd-even staggering at the cost of some resolution. Since most peaks are many channels wide this had only small effects in general, but did make it more difficult to separate peaks that lie very close together.

5.4. Data sorting

The data sorting process for this experiment consisted of using several computer programs to refine, filter and sort the raw data stream. Programs to accomplish these tasks were written for that purpose and tested on multiple data sets under consideration. All programming was done in the C++ computer language.

5.4.1. Filtering the raw data stream

The first step in the process of analyzing the data was to remove the bad events, compress the energy scale as described, and sort the resulting events by multiplicity. Although there is interesting physics to be found in the study of high multiplicity events, in this experiment we were not interested in events with multiplicities greater than two. For this reason, an event with a multiplicity greater than two was broken down into several multiplicity-two events. For example, a multiplicity-three event can be treated as three unique multiplicity-two events.

The next step was to make sure that the data from each run were gain matched so that the energies of the strong peaks matched the previous measurements summarized in

the Nuclear Data Sheets [12]. In the case of the ^{166m}Ho decay it was decided that the energy calibration was good enough without a gain matching process. However, the ^{166}Tm decay spans a much larger energy range and it was decided that this data needed to be gain matched. For reference the 38 peaks used for the ^{166}Tm gain matching are presented in Table 5-1. Note that the three lowest energy peaks are actually a weighted average energy of groups of x-rays and that the 82.3-keV peak is the one gamma ray emitted by the ^{166}Yb parent.

Table 5-1: Peaks used for gain matching of ^{166}Tm data set. Energies presented are those found in the Nuclear Data Sheets [12]. ^{x} indicates an energy that comes from a weighted average of x-ray energies. ^{a} indicates a peak that comes from the ^{166}Yb parent.

Peak #	Energy	Peak #	Energy	Peak #	Energy
1^{x}	49.761	14	496.935	27	1176.7
2^{x}	55.613	15	594.409	28	1203.87
3^{x}	57.762	16	598.764	29	1235.43
4	80.574	17	672.242	30	1273.54
5^{a}	82.29	18	674.788	31	1300.73
6	130.9	19	691.25	32	1347.04
7	147.301	20	705.333	33	1374.19
8	184.405	21	757.798	34	1867.94
9	215.185	22	778.814	35	1895.12
10	280.461	23	785.904	36	2052.36
11	345.569	24	810.29	37	2079.53
12	404.004	25	875.65	38	2092.13
13	459.6	26	1152.35		

The gain matching was accomplished using a fourth-degree polynomial fit on a plot of energies in the "raw" data and the energies quoted in the Nuclear Data Sheets

[12]. The energy of every gamma ray was then shifted according to this fit function so that any non-linear properties of the electronics were corrected for. This allowed the data from all runs to be combined and treated as a whole.

5.4.2. Building the 'true-singles' spectrum

The next step is to correct the data for the detector efficiencies. Ideally the absolute detector efficiencies would be calculated using a calibrated source with known activity. Unfortunately, these data were not collected. Therefore the source itself was used to do the efficiency calibration. However, in order to calculate the efficiency of a detector we must carefully account for all the gamma rays observed by that detector at as wide a range of energies as possible. At this point it is important to note the difference between what we have called "multiplicity-one" events and what experimentalists in this field would call "singles" events. Singles events are those that would be observed by a single detector that is unconcerned with whether the gamma rays it observes are in coincidence or not. A multiplicity-one event, on the other hand, is essentially an anti-coincidence event, i.e. one for which no other gamma ray was observed within the coincidence timing window. Multiplicity-one events are therefore not the same as singles events. In particular, multiplicity-one events under-represent those gamma rays that occur often in coincidence.

In addition it was discovered that the electronics of the 8π were such that when a multiplicity-two or higher event was detected, the scaled-down counter would trigger

only once. Thus if the scale-down factor was set to 24, it was not actually letting through every 24^{th} gamma ray, but some number even less than that.

Both of these factors were eventually accounted for by re-creating a gamma-ray spectrum that represents the overall emissions of the sample in the way that a singles spectrum does. This spectrum, known as the "true-singles" spectrum was constructed as follows. An effective scale-down factor was calculated to offset the miscounting that occurred as the data was recorded. The multiplicity-one event spectrum was scaled up by this factor, at which point all other events (multiplicities two and higher) were added back into the spectrum. This combined spectrum was then scaled back down to reflect the correct Gaussian statistics of the actual data.

A true-singles spectrum was constructed in this way for each of the 20 detectors in the array and it was these spectra that were used in the detector efficiency calculations.

5.4.3. Detector efficiency

Due to the competing ways in which a germanium detector absorbs a gamma ray, the efficiency with which a detector will capture a gamma ray is energy dependent. Moreover, each detector used will have a different energy dependent response, depending primarily on the effective volume of the Ge crystal, but also upon other factors such as neutron damage from use in in-beam experiments. To represent this effect we define an energy dependent factor, ε_γ known as the efficiency

$$I_\gamma = \frac{Area_\gamma}{\varepsilon_\gamma} \tag{5-1}$$

where I_γ is the relative intensity of a gamma ray (usually normalized to the strongest peak in the spectrum) and $Area_\gamma$ is the experimentally measured area of the peak corresponding to that gamma ray.

It is impossible to measure the efficiency at all energies. However, the physical theory behind the processes by which a gamma ray is absorbed leads us to conclude that efficiency will be a smoothly varying function of energy. Thus, a relative-efficiency function was extrapolated from the data. The relative efficiencies were calculated for selected strong peaks from across the largest possible range of energies using literature intensities from the Nuclear Data Sheets [12]. These relative efficiency data points were then plotted against the energy of the gamma rays on a log-log scale. The resulting plot was then fitted to a 4^{th} order polynomial using a least-squares regression. A sample relative-efficiency curve is shown in Figure 5-5.

Due to the length of time between the two experiments described here efficiency curves were calculated separately for the ^{166m}Ho and ^{166}Tm experiments. Note that due to the importance of the 80.5-keV transition present in both decays it was particularly important to pin down the relative efficiency curve at low energy. This was difficult due to the rapidly changing response curve in that energy range. In the ^{166}Tm decay the erbium x-rays were used as an additional low-energy data point on the efficiency curves.

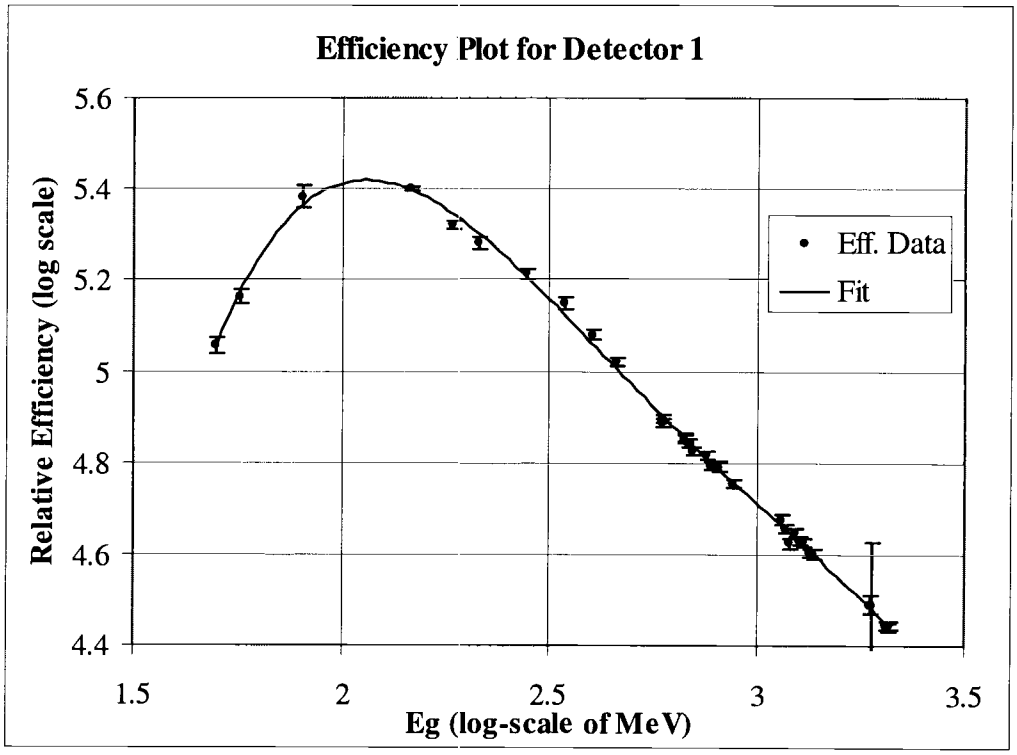

Figure 5-5: Typical relative efficiency plot and fit. The log-log efficiency data are fit to a 4th-order polynomial. These data come from detector 1 in the ^{166}Tm decay. Note that the vertical scale is arbitrary

5.4.4. Creating angle matrices

The primary focus of this investigation was to measure the E2/M1 mixing ratios of various gamma-ray transitions in the ^{166}Er nucleus. A previously described, this is accomplished by measuring the angular correlation of the gamma rays emitted in coincidence. For this reason it was important to know the angle between detectors for each coincidence event recorded.

Due to the symmetry of the 8π instrument, it turns out that there are only five unique opening angles between all 190 pairs of detectors: 41.8°, 70.5°, 109.5° 138.2°, and 180°. The angles formed by each detector pair can be found by consulting Table 5-2.

Table 5-2: Opening angles for each detector pair. The key is as follows: ■ → 41.8°, ● → 70.5°, ○ → 109.5°, □ → 138.2°, ◊ → 180° and ▬ → 0° which is a detector with itself (and is not used in the analysis). Note that the redundant upper right of the table has been left blank. The five unique angles (not including 0°) appear in the proportions 3:6:6:3:1 respectively.

	0	1	2	3	4	5	6	7	8	9	10	11	12	13	14	15	16	17	18	19
0	▬																			
1	■	▬																		
2	●	■	▬																	
3	■	●	●	▬																
4	●	●	■	■	▬															
5	○	●	■	○	●	▬														
6	●	■	●	○	○	●	▬													
7	■	●	○	●	○	□	●	▬												
8	●	○	○	■	●	□	□	●	▬											
9	○	○	●	●	■	●	□	□	●	▬										
10	○	●	●	□	○	■	■	○	◊	○	▬									
11	●	●	○	○	□	○	■	■	○	◊	●	▬								
12	●	○	□	●	○	◊	○	■	■	○	□	●	▬							
13	○	□	○	●	●	○	◊	○	■	■	□	□	●	▬						
14	□	○	●	○	●	■	○	◊	○	■	●	□	□	●	▬					
15	□	○	○	◊	□	●	●	○	□	○	■	●	○	○	●	▬				
16	○	○	□	□	◊	○	●	●	○	□	●	■	●	○	○	■	▬			
17	○	□	◊	○	□	□	○	●	●	○	○	●	■	●	○	●	■	▬		
18	□	◊	□	○	○	○	□	○	●	●	○	○	●	■	●	●	●	■	▬	
19	◊	□	○	□	○	●	○	□	○	●	●	○	○	●	■	■	●	●	■	▬

There are more detector pairs that create some of these angles than others. Specifically out of the 190 unique detector pairs that can be created from combinations of all 20 detectors, 60 detector pairs form the 70.5° angle, 60 form the supplementary angle 109.5°, 30 form the angle 41.8°, 30 others form the supplementary angle 138.2°, and only 10 form the 180° angle. For this reason the statistics of the 180° angle are often the limiting factor in measuring angular correlations.

The task of combining the mass of data collected into a coherent angular correlation measurement was accomplished by creating an "angle matrix" for each of these five angles. To do so, each coincidence event in the data stream was first corrected for the efficiency of the detectors and energies involved and then added into the energy-energy matrix of the angle that that pair of detectors forms. For example, if a coincidence event consists of a 100-keV gamma ray in detector 3 and a 500-keV gamma ray in detector 9 we would first look up the angle formed by this pair, which is 70.5°, we would then add $\frac{1}{\varepsilon(\det 3,\ 100\ \mathrm{keV})\cdot\varepsilon(\det 9,\ 500\ \mathrm{keV})}$ to the [100,500] location in the 70.5° matrix. We would also add the same quantity to the [500,100] location in the 70.5° matrix, creating a symmetric matrix and removing any concern about which energy happens to be listed first in the data stream. The resulting matrix has a certain value in each energy-energy location that represents an efficiency-corrected count of how many times that energy-energy pair occurred. Thus, data from all detector pairs can be effectively combined into these five angle matrices.

In this process both an efficiency-corrected angle matrix and a "raw", uncorrected angle matrix were created. The raw matrix was used to approximate the errors introduced by efficiency correction, as described in Section 5.5.4.

5.5. Angular correlation measurements

5.5.1. Pulling a gate

Measuring a particular angular correlation involves a two-step process. First, a "slice" must be taken of each of the five angle matrices discussed in the previous section. This entails setting a window on the energy-energy angle matrix and creating a gamma-ray spectrum from the counts within the window. As an illustrative example let us consider measuring the angular correlation of the 810-keV gamma ray (which connects the 5^+ state of the gamma band to the 4^+ state of the ground band) in coincidence with the 184-keV gamma ray (which connects the 4^+ and 2^+ states of the ground band). We would first set an energy window on each matrix corresponding to the 184-keV gamma ray. For example, we might take every location in the matrix whose first energy is listed between 183 and 185 keV and combine them to create a counts vs. energy spectrum. This spectrum now represents a summary of all gamma rays that were in coincidence with a gamma ray that had an energy between 183 and185 keV at that particular angle. This process is known as "creating a slice".

Due to the Compton background that is constantly present in this type of experiment, there is a small number of background coincidences that has been counted in

this slice. To account for these background coincidences we also create a similar slice from a nearby energy range that we are confident contains no peaks at all. This slice should now represent the background coincidences that are also present in our peak slice. Accounting for any difference in size between our peak window and our background window we then subtract the background window from the peak window leaving only real coincidences and the accidental coincidences that are due to a gamma ray with the correct energy but that didn't come from the same nucleus. The five spectra created in this fashion are collectively referred to as the "184 gate" as they represent gamma rays in coincidence with the 184-keV gamma ray from all the data collected.

5.5.2. Fitting peaks in a gate

In each of these spectra we can now measure the area of the other gamma ray we are concerned with, the 810-keV peak. This was done using a powerful analysis tool called GF3 which is specifically designed for analyzing gamma ray spectra generated by Ge detectors. GF3 is part of the Radware software suite created by David C. Radford [47]. The fitting routine uses a chi-squared minimization method that includes a skewed Gaussian peak shape, a quadratic background function and a step-function background that accounts for Compton scattering. This program is quite adept at fitting multiple close-lying peaks, though there are limits to this resolution of doublets and multiplets. An example fit of a section of the 42° spectrum from the 184-keV gate produced by the ^{166}Tm decay is shown in Figure 5-6.

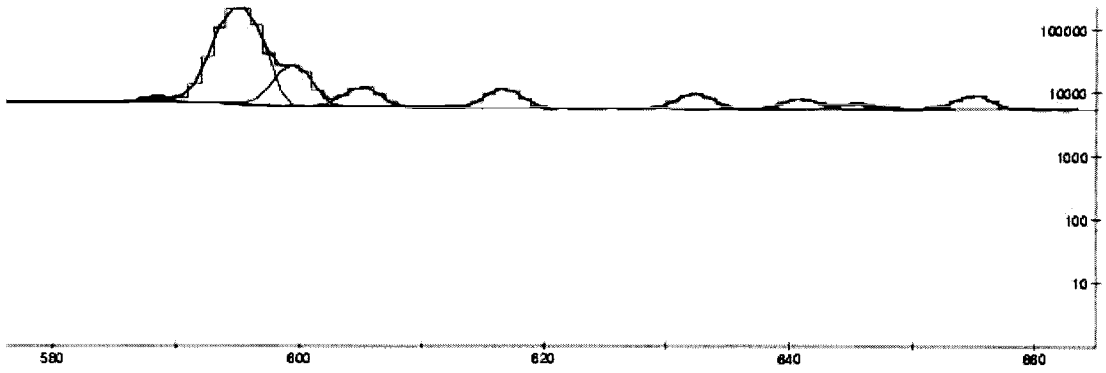

Figure 5-6: Example GF3 gamma-ray spectrum fit showing the resolution of multiplets in the 42° spectrum of the 184-keV gate produced by the decay of ^{166}Tm. The raw spectrum is shown by the step-like channels and the fitted function is shown as a smooth line, with the component peaks and fitted background functions displayed below it.

One issue to consider in measuring the angular correlation is the possibility of "Compton backscatter". In certain circumstances a gamma ray may encounter one detector, scatter backwards to some degree and be detected in another detector. This would happen fast enough that the two partial gamma rays would be interpreted as a coincidence by the detector electronics. Due to the strong energy dependence of the Compton scattering formula [2] this can occur only for a small range of energies. In fact, when this occurs for gamma rays between 200 and 3,000 keV, one of the partial gamma rays will always be between 100 and 240 keV. Thus we can see that this will be a concern for only a few gamma rays. Unfortunately, right in the middle of this range is one of the strongest gamma rays in either decay. The 184 keV 4^+ to 2^+ ground-band transition is used as a gate for many measurements, and so it is important to consider the effects this backscattering could have. A careful analysis of all the strong gamma rays in

each decay shows that the only potential problem comes from the 779-keV gamma ray. This gamma could backscatter in such a way that it would leave 192 keV in a particular detector and then deposit the remaining 586 keV in the detector opposite the first. This could, in principle cause trouble with the 180° measurement of the 594-184 angular correlation. However, given that the typical resolution of the detectors is well under 3 keV, we believe this effect did not contribute to the data in any meaningful way. Previous measurements of angular correlations that use the 184-keV gate [26] with a NaI detector may have suffered from of this potential problem.

Once we have measured the area of the 810-keV peak in the spectra of all five angles we are ready to plot our experimental angular correlation data.

5.5.3. Correcting for accidental coincidences

Before using the data to calculate the angular correlation coefficients we must first account for the still present accidental coincidences. This is accomplished by using self-coincidences of the gate to determine the overall accidental coincidence rate and then correcting the peak in question based on its relative intensity to that of the gate.

First, we measure the self-coincidences present in the gate. In our example this would mean measuring the area of the 184-keV peak in the 184 gate. Since we know that there can be no legitimate coincidences between the 184-keV gamma ray and itself, we can conclude that this entire area must come from accidental coincidences. We can then calculate the amount of accidental coincidences in another peak in the same spectrum, such as the 810-keV peak, by

$$\text{Acc}(810) = \text{Self-coinc}(184) \cdot \frac{I_{\text{rel.}}(810)}{I_{\text{rel.}}(184)} \tag{5-2}$$

where $I_{\text{rel.}}$ is the relative intensity taken from the Nuclear Data Sheets. This number of counts is then subtracted from the area of the 810 peak to remove the contribution of accidental coincidences.

By repeating this process for each of the five angles we can arrive at a set of angular correlation measurements that are ready to be analyzed further.

5.5.4. Calculating angular coefficient coefficients

As mentioned before it is the extreme symmetry of the 8π apparatus that creates only five unique angles among all 190 detector pair combinations. This is somewhat contrary to the purpose of extracting angular correlations in that one would normally like to measure the angular correlation at as many angles as possible. Further hindering this process is the fact that the angular correlation function, Equation (2-14), is symmetric about 90°, i.e. the angular correlation function treats the angles 41.8° and 138.2° as the same angle. In some sense this further reduces the sensitivity of our measurement of angular correlations.

The angular correlation function $W(\theta)$ is plotted with counts on the vertical axis and angle on the horizontal axis. The five data points can then be fitted to the theoretical angular correlation function given in Equation (2-22) (reproduced here for ease of reference).

$$W(\theta) = N(1 + A_{22}Q_2G_2P_2(\cos\theta) + A_{44}Q_4G_4P_4(\cos\theta)) \tag{2-22}$$

The variables N and the two $A_{kk}Q_kG_k$ coefficients were calculated by a minimizing the chi-squared function given by

$$\chi^2 = \sum_{\theta} \frac{\left(W(\theta)_{\text{exp}} - W(\theta)_{\text{theory}}\right)^2}{\left(\delta W(\theta)_{\text{exp}}\right)^2} \tag{5-3}$$

where there is one term in the sum for each of the five unique angles used in this experiment. $W(\theta)_{\text{exp}}$ is the experimental area measured for the coincidence in question at the angle θ, $\delta W(\theta)_{\text{exp}}$ is the experimental uncertainty in this quantity and $W(\theta)_{\text{theory}}$ is the theoretical value of the angular correlation function for a given value of N and the two $A_{kk}Q_kG_k$ coefficients. Minimizing this function for all three unknown quantities gives their best fit value. The standard rules of error propagation are used to find the uncertainties in these best fit values.

The effects of finite detector size (Q_{kk}), and oriented level lifetime (G_k) are then divided out, producing the A_{kk} coefficients (recall that Q_{00} and G_0 are unity). An example plot of the 810-184 angular correlation function is shown in Figure 5-7.

The uncertainties for the angular correlation functions were calculated using a combination of the fitting uncertainty generated by GF3 (which include statistical uncertainties as well as uncertainties caused by the fitting routine) and uncertainty due to the efficiency correction applied to the data. The efficiency uncertainty was calculated in an unusual manner due to the profound averaging effects of combining the 190 detector pairs into five angle matrices. The process described so far was done for both the

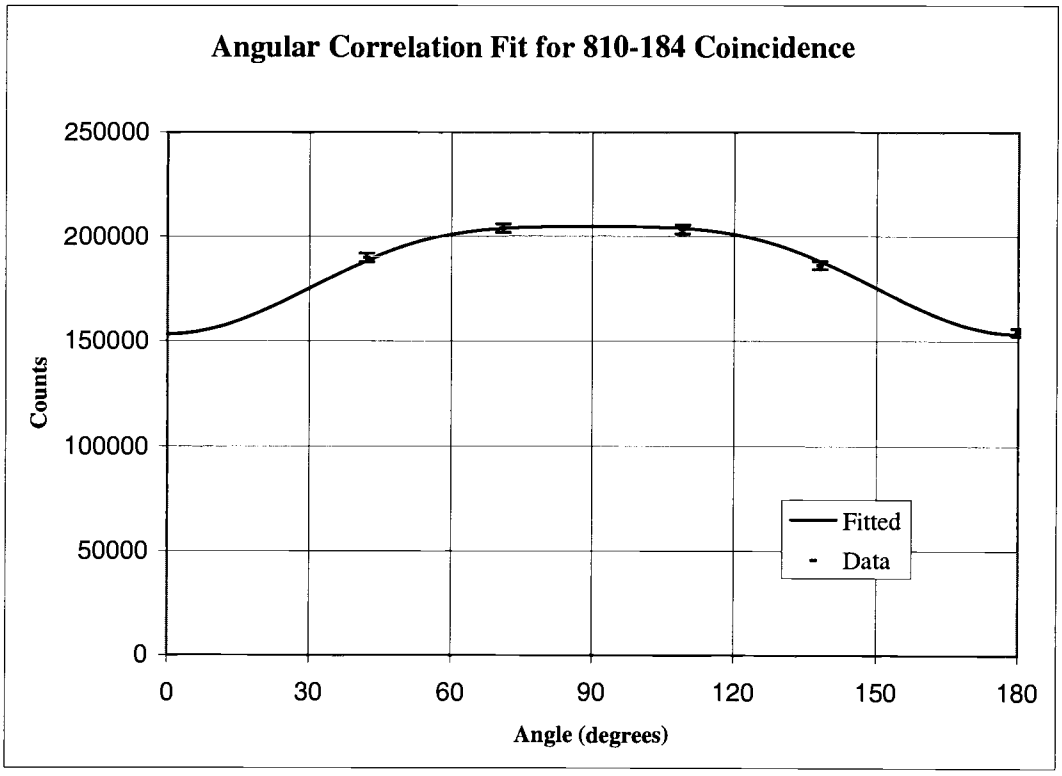

Figure 5-7: Example angular correlation fit. The angular correlation data for the 810-184-keV cascade are plotted with error bars and fitted to the theoretical form of $W(\theta)$ given in Equation (2-22).

efficiency-corrected and raw angle matrices (described in Section 5.4.4). The final fitted area for the raw coincidences was divided by the efficiency-corrected coincidence area to produce an effective efficiency correction parameter.

$$\varepsilon_{\text{eff}} = \frac{Area_{\text{raw}}}{Area_{\text{corrected}}} \tag{5-4}$$

The effective efficiencies were then compared across the five angles. In this way we could estimate how much the efficiency correction varied in the experiment. The standard deviation of these five effective efficiency values was then takes as the uncertainty in the

efficiency and combined (as a relative error) with the uncertainty produced by the GF3 fits.

The Q_{kk} coefficients (see Section 2.6) were calculated for gamma rays from 100 to 2000 keV. As noted previously these correction factors are generally on the order of 2-5%, and are relatively insensitive to the gamma-ray energy. Q_{kk} is calculated by the product of two Q_k values (one for each gamma ray), which are presented in Table 5-3.

Table 5-3: Calculated Q_k coefficients for the 8π detector array. Coefficients are calculated every 100 keV between 100 and 2,000 keV.

E_γ (keV)	Q_2	Q_4
100	0.991	0.971
200	0.992	0.973
300	0.992	0.973
400	0.992	0.974
500	0.992	0.974
600	0.992	0.975
700	0.992	0.975
800	0.993	0.975
900	0.993	0.976
1000	0.993	0.976
1100	0.993	0.976
1200	0.993	0.976
1300	0.993	0.976
1400	0.993	0.976
1500	0.993	0.976
1600	0.993	0.976
1700	0.993	0.977
1800	0.993	0.977
1900	0.993	0.977
2000	0.993	0.977

The G_k coefficients deviate from unity only when the lifetime of an intermediate oriented state is long enough to allow the environment of the nucleus to affect the

populations of the magnetic substates (see Section 2.6). In these experiments the 81 keV 2^+ ground band level is low enough in energy that its lifetime is 1.82 ns. This is on the order of 1000 times longer than the lifetime of the typical nuclear level, which is the picosecond range. Because the exact environment of the liquid source sample is impossible to determine, effective G_k factors must be measured for each experiment. To determine the G_k factors for this first 2^+ level, several measurements of well understood angular correlations were performed and compared to their theoretical values. In particular, angular correlations that consist of monotonically decreasing spin sequences with $\Delta J = 2$ for each transition give large, well understood A_{22} coefficients. Table 5-4 shows six measured values of A_{22} for the 81-keV state in ^{166m}Ho along with their weighted average. All six A_{22} values (which are unitless) have the same theoretical value of $A_{22} = 0.102$.

Table 5-4: Angular correlations used to calculate G_2 for the 81-keV level in ^{166m}Ho. The six A_{22} values shown have the same theoretical value of 0.102. Unobserved intermediate gamma rays are shown in parentheses.

Gamma-Ray Energies	Spin sequence	A_{22}	+/-
184-81	4-2-0	0.0788	0.0145
280-(184)-81	6-4-2-0	0.0782	0.0190
365-(280)-(184)-81	8-6-4-2-0	0.0757	0.0352
875-81	4-2-0	0.0933	0.0734
951-(184)-81	6-4-2-0	0.0811	0.0363
1010-(280)-(184)-81	8-6-4-2-0	0.2242	0.2209
	Weighted Avg.	0.0791	0.0104

From these data the G_2 value for the 81-keV level in the ^{166m}Ho decay was determined to be $G_2 = 0.78 \pm 0.10$. This value compares favorably with other similar studies [15,24].

A similar calculation was done for the 81-keV level in the ^{166}Tm decay, using the data shown in Table 5-5. Only three values could be used in this case due to the lack of high spins populated in this decay.

Table 5-5: Known angular correlations used to calculate G_2 for the 81-keV level in ^{166}Tm. The three A_{22} values shown have the same theoretical value of 0.102. Unobserved intermediate gamma rays are shown in parentheses.

Gamma-Ray Energies	Spin sequence	A_{22}	+/-
184-81	4-2-0	0.0754	0.0225
280-(184)-81	6-4-2-0	0.2058	0.1048
875-81	4-2-0	0.1042	0.0372
	Weighted Avg.	0.0872	0.0190

From these data the G_2 value for the 81-keV level in the ^{166}Tm decay was determined to be $G_2 = 0.85 \pm 0.19$. This value also compares favorably with other similar studies [15,24].

The G_4 value for this level in the ^{166}Tm decay was calculated using the strong gamma ray cascade 705-81 keV. The 705-keV gamma ray is emitted in the transition from the 2^+ gamma band state to the 2^+ ground band state. This angular correlation does not have a well known theoretical value, due to the mixing of E2 and M1 multipolarities in the 705-keV gamma ray. However, all measurements of this mixing ratio, including the present work (see Section 6.2.1) have given very large values. Since the B_4 coefficient

is asymptotic at large values of $\delta(705)$, we could safely assume that the value of the A_{44} would be very close to $A_{44,th} = 0.327$. The measured coefficient for this cascade was $A_{44,exp} = 0.214 \pm 0.023$, which yields a value of $G_4 = 0.66 \pm 0.07$.

Due to the lack of such an angular correlation in the ^{166m}Ho decay, the G_4 value for the 81 keV in the ^{166}Tm decay was also used in the ^{166m}Ho analysis.

With both the Q_k and G_k values corrected for, the measured A_{kk} coefficients can now be compared with previous measurements and used in further analysis.

5.6. Extracting mixing ratios

The mixing ratio δ has often been a good experimental check on the theory of nuclear structure. Rather than simply measuring the intensities of transitions as a test of theoretical models, the mixing ratio allows a glimpse of the cause of those intensities. A given transition rate may match well with theory, but if theory predicts that the intensity stems from an enhancement of E2 transitions, while the $\delta(\mathrm{E2/M1})$ mixing ratio is small, then the theory will have to be reexamined.

In many experiments the value of δ is extracted from the A_{kk} coefficients produced by angular correlation measurements. As described in Section 2.5, these coefficients are quadratic functions of δ. In addition, the A_{22} coefficient is sensitive to the sign of δ. A plot of the A_{kk} coefficients vs. δ can be a good way to understand the relationship between these quantities.

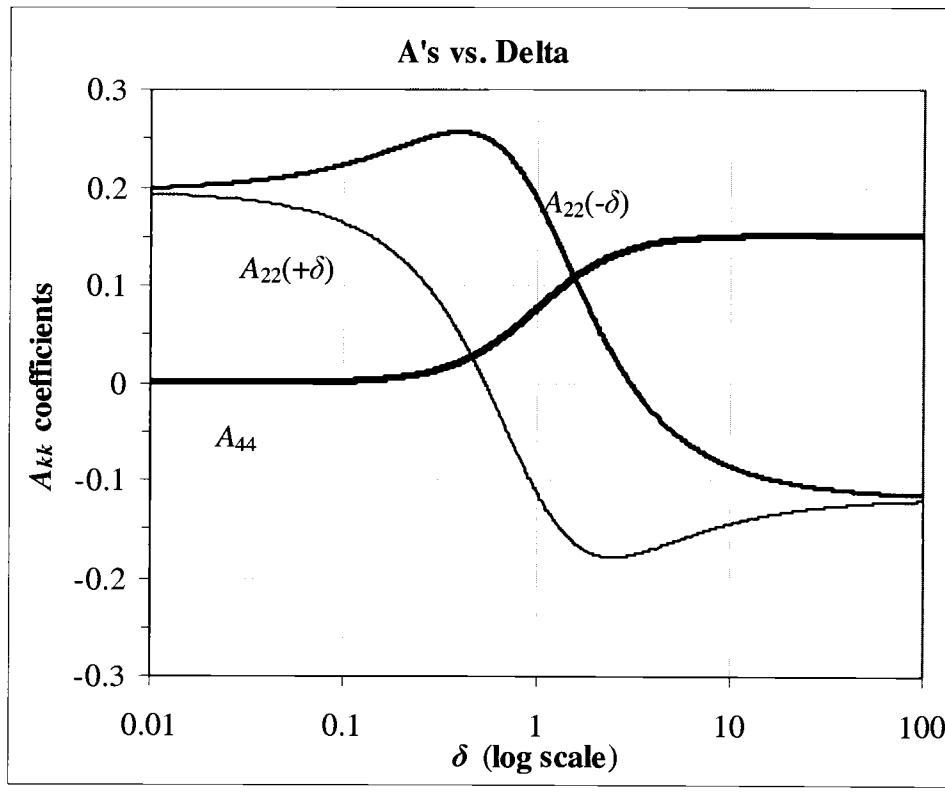

Figure 5-8: Plot of A_{kk} coefficients vs. δ for a 4-4-2 angular correlation. A_{22} is sensitive to the sign of delta and so is plotted once for positive values of delta and once for negative values. Note the common asymptotic behavior of $A_{22}(+\delta)$ and $A_{22}(-\delta)$ when δ is very small or very large.

Figure 5-8 shows such a plot for an angular correlation sequence 4-4-2 (such as the 691-184-keV gamma-to-ground-to-ground coincidence). Here we can see that a different sign of δ does indeed give a different value, but the two values come to the same asymptotic limit if δ is very large or very small. A_{44} is also very insensitive to δ for large or small values of delta and does not depend on the sign of delta.

5.6.1. Extracting $1/\delta$ instead of δ

In situations where δ is expected to be large, as in the case of gamma-band to ground-band transitions, it is our opinion that solving for $1/\delta$ gives more information and is more useful than solving for δ itself.

As seen in Figure 5-8, the angular correlation coefficients, and therefore the $W(\theta)$ function itself, converge to a single value as δ approaches positive or negative infinity. For this reason an experimental determination of δ is often unable to tell the difference between a large positive and large negative value (imagine an experimental value of $-0.11 \pm .03$ for A_{22} in Figure 5-8). It is common in these situations to come across a value of δ in the literature that extends to infinity. The reality of this measurement is often that while the data indicated a certain large value of delta, the uncertainty limits could not exclude the possibility of a large value of delta *with the opposite sign*. If the authors had instead quoted a value of $1/\delta$ they could quote their full uncertainties and make it clear to the reader that while they are confident that δ is large, they cannot conclusively state the sign of δ. For example, a measurement of $1/\delta = 0.010 \pm 0.011$ means that delta is likely positive, and if it is negative it is very large. In either case this transition is more than 99.95% E2 (the %E2 calculation, Equation (2-16), depends only on δ^2). In the past, such a measurement would probably be quoted as $\delta = 100^{+\infty}_{-53}$. However, there are a few circumstances, such as the ^{166}Er nucleus that is the focus of this work, in which the sign of delta is of some interest and so a statement of $1/\delta$ can clarify the measurement.

In addition, averaging large values of delta can be very difficult. Imagine three measurements of a certain mixing ratio: $\delta_a = 108^{+\infty}_{-56}$, $\delta_b = 100^{+\infty}_{-53}$ and $\delta_c = 93^{+\infty}_{-49}$. Attempting to average these values directly is both difficult and can potentially leave out useful information. By recasting these as $1/\delta_a = 0.0093 \pm 0.0100$, $1/\delta_b = 0.010 \pm 0.011$ and $1/\delta_c = 0.0107 \pm 0.0120$ we can easily do a weighted average of these, resulting in $1/\delta_{avg} = 0.0099 \pm 0.0063$, which *does* exclude the possibility of a negative result.

Thus, in this work when the δ value was expected to be large, it was $1/\delta$ that was actually calculated and, when possible, averaged. For the sake of convenience we will still refer to "extracting δ" even though we were actually solving for $1/\delta$ in many cases.

The mixing ratio δ was calculated in several different ways in this study. However, these different methods can be broken down into two distinct groups. In one group δ is calculated from the angular correlation coefficients, or from a combination of same. In the second group, delta is calculated directly from the angular correlation data by means of a chi-squared minimization process. In both cases, multiple angular correlation measurements may go into extracting each value of δ.

5.6.2. Extracting δ from A_{kk} with a pure transition

The δ of a gamma ray can be most easily extracted from angular correlation coefficients by using a coincidence with another gamma ray of pure multipolarity. In this method δ can be easily extracted from either A_k or a B_k depending on whether the mixed gamma ray comes first or last in the coincidence cascade. We can then use the equations

given in Section 2.5 to solve for δ. For example, in the 810-184-keV angular correlation, the A_{22} coefficient is a combination of a $B_2(810)$ and an $A_2(184)$. The $A_2(184)$ can be calculated from theory because we expect the 184-keV gamma ray, which links the 4^+ and 2^+ levels in the ground band, to be a pure-E2 transition. Any M3 component would be at least seven orders of magnitude weaker, and probably even less due to the enhancement of E2 radiation between collective states. This lets us extract an experimental value for $B_2(810)$, which is a quadratic function of the mixing ratio $\delta(810)$, given by Equation (2-18). This quadratic can be solved, yielding two values of $\delta(810)$ based on the experimental A_{22} coefficient.

A similar process using the A_{44} coefficient yields another two values, and in principle one of the δ values from A_{44} should match one of the δ values from A_{22} and the two values can be averaged. However due to the vanishing of the constant and linear terms in the B_4 numerator, this coefficient is much less sensitive to δ. For this reason it has long been standard practice to calculate the two δ values from the A_{22} coefficient and then use the A_{44} coefficient to choose between them.

In this method the uncertainties in δ are calculated using the uncertainties in the A_{kk} coefficients and standard propagation of error methods.

5.6.3. Extracting δ from a ratio of A_{kk} coefficients

A clever way of extracting a δ when you cannot use a pure gamma ray in coincidence is to use a ratio of angular correlation coefficients. For example, consider the 705 keV 2^+ gamma to 2^+ ground transition in the ^{166}Tm decay. We can get one

measurement of $\delta(705)$ using the 81 keV 2^+ to 0^+ ground-band transition as a pure coincidence, but there are no other pure multipolarity gamma rays in coincidence with this transition. However this gamma ray is in coincidence with several strong transitions from other high lying levels fed in the ^{166}Tm decay, such as the 672-keV gamma ray that comes from the 1458-keV level. In theory, we could measure the δ of the 672-keV gamma ray using the 785-keV 2^+ gamma to 0^+ ground pure transition. We could then use $\delta(672)$ in combination with the 672-705-keV angular correlation data to solve for $\delta(705)$. However, in practice this method expands the uncertainties of the final δ so much that it becomes nearly useless.

However, there is a way to use the 672-keV transition, and others like it, to solve for $\delta(705)$ without introducing additional uncertainty. Consider that the A_{22} coefficient of the 672-705 angular correlation fit consists of $B_2(672)$ times $A_2(705)$. The A_{22} coefficient of the 672-785 angular correlation fit consists of the same $B_2(672)$ times $A_2(785)$, which is directly calculable because the 785 is a pure transition (2^+ gamma to 0^+ ground). Now, if we take the ratio of these two angular correlation coefficients we have

$$\frac{A_{22}(672-705)}{A_{22}(672-785)} = \frac{B_2(672)A_2(705)}{B_2(672)A_2(785)} = \frac{A_2(705)}{A_2(785)}$$

From here we can solve for $A_2(705)$ and use this as we have previously to solve for $\delta(705)$. Thus, without introducing any error associated with the actual properties of the 672-keV transition we can use it to get another measurement of $\delta(705)$. In fact, this

method can be used with any higher lying gamma ray, regardless of whether it feeds the 2^+ gamma level directly or not. In the same way that the $B_2(672)$ cancelled out in the above expression, the deorientation coefficient U_k associated with any unobserved intermediate radiations will also cancel out. In a decay that feeds higher lying states strongly, such as both the decays in this work, this method offers many additional data points for an otherwise difficult to measure δ.

In this method the uncertainties in δ are calculated using the uncertainties in the A_{kk} coefficients and standard propagation of error methods.

5.6.4. Extracting δ from an A_{kk} ratio with a mixed transition

The above method cannot be used for gamma rays emitted from odd spin levels in the gamma band because there are no pure-multipole gamma rays emitted from the same level (e.g. the 3^+ gamma band state can decay only to the 2^+ or 4^+ ground band states by mixed E2+M1 radiations). However, the same principle can be used by considering a cascade with a mixed transition that feeds the gamma ray of interest. Consider the 779 keV 3^+ gamma to 2^+ ground gamma ray, fed by the 599-keV gamma ray that is emitted from the 1458-keV level. We can use the 599-594 angular correlation in much the same way that we used the angular correlation with a pure transition in the previous case. We know that $A_{22}(598-594) = B_2(598)A_2(594)$ where the $A_2(594)$ is a function of mixing ratio $\delta(594)$ as per Equation (2-20). We plan to divide the $A_{22}(598-779)$ coefficient by $A_{22}(598-594)$ in much the same way as in the previous section, but this time there is the

additional uncertainty of having to use the experimentally determined $\delta(594)$ in the calculation. However, $\delta(594)$ has been measured with high accuracy through other methods in this study, in good agreement with previous measurements. As with the previous method, this procedure can be extended to any gamma ray that is in appreciable coincidence with the 594 and 779-keV gamma rays, regardless of whether it feeds them directly or not.

In this method the uncertainties in $\delta(594)$ (continuing our example) must be taken into account when determining the experimental uncertainty in $\delta(779)$. Using standard propagation of error methods we put in the maximum and minimum values for $\delta(594)$ and then use the largest and smallest limits of the extracted $\delta(779)$ to determine the final limits of uncertainty.

5.6.5. Extracting δ by chi-squared minimization

The second category of ways to calculate δ involves using the angular correlation data directly. Let us again first consider an angular correlation in which the mixed gamma ray in question is in coincidence with a pure multipolarity gamma ray. First, the theoretical angular correlation function $W(\theta)$ is recast in terms of δ, including corrections such as the Q_k and G_k factors. This function is then fit to the experimental data using a chi-squared minimization method that parallels the method described in Section 5.5.4. It should be noted here that recasting $W(\theta)$ in terms of δ does not remove N as a variable. For this reason, the value of N determined in the angular correlation fit is

used for the chi-squared minimization. Once a minimum has been located, N is adjusted to find an even deeper minimum. These adjustments are always smaller than the experimental uncertainty in N and are usually on the order of 0.1%.

As $W(\theta)$ is still a quadratic function of δ we still expect there to be two minima in the chi-squared function. In good cases, such as the example shown in Figure 5-9 one minimum is clearly deeper and sharper than the other. In less straight-forward cases, such as that shown in Figure 5-10, the two minima may be nearly the same depth and other factors may influence us to choose one over the other.

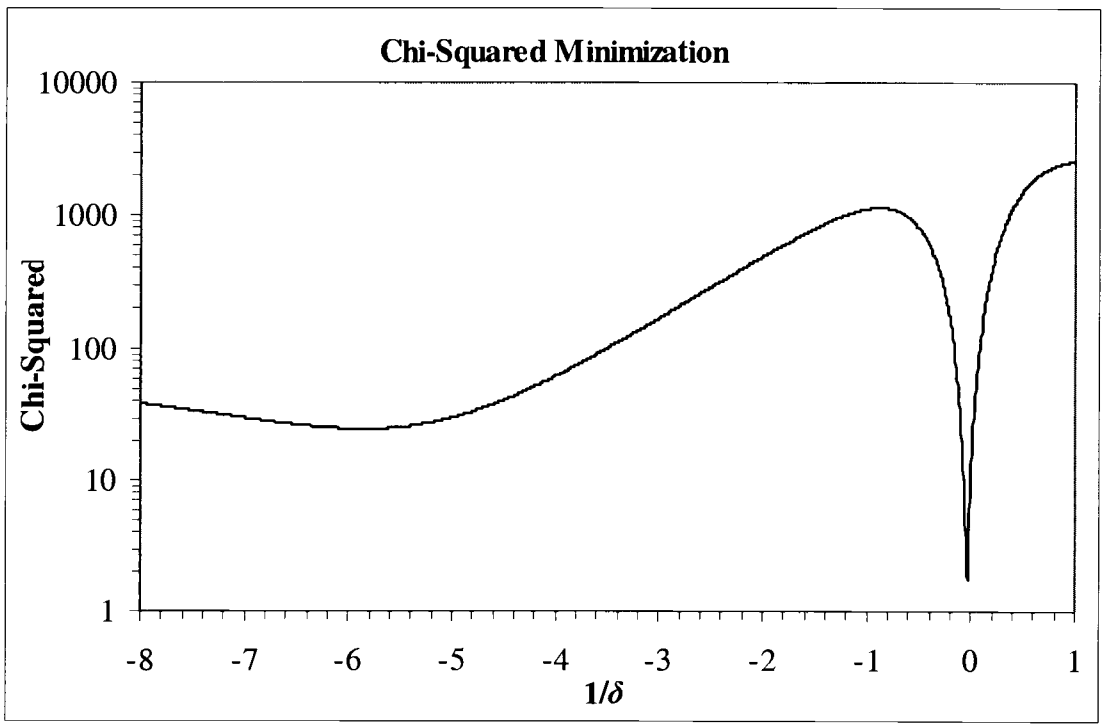

Figure 5-9: Example of a chi-squared minimization where the choice between the two possible minima is clear. This plot comes from the ^{166}Tm decay and is the plot of the chi-squared function for the 810-184-keV angular correlation. Note that the x-axis is $1/\delta$, which allows the very large value of δ to be located more effectively.

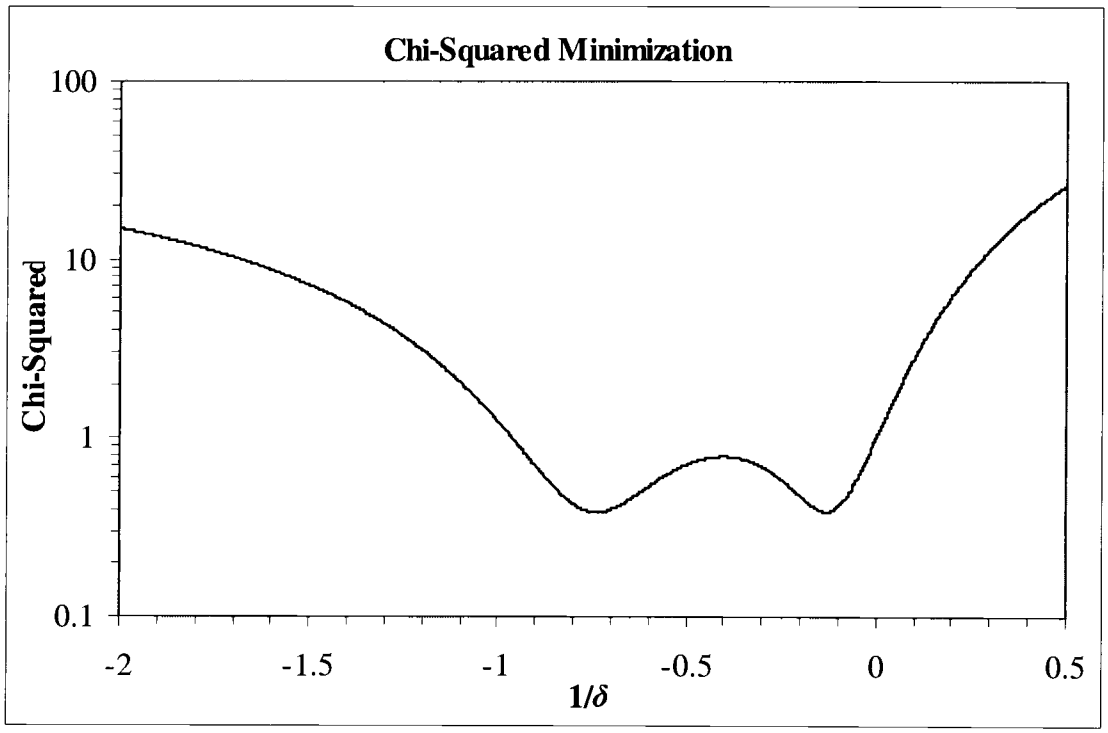

Figure 5-10: Example of a chi-squared minimization where the choice between the two possible minima is not clear at all and other factors are used to choose the favored solution. This plot comes from the ^{166m}Ho decay and is the plot of the chi-squared function for the 691-260-keV angular correlation. Note that the x-axis is $1/\delta$.

In this method the experimental uncertainties are determined by taking the values of delta given by adding one to the chi-squared minimum. This can be visualized by imagining the spread of delta values that is included below a line one unit above the chi-squared minimum (as shown in Figure 5-11, a magnified version of Figure 5-9).

In Figure 5-11 we can see that this will correspond to a small range of $1/\delta$ (but remember that δ is very sensitive to $1/\delta$ in this range). In contrast, the same process applied to the plot in Figure 5-10 indicates that include both minima will be included by the uncertainty.

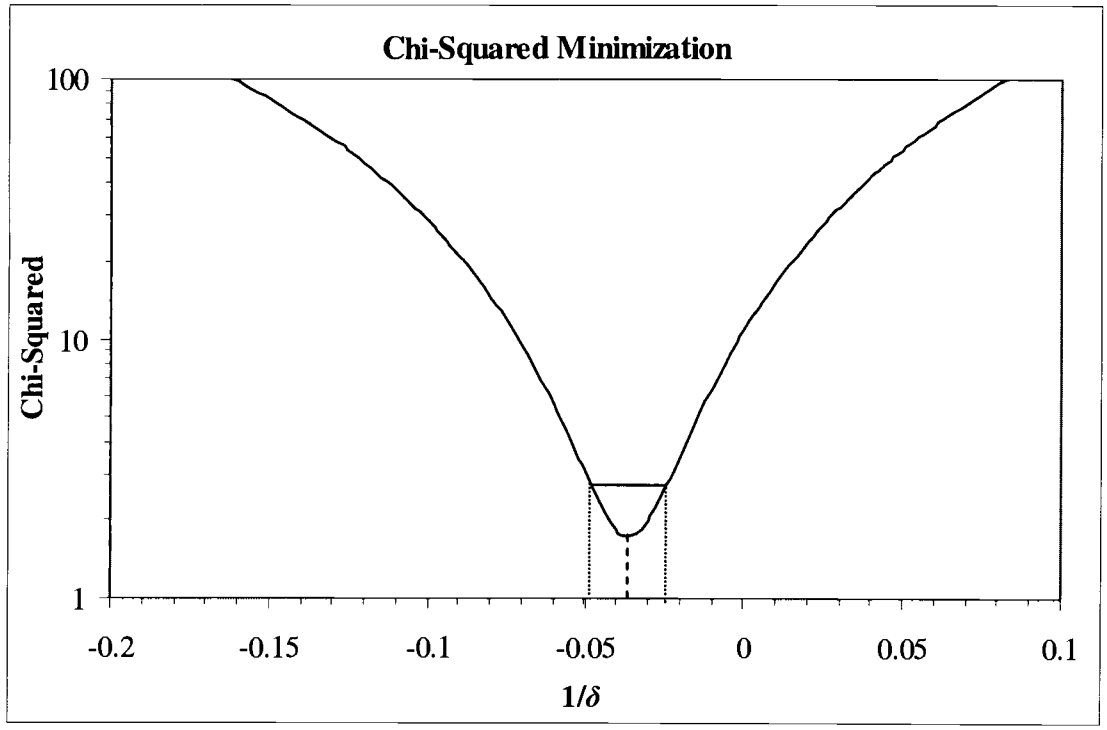

Figure 5-11: Magnified plot of chi-squared illustrating the method of finding uncertainty limits in a chi-squared minimization. The straight line in the figure is one unit above the minimum chi-squared value. The ends of the line represent the limits of uncertainty for the value of $1/\delta$. The $1/\delta$ value determined by this plot is $-(0.0362^{+0.0102}_{-0.0078})$ which corresponds to a δ value of $-(27.6^{+10.8}_{-4.9})$.

This chi-squared minimization method is preferable to extracting δ from the A_{22} coefficient because in some sense that method leaves out the information contained in the A_{44} coefficient. The chi-squared minimization method uses all the experimental data available. In addition, it has been previously noted [27] that the uncertainties produced by extracting δ from the A_{22} coefficient are smaller than those produced by the chi-squared minimization method raising some questions about the validity of those limits. See the end of Section 7.1 for a brief analysis of this issue in our data.

A major problem with the traditional method of determining δ from the A_{22} coefficient is that it may not immediately show that a δ value of up to infinity is possible. As noted, this issue can be addressed by solving for $1/\delta$. If the limits on this value encompass zero, it is obvious that δ itself could then be either positive or negative.

6. Experimental Results

We first present some spectra to show the basic character of the data we collected. Since the primary focus of this work was to measure the properties of the gamma band states, the second section presents our results for the $\delta(\mathrm{E2/M1})$ mixing ratios for the gamma-to-ground transitions and the third section presents results for the three intra-gamma-band transitions for which we were able to measure $\delta(\mathrm{E2/M1})$.

6.1. Experimental spectra

Figure 6-1 shows the singles spectrum collected for the ^{166m}Ho decay. This spectrum is the "true" singles spectrum described in Section 5.4.2 and accurately represents the total statistics collected for this decay.

Figure 6-2 shows the singles spectrum collected for the ^{166}Tm decay. This spectrum is the "true" singles spectrum and accurately represents the total statistics collected for this decay.

Figure 6-3 shows the so-called 184 gate for the ^{166m}Ho decay. This spectrum represents a background-subtracted gate on the 184-keV gamma ray in the ^{166m}Ho decay. See Section 5.5.1 for a description of how a gate such as this was created.

Figure 6-4 shows the 184 gate for the ^{166}Tm decay. This spectrum represents a background-subtracted gate on the 184-keV gamma ray in the ^{166}Tm decay.

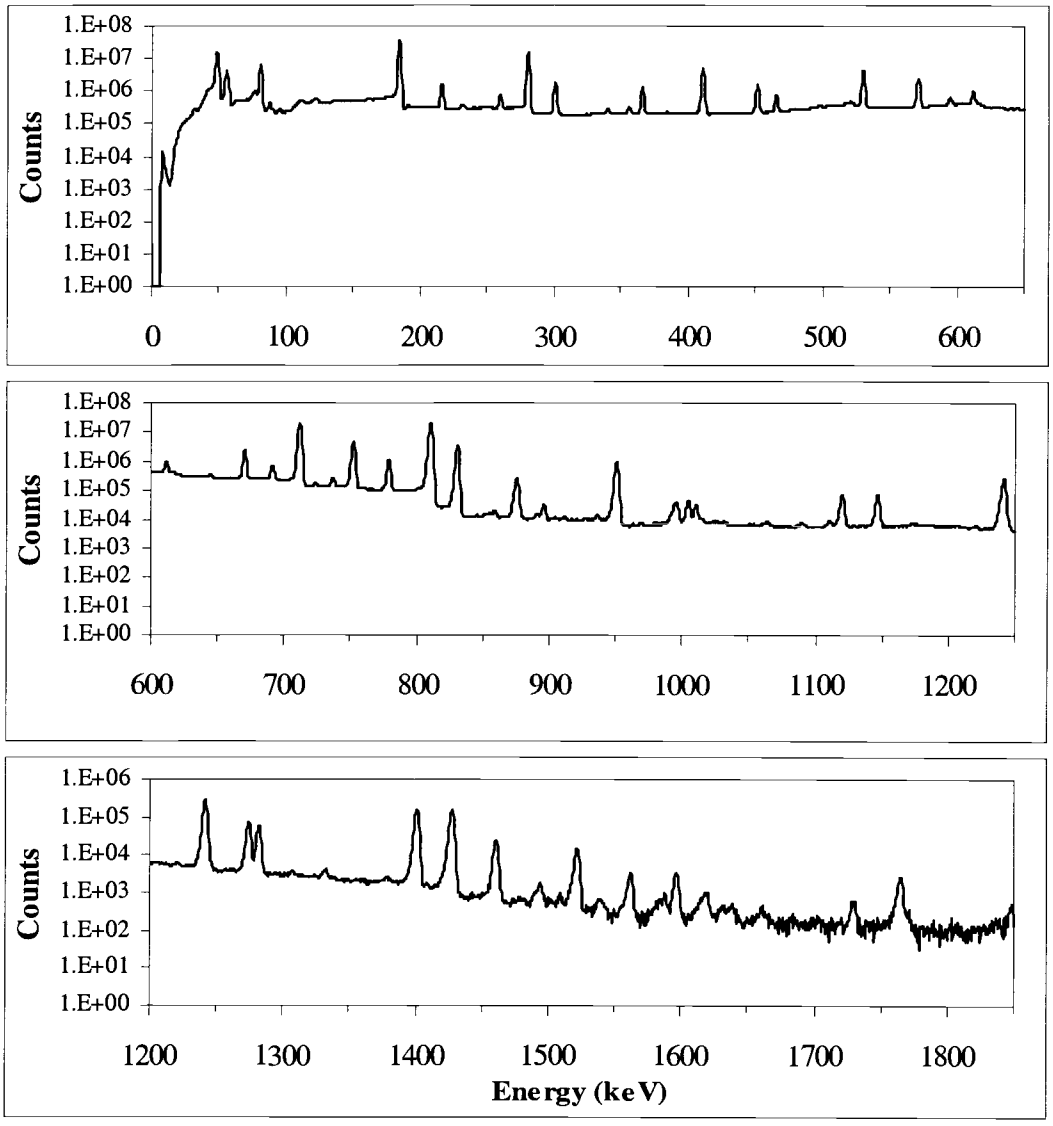

Figure 6-1: ^{166m}Ho full singles spectrum. For convenience there is some overlap in the energy ranges. Note that the vertical scale changes for each partial spectrum.

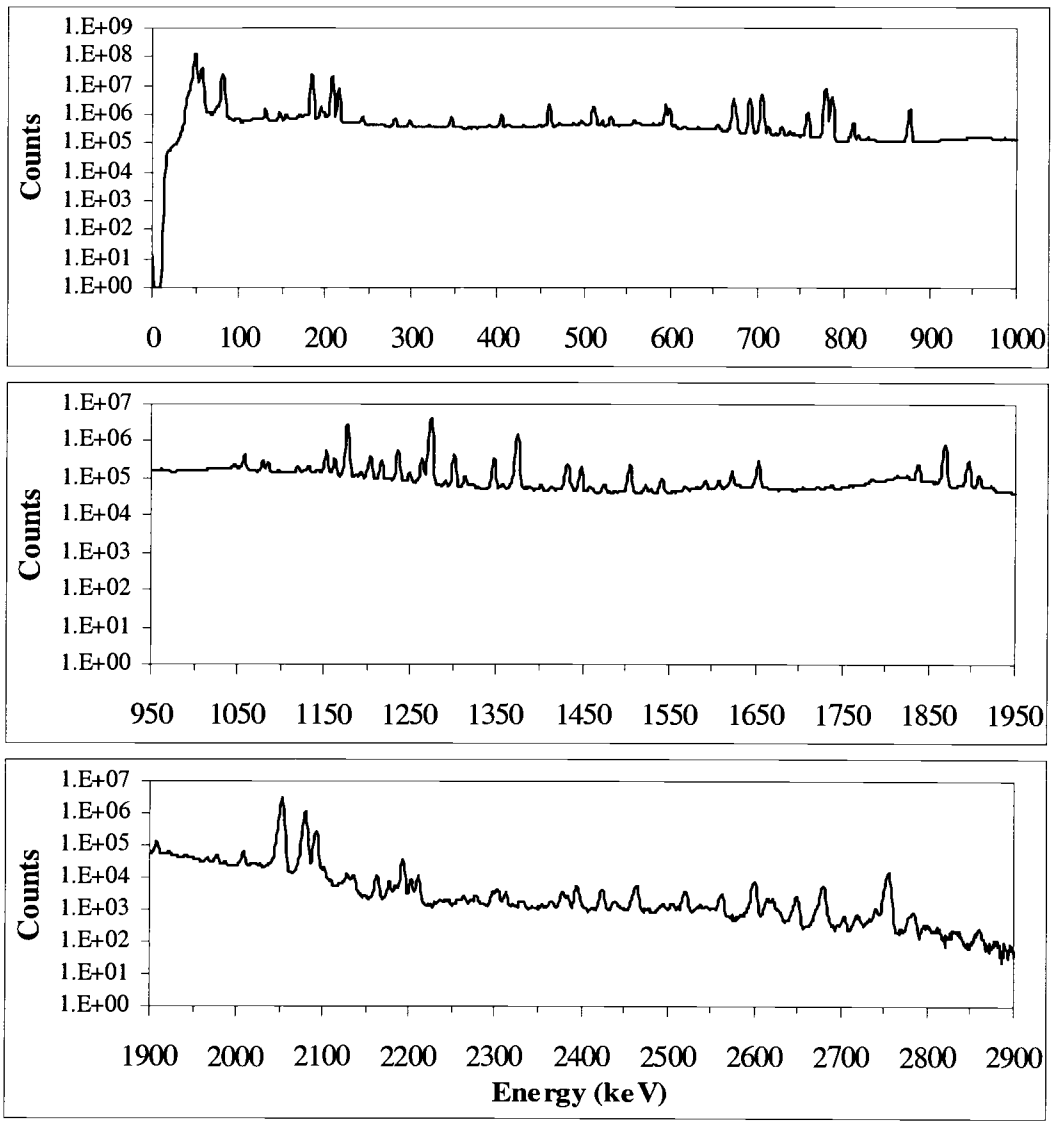

Figure 6-2: ^{166}Tm full singles spectrum. For convenience there is some overlap in the energy ranges. Note that the vertical scale changes for each partial spectrum.

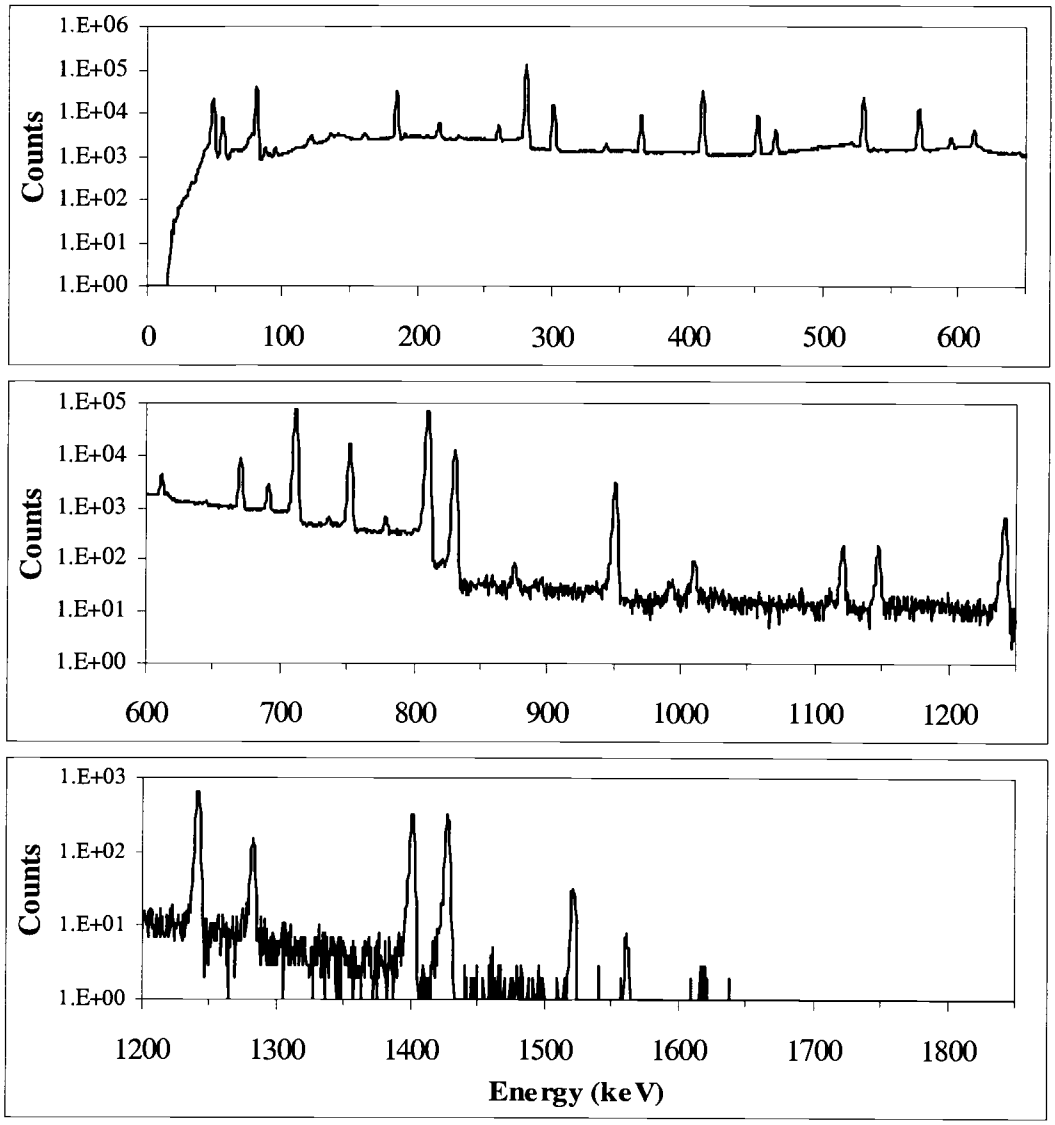

Figure 6-3: ^{166m}Ho 184 gate. This spectrum represents a background-subtracted gate on the 184-keV gamma ray in the ^{166m}Ho decay.

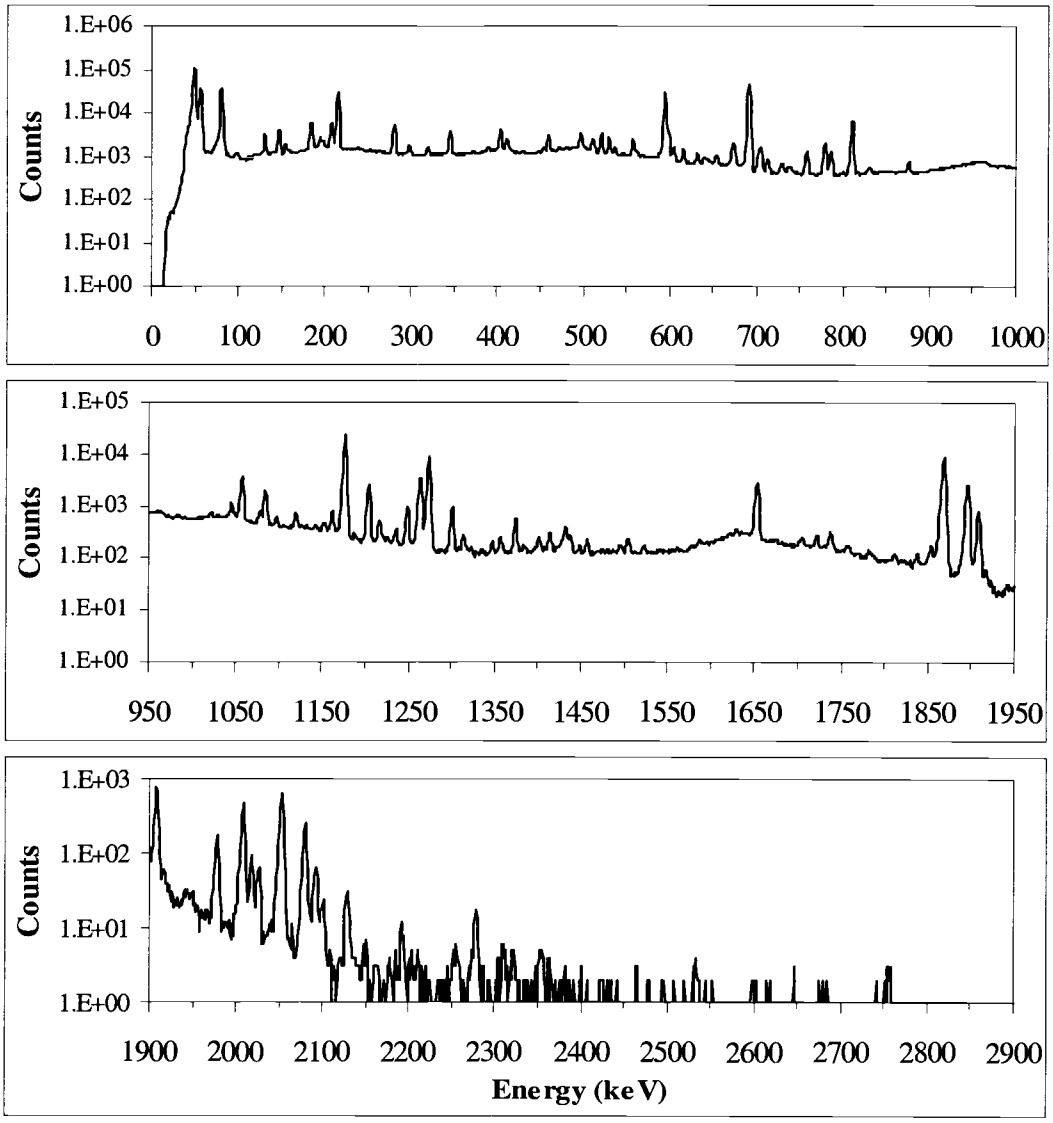

Figure 6-4: ^{166}Tm 184 gate. This spectrum represents a background-subtracted gate on the 184-keV gamma ray in the ^{166}Tm decay.

6.2. Gamma band to ground band δ(E2/M1) mixing ratios

In the following 10 subsections results are presented for each gamma-to-ground transition in order of initial spin. Each section describes the following: The angular correlation measurements used in the analysis, the angular correlation fits associated with these data, the methods by which the δ(E2/M1) mixing ratio was calculated for each angular correlation, the individual calculated values for δ and the final weighted average of these values. Presented in Table 6-1 for convenience are the final values for ten gamma-to-ground transitions measured in the present work. Recall that throughout this work it was actually $1/\delta$ that was calculated, and the values of δ are then inferred. In a few instances this may cause the error limits of δ to be asymmetric with the error bar that extends towards zero being larger than the one extending toward infinity. This is contrary to the usual error bars on δ but comes from irregular shapes of the chi-squared minimization curves.

In order to help the reader understand the coincidence relationships described in the following sections Figure 6-5, Figure 6-6 and Figure 6-7 present partial decay schemes for ^{166}Er. Figure 6-5 shows the ground and gamma bands and shows the intra-band transitions. Figure 6-6 shows all gamma-to-ground transitions up to initial spin 8. Figure 6-7 shows transitions from higher-lying states that feed the gamma band directly. Between them these three diagrams show all coincidence cascades used for the measurements presented in the following ten sections.

Table 6-1: Summary of gamma-to-ground mixing ratios. The "+" and "-" columns represent the uncertainty limits of the value in the preceding column. For those transitions where δ overlaps infinity see the text for limiting values. Note that throughout we have intentionally quoted every $1/\delta$ value to four decimal places regardless of its uncertainty. This is done because δ is so sensitive to small changes in $1/\delta$.

$E(\gamma)$	J_i to J_f	δ	+	-	$1/\delta$	+	-
705	**2^+ to 2^+**	-128	83	∞	**-0.0078**	**0.0147**	**0.0147**
779	**3^+ to 2^+**	-21.5	1.6	1.8	**-0.0464**	**0.0036**	**0.0036**
594	**3^+ to 4^+**	-7.6	0.4	0.4	**-0.1309**	**0.0068**	**0.0068**
691	**4^+ to 4^+**	-41	15	50	**-0.0242**	**0.0133**	**-0.0133**
810	**5^+ to 4^+**	-25.3	3.5	4.9	**-0.0395**	**0.0064**	**0.0064**
530	**5^+ to 6^+**	-33.7	1.8	2.0	**-0.0297**	**0.0017**	**0.0017**
671	**6^+ to 6^+**	+9.2	3.7	4.2	**+0.1082**	**0.0899**	**-0.0312**
831	**7^+ to 6^+**	-15.4	2.0	2.7	**-0.0649**	**0.0098**	**-0.0098**
465	**7^+ to 8^+**	-110	64	∞	**-0.0091**	**0.0127**	**-0.0127**
645	**8^+ to 8^+**	+2.4	26.4	0.9	**+0.4088**	**0.2527**	**-0.3742**

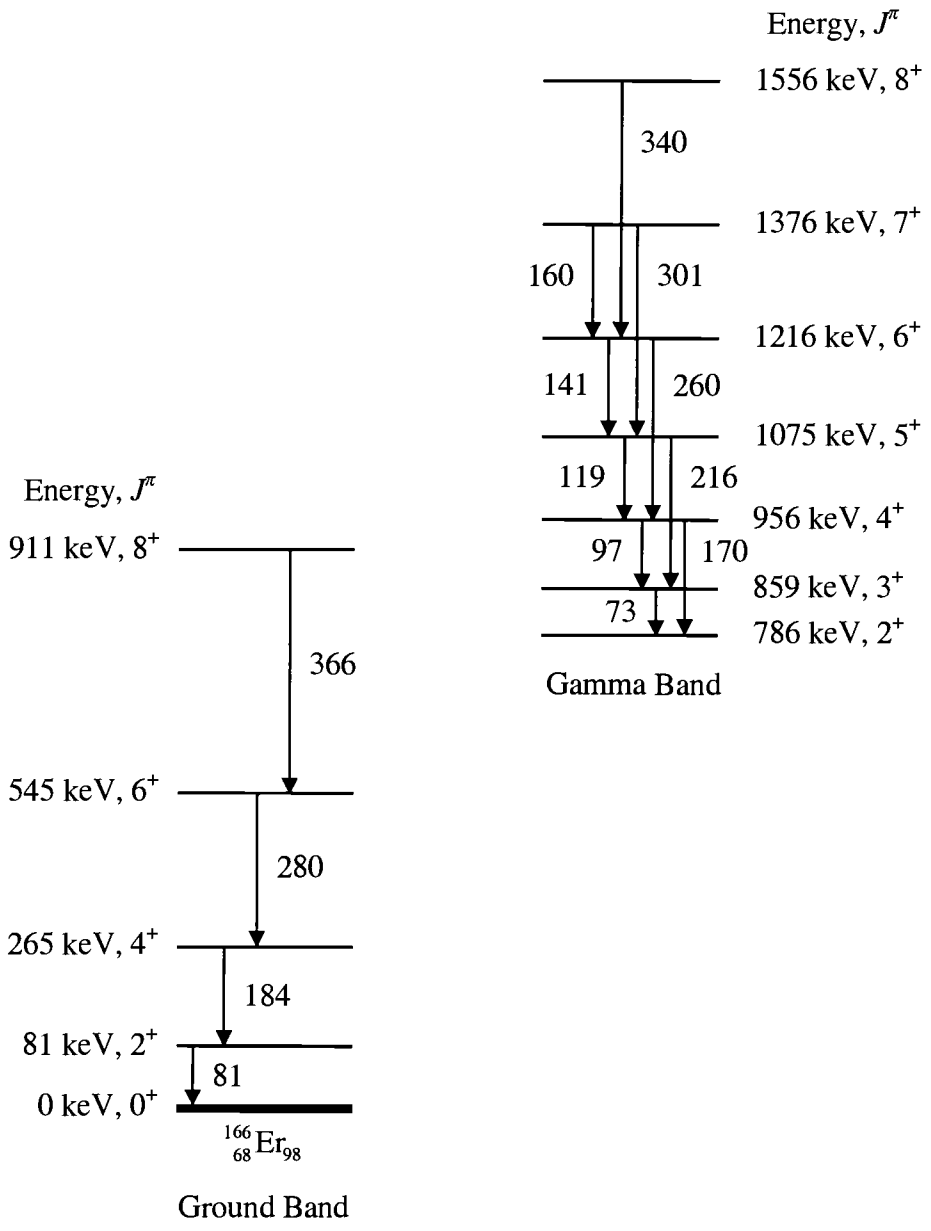

Figure 6-5: Partial decay scheme showing the gamma and ground bands of ^{166}Er. Intra-band transitions are also shown. Each excited state is labeled with its energy, spin and parity. Gamma rays are labeled by energies in keV. Labels are horizontally adjacent to the gamma ray they label.

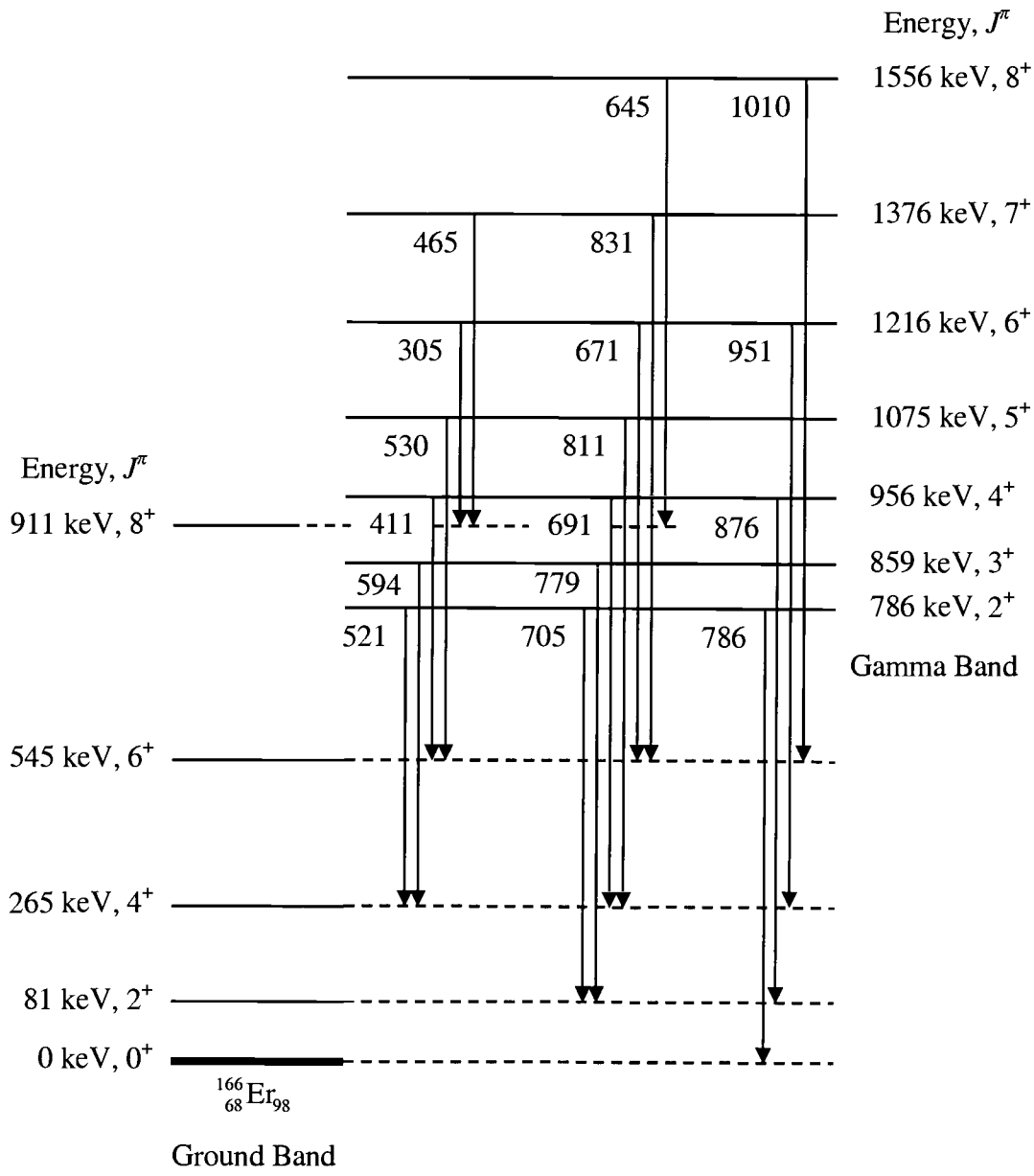

Figure 6-6: Partial decay scheme showing gamma-to-ground transitions in ^{166}Er. Each excited state is labeled with its energy, spin and parity. Gamma rays are labeled by energies in keV. Labels are horizontally adjacent to the gamma ray they label.

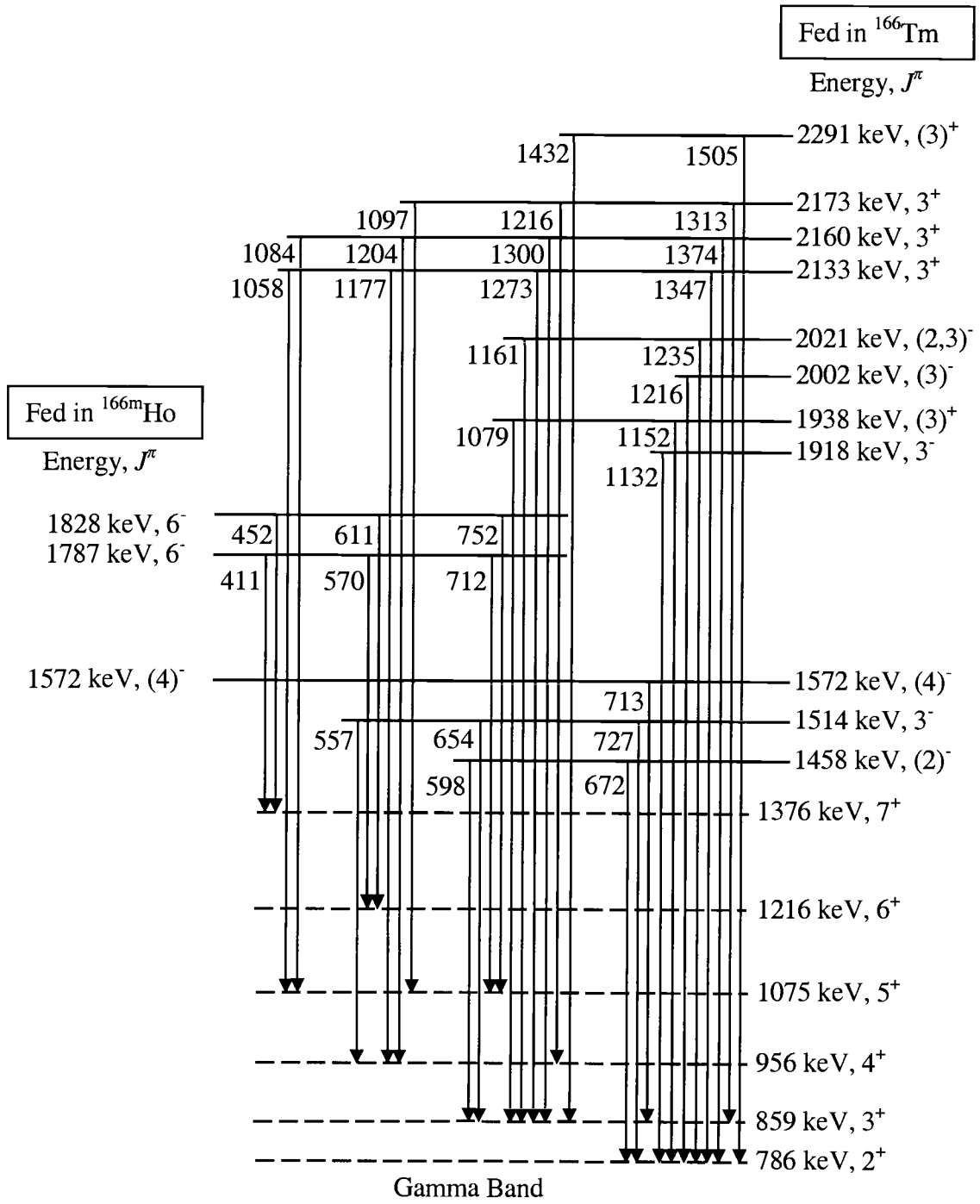

Figure 6-7: Partial decay scheme showing gamma rays that directly feed the gamma band in ^{166}Er. Gamma ray labels (in keV) are to the left of the gamma ray they label. States with lines extending to the right are fed in the ^{166}Tm decay, while those that extend left are fed in the ^{166m}Ho decay.

6.2.1. The 2^+ gamma to 2^+ ground transition (705 keV)

The 2^+ to 2^+ gamma-to-ground transition, which has an energy of 705 keV, is not fed in the ^{166m}Ho decay with any appreciable strength, so only the ^{166}Tm data were used to calculate the $\delta(\mathrm{E2/M1})$ mixing ratio for this gamma ray. In only one case could the chi-squared minimization method be used for this gamma ray (see Section 5.6 for a description of the various methods used to solve for δ). However, this angular correlation involved the 81 keV 2^+ to 0^+ ground-band transition, which is subject to the G_k correction factors. The uncertainty introduced by the inclusion of the G_k correction factors in the chi-squared minimization was such that no useful information could be gleaned from this angular correlation. Fortunately, nine other data points were obtained using the ratio of A_{kk} coefficients method. The angular correlations for these nine coincidences are presented in Table 6-2. Note that in this case all the gamma rays used with the 705-keV gamma ray fed the 2^+ gamma band state directly.

Recall that the ratio of A_{kk} coefficients method can be used even for a doublet such as the 1216-keV doublet. Both of the 1216-keV transitions feed the 705-keV transition in different ways, but all of the factors relating to the complex feeding of the 705-keV transition will cancel out in the ratio. The $\delta(\mathrm{E2/M1})$ values produced by these measurements are presented in Table 6-3, along with their weighted average. In this study we are not able to exclude a positive result for $\delta(705)$ but we can place the limits that $\delta(705) > 145$ or $\delta(705) < -45$.

Table 6-2: Summary of angular correlation fits for the coincidences used to determine $\delta(705)$. $E(\gamma_U)$ refers to the energy (in keV) of the gamma ray that comes first in the cascade, $E(\gamma_L)$ to the second. Each energy is followed by the spin and parities of the levels the gamma ray connects. Uncertainties in the last two digits of the A_{kk} values are expressed in italics. Cascade refers to whether the two gamma rays presented are connected directly or if there are unobserved gamma rays that connect them. Correlations are listed in order of increasing $E(\gamma_L)$.

Source	$E(\gamma_U)$	J_i to J_f	$E(\gamma_L)$	J_i to J_f	A_{22}	A_{44}	Cascade
Tm	672	$(2)^-$ to 2^+	705	2^+ to 2^+	-0.052 *10*	-0.006 *10*	Direct
Tm	728	3^- to 2^+	705	2^+ to 2^+	0.033 *32*	-0.033 *34*	Direct
Tm	1132	3^- to 2^+	705	2^+ to 2^+	-0.015 *51*	0.003 *54*	Direct
Tm	1152	$(3)^+$ to 2^+	705	2^+ to 2^+	0.016 *21*	-0.004 *22*	Direct
Tm	1216	Doublet	705	2^+ to 2^+	-0.001 *33*	0.023 *34*	Direct
Tm	1235	$(2,3)^-$ to 2^+	705	2^+ to 2^+	-0.042 *19*	-0.001 *19*	Direct
Tm	1347	3^+ to 2^+	705	2^+ to 2^+	0.077 *24*	-0.025 *26*	Direct
Tm	1374	3^+ to 2^+	705	2^+ to 2^+	0.047 *13*	0.021 *14*	Direct
Tm	1505	$(3)^+$ to 2^+	705	2^+ to 2^+	0.091 *30*	0.019 *32*	Direct
Tm	672	$(2)^-$ to 2^+	785	2^+ to 0^+	0.216 *10*	-0.004 *11*	Direct
Tm	728	3^- to 2^+	785	2^+ to 0^+	-0.072 *35*	-0.037 *35*	Direct
Tm	1132	3^- to 2^+	785	2^+ to 0^+	-0.025 *64*	0.025 *66*	Direct
Tm	1152	$(3)^+$ to 2^+	785	2^+ to 0^+	-0.057 *25*	-0.012 *25*	Direct
Tm	1216	Doublet	785	2^+ to 0^+	-0.036 *37*	-0.023 *38*	Direct
Tm	1235	$(2,3)^-$ to 2^+	785	2^+ to 0^+	0.264 *22*	-0.013 *24*	Direct
Tm	1347	3^+ to 2^+	785	2^+ to 0^+	-0.367 *26*	-0.024 *24*	Direct
Tm	1374	3^+ to 2^+	785	2^+ to 0^+	-0.163 *15*	-0.015 *15*	Direct
Tm	1505	$(3)^+$ to 2^+	785	2^+ to 0^+	-0.271 *36*	0.023 *35*	Direct

It bears repeating that measurements using the ratio of A_{kk} coefficients method are independent of the nature of the gamma ray that feeds the two angular correlations. Thus, even though there may be some uncertainty in spin assignment for the level which a

gamma ray comes from, and nothing may be known about its multipole character, these considerations are all removed when the ratio is taken.

Table 6-3: Summary of $\delta(705)$ values. In this measurement we are not able to rule out a positive value for $\delta(705)$ though we can say with confidence that it is very large. The averaged value of $1/\delta$ indicates that $\delta(705) > 145$ or $\delta(705) < -45$. $E(\gamma_C)$ indicates the energy of the gamma ray which was used in coincidence for this measurement. In the method column, A indicates the A_{kk} coefficient from a pure transition method, A/A indicates the ratio of A_{kk} coefficients method, A/A(E_g) indicates the ratio of A_{kk} coefficients with a mixed intermediate method, $\chi 2$ indicates the chi-squared minimization method and $\chi 2(E_g)$ indicates the chi-squared minimization with a mixed transition method. Note that some methods produce symmetric uncertainty limits, which is noted by NA in the "-" column.

Source	Method	$E(\gamma_C)$	J_i to J_f	δ	+	-	$1/\delta$	+	-
Tm	A/A	672	$(2)^-$ to 2^+	-75	48	∞	-0.0132	0.0233	NA
Tm	A/A	728	3^- to 2^+	-8	6	∞	-0.1250	0.2784	NA
Tm	A/A	1132	3^- to 2^+	3	∞	-2	0.3828	5.3792	NA
Tm	A/A	1152	$(3)^+$ to 2^+	-28	24	∞	-0.0352	0.1894	NA
Tm	A/A	1216	Doublet	9	∞	-7	0.1122	0.4317	NA
Tm	A/A	1235	$(2,3)^-$ to 2^+	38	∞	-21	0.0262	0.0332	NA
Tm	A/A	1347	3^+ to 2^+	356	∞	-328	0.0028	0.0317	NA
Tm	A/A	1374	3^+ to 2^+	-29	16	∞	-0.0349	0.0418	NA
Tm	A/A	1505	$(3)^+$ to 2^+	-16	8	-1877	-0.0618	0.0613	NA
		Weighted Average		-128	83	∞	**-0.0078**	**0.0147**	**0.0147**

6.2.2. The 3^+ gamma to 2^+ ground transition (779 keV)

The 3^+ to 2^+ gamma-to-ground transition, which has an energy of 779 keV, is fed in both the ^{166m}Ho and ^{166}Tm decays. It is found in coincidence with the 81 keV 2^+ to 0^+ ground-band transition with sufficient strength to be of use in finding a value for δ in

both decays. In addition, two transitions in the ^{166m}Ho decay and nine in the ^{166}Tm decay feed this gamma strongly enough to be used to find δ values. The 24 relevant angular correlation fits are presented in Table 6-4.

The $\delta(\mathrm{E2/M1})$ values produced by these measurements and the methods used are presented in Table 6-5, along with their weighted average. The agreement between all thirteen measurements in this case is remarkable, and the weighted average reduces the uncertainty limits significantly.

As noted, the ratio of A_{kk} coefficients with a mixed transition was used for 11 of these measurements. In these ratios, the mixing ratio for the 594 keV 3^+ to 4^+ gamma-to-ground transition is used, but as shown in the next section, the value is relatively large and has a narrow uncertainty range. The large value means that the $A_2(594)$ coefficient is relatively insensitive to changes in $\delta(594)$. In fact, this insensitivity is such that applying the uncertainty limits of $\delta(594)$ has only negligible effects on the values calculated for $\delta(779)$.

Table 6-4: Summary of angular correlation fits for the coincidences used to determine $\delta(779)$. See Table 6-2 for table notation.

Source	$E(\gamma_U)$	J_i to J_f	$E(\gamma_L)$	J_i to J_f	A_{22}	A_{44}	Cascade
Tm	779	3^+ to 2^+	81	2^+ to 0^+	-0.201 *23*	-0.061 *23*	Direct
Ho	779	3^+ to 2^+	81	2^+ to 0^+	-0.196 *36*	-0.118 *45*	Direct
Ho	713	Doublet	594	3^+ to 4^+	0.009 *19*	0.000 *24*	Indirect
Ho	752	6^- to 5^+	594	3^+ to 4^+	0.021 *32*	0.034 *42*	Indirect
Tm	599	$(2)^-$ to 3^+	594	3^+ to 4^+	-0.035 *19*	0.024 *20*	Direct
Tm	654	3^- to 3^+	594	3^+ to 4^+	0.013 *30*	0.005 *31*	Direct
Tm	713	$(4)^-$ to 3^+	594	3^+ to 4^+	-0.029 *30*	-0.010 *31*	Direct
Tm	1079	$(3)^+$ to 3^+	594	3^+ to 4^+	0.017 *41*	-0.022 *43*	Direct
Tm	1162	$(2,3)^-$ to 3^+	594	3^+ to 4^+	-0.009 *34*	0.037 *35*	Direct
Tm	1274	3^+ to 3^+	594	3^+ to 4^+	0.0353 *81*	-0.0006 *85*	Direct
Tm	1301	3^+ to 3^+	594	3^+ to 4^+	0.049 *20*	-0.012 *21*	Direct
Tm	1313	3^+ to 3^+	594	3^+ to 4^+	0.001 *48*	0.032 *50*	Direct
Tm	1432	$(3)^+$ to 3^+	594	3^+ to 4^+	0.054 *35*	-0.044 *36*	Direct
Ho	713	Doublet	779	3^+ to 2^+	0.056 *48*	0.014 *66*	Indirect
Ho	752	6^- to 5^+	779	3^+ to 2^+	-0.09 *11*	0.07 *14*	Indirect
Tm	599	2^- to 3^+	779	3^+ to 2^+	0.081 *24*	0.013 *26*	Direct
Tm	654	3^- to 3^+	779	3^+ to 2^+	-0.112 *55*	0.002 *56*	Direct
Tm	713	$(4)^-$ to 3^+	779	3^+ to 2^+	0.053 *55*	-0.014 *57*	Direct
Tm	1079	$(3)^+$ to 3^+	779	3^+ to 2^+	-0.093 *64*	-0.013 *65*	Direct
Tm	1162	$(2,3)^-$ to 3^+	779	3^+ to 2^+	0.087 *49*	0.036 *51*	Direct
Tm	1274	3^+ to 3^+	779	3^+ to 2^+	-0.119 *12*	0.014 *13*	Direct
Tm	1301	3^+ to 3^+	779	3^+ to 2^+	-0.138 *35*	-0.026 *35*	Direct
Tm	1313	3^+ to 3^+	779	3^+ to 2^+	-0.06 *10*	-0.14 *11*	Direct
Tm	1432	$(3)^+$ to 3^+	779	3^+ to 2^+	-0.149 *78*	-0.021 *79*	Direct

Table 6-5: Summary of $\delta(779)$ values. See Table 6-3 for notation.

Source	Method	$E(\gamma_C)$	J_i to J_f	δ	+	-	$1/\delta$	+	-
Tm	χ2	81	2^+ to 0^+	-21	16	∞	-0.0474	0.0694	0.133
Ho	χ2	81	2^+ to 0^+	-11.4	6.9	∞	-0.0881	0.0921	0.136
Ho	A/A(594)	713	Doublet	-13.4	3.2	6.1	-0.0744	0.0233	NA
Ho	A/A(594)	752	6^- to 5^+	-19.7	6.1	15.8	-0.0507	0.0226	NA
Tm	A/A(594)	599	2^- to 3^+	-26.5	7.9	19.3	-0.0377	0.0159	NA
Tm	A/A(594)	654	3^- to 3^+	-17.5	4.2	8.1	-0.0572	0.0181	NA
Tm	A/A(594)	713	$(4)^-$ to 3^+	-32	18	∞	-0.0309	0.0380	NA
Tm	A/A(594)	1079	$(3)^+$ to 3^+	-18.8	6.7	23.6	-0.0532	0.0296	NA
Tm	A/A(594)	1162	$(2,3)^-$ to 3^+	-17.2	5.3	14.1	-0.0582	0.0263	NA
Tm	A/A(594)	1274	3^+ to 3^+	-21.8	2.0	2.4	-0.0460	0.0046	NA
Tm	A/A(594)	1301	3^+ to 3^+	-23.7	4.5	7.1	-0.0423	0.0098	NA
Tm	A/A(594)	1313	3^+ to 3^+	-15.9	7.3	90.9	-0.0630	0.0536	NA
Tm	A/A(594)	1432	$(3)^+$ to 3^+	-23.9	6.6	14.6	-0.0419	0.0159	NA
		Weighted Average		-21.5	1.6	1.8	**-0.0464**	**0.0036**	**0.0036**

6.2.3. The 3^+ gamma to 4^+ ground transition (594 keV)

The 3^+ to 4^+ gamma-to-ground transition, which has an energy of 594 keV, is fed in both the ^{166m}Ho and ^{166}Tm decays. This transition is in coincidence with both the 184 keV 4^+ to 2^+ and the 81 keV 2^+ to 0^+ ground-band transitions in both decays. The angular correlation fits for these four coincidences are presented in Table 6-6. Note that even though the 594-keV gamma ray does not directly feed the 81-keV gamma ray, there is only one path for the cascade to take (i.e. via the pure 184-keV transition), thus the 81-594-keV angular correlation is still marked as "direct" as opposed to an angular correlation where there are several paths for the cascade to take, or where the intermediate radiation is of mixed multipolarity. This same notation will hold for angular

correlations involving any ground band gamma ray that is not directly fed by the gamma-to-ground transition.

Table 6-6: Summary of angular correlation fits for the coincidences used to determine $\delta(594)$. See Table 6-2 for table notation.

Source	$E(\gamma_U)$	J_i to J_f	$E(\gamma_L)$	J_i to J_f	A_{22}	A_{44}	Cascade
Tm	594	3^+ to 4^+	81	2^+ to 0^+	0.0433 *57*	-0.1359 *59*	Direct
Ho	594	3^+ to 4^+	81	2^+ to 0^+	0.1536 *38*	-0.1672 *51*	Direct
Tm	594	3^+ to 4^+	184	4^+ to 2^+	0.08757 *91*	-0.0916 *10*	Direct
Ho	594	3^+ to 4^+	184	4^+ to 2^+	0.0850 *27*	-0.1009 *35*	Direct

The δ(E2/M1) values produced by these measurements are presented in Table 6-7, along with their weighted average. The measurement in the 184-keV gate of the ^{166}Tm decay dominates this determination.

Table 6-7: Summary of $\delta(594)$ values. See Table 6-3 for notation.

Source	Method	$E(\gamma_C)$	J_i to J_f	δ	+	-	$1/\delta$	+	-
Tm	χ2	81	2^+ to 0^+	-40	30	∞	-0.0251	0.0741	0.0789
Ho	χ2	81	2^+ to 0^+	-4.6	1.7	3.0	-0.2164	0.0844	0.1296
Tm	χ2	184	4^+ to 2^+	-7.52	0.37	0.42	-0.1330	0.0070	0.0070
Ho	χ2	184	4^+ to 2^+	-10.8	2.8	5.9	-0.0928	0.0328	0.0332
		Weighted Average		-7.64	0.38	0.42	**-0.1309**	**0.0068**	**0.0068**

The average value of δ for this transition is used to calculate $\delta(779)$ using the ratio of A_{kk} coefficients with a mixed intermediate method (see the previous section).

6.2.4. The 4^+ gamma to 4^+ ground transition (691 keV)

The 4^+ to 4^+ gamma-to-ground transition, which has an energy of 691 keV, is fed in both the ^{166m}Ho and ^{166}Tm decays. This transition is in coincidence with both the 184 keV 4^+ to 2^+ and the 81 keV 2^+ to 0^+ ground-band transitions in both decays. In addition this transition is in coincidence with one other strong gamma ray in the ^{166m}Ho decay and five others in the ^{166}Tm decay. These other gamma rays can be used in the ratio of A_{kk} method to find δ. The angular correlation fits for the 13 coincidences used are presented in Table 6-10.

The data from the 81 and 184-keV gates in both decays were used with the chi-squared minimization method to find values of $\delta(691)$. However, these calculations produced results that were scattered and did not correspond well with our other measurements. These data were also used to calculate $\delta(691)$ using the A_{kk} coefficients with a pure transition method. This produced a more satisfactory and consistent set of values. The $\delta(\mathrm{E2/M1})$ values produced by these measurements and from the other five applicable angular correlations are presented in Table 6-9, along with their weighted average.

Table 6-8: Summary of angular correlation fits for the coincidences used to determine $\delta(691)$. See Table 6-2 for table notation.

Source	$E(\gamma_U)$	J_i to J_f	$E(\gamma_L)$	J_i to J_f	A_{22}	A_{44}	Cascade
Tm	691	4^+ to 4^+	81	2^+ to 0^+	-0.109 *62*	0.031 *63*	Direct
Ho	691	4^+ to 4^+	81	2^+ to 0^+	-0.047 *57*	0.016 *74*	Direct
Tm	691	4^+ to 4^+	184	4^+ to 2^+	-0.1110 *66*	0.1400 *67*	Direct
Ho	691	4^+ to 4^+	184	4^+ to 2^+	-0.146 *18*	0.156 *23*	Direct
Ho	260	6^+ to 4^+	691	4^+ to 4^+	-0.077 *22*	0.012 *29*	Direct
Tm	558	3^- to 4^+	691	4^+ to 4^+	0.088 *33*	0.006 *35*	Direct
Tm	1177	3^+ to 4^+	691	4^+ to 4^+	0.2043 *93*	-0.018 *10*	Direct
Tm	1204	3^+ to 4^+	691	4^+ to 4^+	0.307 *19*	-0.111 *21*	Direct
Tm	1217	Doublet	691	4^+ to 4^+	0.296 *70*	-0.088 *77*	Direct
Tm	558	3^- to 4^+	875	4^+ to 2^+	-0.136 *52*	-0.014 *51*	Direct
Tm	1177	3^+ to 4^+	875	4^+ to 2^+	-0.325 *13*	-0.011 *12*	Direct
Tm	1204	3^+ to 4^+	875	4^+ to 2^+	-0.468 *27*	-0.080 *25*	Direct
Tm	1217	Doublet	875	4^+ to 2^+	-0.47 *11*	-0.202 *97*	Direct

Table 6-9: Summary of $\delta(691)$ values. See Table 6-3 for notation.

Source	Method	$E(\gamma_C)$	J_i to J_f	δ	+	-	$1/\delta$	+	-
Tm	A	81	2^+ to 0^+	25	∞	21	0.0401	0.2300	NA
Ho	A	81	2^+ to 0^+	-6.0	2.9	63.9	-0.1674	0.1531	NA
Tm	A	184	4^+ to 2^+	-54	29	∞	-0.0186	0.0216	NA
Ho	A	184	4^+ to 2^+	8.8	26.0	3.8	0.1134	0.0847	NA
Ho	$\chi 2$	260	6^+ to 4^+	-8	5	∞	-0.1310	0.7653	0.282
Tm	A/A	558	3^- to 4^+	-24	20	∞	-0.0415	0.1799	NA
Tm	A/A	1177	3^+ to 4^+	-38	17	155	-0.0262	0.0210	NA
Tm	A/A	1204	3^+ to 4^+	-22.0	9.1	54.1	-0.0455	0.0323	NA
Tm	A/A	1217	3^+ to 4^+	-41	34	∞	-0.0244	0.1149	NA
		Weighted Average		-41	15	50	**-0.0242**	**0.0133**	**-0.0133**

6.2.5. The 5^+ gamma to 4^+ ground transition (810 keV)

The 5^+ to 4^+ gamma-to-ground transition, which has an energy of 810 keV, is fed in both the ^{166m}Ho and ^{166}Tm decays. This transition is in coincidence with the 184 keV 4^+ to 2^+ and the 81 keV 2^+ to 0^+ ground-band transitions in both decays, as well as with the pure-E2 301 keV 7^+ to 5^+ intra-gamma band transition in the ^{166m}Ho decay. Two other mixed multipolarity transitions in the ^{166m}Ho decay and three pure 3^+ to 5^+ transitions in the ^{166}Tm decay feed the 810-keV gamma ray with sufficient strength to enable us to find a δ value. The 12 applicable angular correlation fits are presented in Table 6-10.

The two mixed multipolarity gamma rays that feed this transition in the ^{166m}Ho decay used in the chi-squared minimization method. However, since these transitions are not pure multipolarity, their mixing ratios were calculated and then used in the chi-squared minimization for $\delta(810)$. The calculated mixing ratios for the 712 and 753 keV gamma rays, using the 216 keV 5^+ to 3^+ intra-gamma band transition as a pure gate, are -0.009 ± 0.02 and 0.01 ± 0.04. The uncertainty limits were incorporated into the subsequent chi-squared minimization for $\delta(810)$. The $\delta(\mathrm{E2/M1})$ values produced by these ten angular correlations are presented in Table 6-11, along with their weighted average.

Table 6-10: Summary of angular correlation fits for the coincidences used to determine $\delta(810)$. See Table 6-2 for table notation.

Source	$E(\gamma_U)$	J_i to J_f	$E(\gamma_L)$	J_i to J_f	A_{22}	A_{44}	Cascade
Tm	810	5^+ to 4^+	81	2^+ to 0^+	-0.22 *12*	-0.11 *13*	Direct
Ho	810	5^+ to 4^+	81	2^+ to 0^+	-0.114 *18*	-0.033 *21*	Direct
Tm	810	5^+ to 4^+	184	4^+ to 2^+	-0.153 *11*	-0.056 *11*	Direct
Ho	810	5^+ to 4^+	184	4^+ to 2^+	-0.1558 *82*	-0.0648 *83*	Direct
Ho	301	7^+ to 5^+	810	5^+ to 4^+	-0.017 *14*	-0.022 *17*	Direct
Ho	712	6^- to 5^+	810	5^+ to 4^+	0.021 *11*	-0.008 *12*	Direct
Ho	753	6^- to 5^+	810	5^+ to 4^+	0.009 *15*	-0.008 *17*	Direct
Tm	1058	3^+ to 5^+	810	5^+ to 4^+	-0.014 *28*	-0.123 *28*	Direct
Tm	1085	3^+ to 5^+	810	5^+ to 4^+	-0.017 *38*	-0.162 *39*	Direct
Tm	1097	3^+ to 5^+	810	5^+ to 4^+	-0.069 *75*	-0.135 *76*	Direct
Ho	712	6^- to 5^+	216	5^+ to 3^+	-0.076 *14*	-0.010 *17*	Direct
Ho	753	6^- to 5^+	216	5^+ to 3^+	-0.063 *27*	-0.014 *34*	Direct

Table 6-11: Summary of $\delta(810)$ values. See Table 6-3 for notation.

Source	Method	$E(\gamma_C)$	J_i to J_f	δ	+	-	$1/\delta$	+	-
Tm	χ^2	81	2^+ to 0^+	-3.3	2.9	8.3	-0.2995	0.2135	1.9805
Ho	χ^2	81	2^+ to 0^+	-38	28	∞	-0.0262	0.0542	0.0718
Tm	χ^2	184	4^+ to 2^+	-27.7	6.8	12.3	-0.0361	0.0111	0.0119
Ho	χ^2	184	4^+ to 2^+	-22.4	3.7	5.4	-0.0447	0.0087	0.0089
Ho	χ^2	301	7^+ to 5^+	-27	12	98	-0.0371	0.0291	0.0289
Ho	χ^2(712)	712	Doublet	-20	10	30	-0.0490	0.0290	0.0430
Ho	χ^2(753)	752	6^- to 5^+	-46	37	∞	-0.0218	0.0618	0.0882
Tm	χ^2	1058	3^+ to 5^+	-145	113	∞	-0.0069	0.0249	0.0251
Tm	χ^2	1085	3^+ to 5^+	-25	12	142	-0.0399	0.0339	0.0341
Tm	χ^2	1097	3^+ to 5^+	-11.5	5.2	44.0	-0.0868	0.0688	0.0712
		Weighted Average		-25.3	3.5	4.9	**0.0395**	**0.0064**	**0.0064**

6.2.6. The 5^+ gamma to 6^+ ground transition (530 keV)

The 5^+ to 6^+ gamma-to-ground transition, which has an energy of 530 keV, is fed in both the ^{166m}Ho and ^{166}Tm decays. This transition is in coincidence with the 280 keV 6^+ to 4^+, the 184 keV 4^+ to 2^+ and the 81 keV 2^+ to 0^+ ground-band transitions in both decays. However, Compton backscattering from a higher peak ruins the measurement of both the 81-keV and 184-keV gates for the ^{166}Tm decay. As with the 810-keV transition, this gamma ray is also fed by the pure-E2 301 keV 7^+ to 5^+ transition in the ^{166m}Ho decay. Two other mixed multipolarity transitions in the ^{166m}Ho decay and three pure 3^+ to 5^+ transitions in the ^{166}Tm decay feed the 530-keV gamma ray with sufficient strength to enable us to find a δ value. The 12 applicable angular correlation fits are presented in Table 6-12.

Table 6-12: Summary of angular correlation fits for the coincidences used to determine $\delta(530)$. See Table 6-2 for table notation.

Source	$E(\gamma_U)$	J_i to J_f	$E(\gamma_L)$	J_i to J_f	A_{22}	A_{44}	Cascade
Ho	530	5^+ to 6^+	81	2^+ to 0^+	0.015 *27*	-0.102 *33*	Direct
Ho	530	5^+ to 6^+	184	4^+ to 2^+	0.024 *12*	-0.092 *13*	Direct
Tm	530	5^+ to 6^+	280	6^+ to 4^+	0.012 *18*	-0.121 *19*	Direct
Ho	530	5^+ to 6^+	280	6^+ to 4^+	0.0109 *17*	-0.1163 *21*	Direct
Ho	301	7^+ to 5^+	530	5^+ to 6^+	-0.042 *24*	-0.016 *31*	Direct
Ho	712	6^- to 5^+	530	5^+ to 6^+	0.042 *12*	-0.016 *14*	Direct
Ho	753	6^- to 5^+	530	5^+ to 6^+	0.025 *19*	0.007 *24*	Direct
Tm	1058	3^+ to 5^+	530	5^+ to 6^+	-0.082 *56*	-0.006 *57*	Direct
Tm	1085	3^+ to 5^+	530	5^+ to 6^+	-0.041 *68*	-0.191 *69*	Direct
Tm	1097	3^+ to 5^+	530	5^+ to 6^+	-0.32 *25*	-0.14 *24*	Direct
Ho	712	6^- to 5^+	216	5^+ to 3^+	-0.076 *14*	-0.010 *17*	Direct
Ho	753	6^- to 5^+	216	5^+ to 3^+	-0.063 *27*	-0.014 *34*	Direct

As with the 810 keV gamma ray, two strong gammas in the ^{166m}Ho decay feed the 530-keV gamma ray and were used in the chi-squared minimization method. However, since these transitions are not pure multipolarity, their mixing ratios were calculated and then used in the chi-squared minimization for $\delta(530)$. See the previous section for the values and uncertainties of the mixing ratios for the 712 and 752-keV transitions used to calculate $\delta(530)$. The $\delta(\mathrm{E2/M1})$ values produced by these ten angular correlations are presented in Table 6-13, along with their weighted average.

Table 6-13: Summary of $\delta(530)$ values. See Table 6-3 for notation.

Source	Method	$E(\gamma_C)$	J_i to J_f	δ	+	-	$1/\delta$	+	-
Ho	χ^2	81	2^+ to 0^+	-35	22	∞	-0.0284	0.0514	0.0486
Ho	χ^2	184	4^+ to 2^+	-16.6	3.1	4.7	-0.0603	0.0133	0.0137
Tm	χ^2	280	6^+ to 4^+	-40	16	103	-0.0249	0.0179	0.0171
Ho	χ^2	280	6^+ to 4^+	-34.1	1.9	1.6	-0.0293	0.0013	0.0017
Ho	χ^2	301	7^+ to 5^+	-17	9	∞	-0.0587	0.0627	0.0633
Ho	χ^2(712)	712	6^- to 5^+	-27	16	∞	-0.0372	0.0732	0.0528
Ho	χ^2(753)	752	6^- to 5^+	-46	34	∞	-0.0218	0.0358	0.0602
Tm	χ^2	1058	3^+ to 5^+	-11.3	4.8	28.7	-0.0885	0.0635	0.0645
Tm	χ^2	1085	3^+ to 5^+	+69	∞	58	+0.0145	0.0735	0.0725
Tm	χ^2	1097	3^+ to 5^+	+1.9	4.4	1.6	+0.5305	2.8195	0.3705
		Weighted Average		-33.7	1.8	2.0	**-0.0297**	**0.0017**	**0.0017**

The value produced by the 1097-530 keV angular correlation disagrees with the other values significantly. However as indicated by the angular correlation fit above, which produces unusually large values for A_{22} and A_{44}, this angular correlation is suspect and should perhaps be excluded from the average. However, due to the influence of the

value produced by the 280-530 keV angular correlation, exclusion of the 1097-530 keV has an almost negligible effect on the weighted average.

6.2.7. The 6^+ gamma to 6^+ ground transition (671 keV)

The 6^+ to 6^+ gamma-to-ground transition, which has an energy of 671 keV, is not fed in the ^{166}Tm decay due to the low spin of the ^{166}Tm parent. This transition is in coincidence with the 280 keV 6^+ to 4^+, the 184 keV 4^+ to 2^+ and the 81 keV 2^+ to 0^+ ground-band transitions in the ^{166m}Ho decay. Two other mixed multipolarity transitions in the ^{166m}Ho decay feed the 671-keV gamma ray with sufficient strength to enable us to find a δ value. The seven applicable angular correlation fits are presented in Table 6-14.

Table 6-14: Summary of angular correlation fits for the coincidences used to determine $\delta(671)$. See Table 6-2 for table notation.

Source	$E(\gamma_U)$	J_i to J_f	$E(\gamma_L)$	J_i to J_f	A_{22}	A_{44}	Cascade
Ho	670	6^+ to 6^+	81	2^+ to 0^+	-0.104 *12*	0.072 *14*	Direct
Ho	670	6^+ to 6^+	184	4^+ to 2^+	-0.125 *12*	0.086 *14*	Direct
Ho	670	6^+ to 6^+	280	6^+ to 4^+	-0.128 *11*	0.097 *13*	Direct
Ho	571	6^- to 6^+	670	6^+ to 6^+	-0.132 *14*	0.014 *18*	Direct
Ho	612	6^- to 6^+	670	6^+ to 6^+	-0.103 *24*	0.043 *30*	Direct
Ho	951	6^+ to 4^+	571	6- to 6^+	0.179 *21*	-0.021 *28*	Direct
Ho	951	6^+ to 4^+	612	6- to 6^+	0.140 *40*	-0.055 *54*	Direct

The 951-keV pure-E2 6^+ to 4^+ gamma-to-ground transition is used to find the mixing ratios of the 571 and 612-keV transitions. The chi-squared minimization method gives $0.17^{+0.14}_{-0.16}$ and $0.004^{+0.092}_{-0.128}$ respectively. The error limits of these mixing ratios is incorporated into the chi-squared minimization for $\delta(671)$. When this is done for the

571-keV transition the resulting error bars make the measurement useless, so it is not included below. The δ(E2/M1) values produced by the remaining four angular correlations are presented in Table 6-15, along with their weighted average.

Table 6-15: Summary of δ(671) values. See Table 6-3 for notation.

Source	Method	$E(\gamma_C)$	J_i to J_f	δ	+	-	$1/\delta$	+	-
Ho	χ^2	81	2^+ to 0^+	+9	∞	7	+0.1055	0.3095	0.1510
Ho	χ^2	184	4^+ to 2^+	+8.9	28.4	7.6	+0.1123	0.6273	0.0855
Ho	χ^2	280	6^+ to 4^+	+11.3	43.3	6.5	+0.0884	0.1204	0.0701
Ho	χ^2(612)	612	6^- to 6^+	+8.1	3.8	4.5	+0.1234	0.1546	0.0394
		Weighted Average		+9.2	3.7	4.2	**+0.1082**	**0.0899**	**-0.0312**

6.2.8. The 7^+ gamma to 6^+ ground transition (831 keV)

The 7^+ to 6^+ gamma-to-ground transition, which has an energy of 831 keV, is not fed in the ^{166}Tm decay due to the low spin of the ^{166}Tm parent. This transition is in coincidence with the 280 keV 6^+ to 4^+, the 184 keV 4^+ to 2^+ and the 81 keV 2^+ to 0^+ ground-band transitions in the ^{166m}Ho decay. Two other mixed multipolarity transitions in the ^{166m}Ho decay feed the 831-keV gamma ray with sufficient strength to enable us to find a δ value. The seven applicable angular correlation fits are presented in Table 6-16.

Table 6-16: Summary of angular correlation fits for the coincidences used to determine $\delta(831)$. See Table 6-2 for table notation.

Source	$E(\gamma_U)$	J_i to J_f	$E(\gamma_L)$	J_i to J_f	A_{22}		A_{44}		Cascade
Ho	831	7^+ to 6^+	81	2^+ to 0^+	-0.152	*31*	-0.020	*37*	Direct
Ho	831	7^+ to 6^+	184	4^+ to 2^+	-0.143	*12*	-0.060	*13*	Direct
Ho	831	7^+ to 6^+	280	6^+ to 4^+	-0.143	*10*	-0.048	*11*	Direct
Ho	411	6^- to 7^+	831	7^+ to 6^+	0.043	*11*	0.004	*14*	Direct
Ho	452	6^- to 7^+	831	7^+ to 6^+	0.016	*16*	0.005	*20*	Direct
Ho	411	6^- to 7^+	301	7^+ to 5^+	-0.100	*11*	0.002	*12*	Direct
Ho	452	6^- to 7^+	301	7^+ to 5^+	-0.085	*16*	-0.025	*20*	Direct

The 301-keV pure-E2 7^+ to 5^+ intra-gamma transition is used to find the mixing ratios of the 411 and 452-keV transitions. The chi-squared minimization method gives -0.011 ± 0.013 and 0.023 ± 0.021 respectively. The error limits of these mixing ratios is incorporated into the chi-squared minimization for $\delta(831)$. The $\delta(\mathrm{E2/M1})$ values produced by these five angular correlations are presented in Table 6-17, along with their weighted average.

Table 6-17: Summary of $\delta(831)$ values. See Table 6-3 for notation.

Source	Method	$E(\gamma_C)$	J_i to J_f	δ	+	-	$1/\delta$	+	-
Ho	χ^2	81	2^+ to 0^+	-7.0	3.4	12.2	-0.1431	0.0911	0.1349
Ho	χ^2	184	4^+ to 2^+	-13.9	2.4	3.9	-0.0718	0.0158	0.0152
Ho	χ^2	280	6^+ to 4^+	-15.9	3.0	4.6	-0.0628	0.0140	0.0144
Ho	$\chi^2(411)$	411	6^- to 7^+	-14.8	5.0	10.2	-0.0677	0.0277	0.0343
Ho	$\chi^2(452)$	452	6^- to 7^+	-72	57	∞	-0.0139	0.0359	0.0521
		Weighted Average		-15.4	2.0	2.7	**-0.0649**	**0.0098**	**-0.0098**

6.2.9. The 7^+ gamma to 8^+ ground transition (465 keV)

The 7^+ to 8^+ gamma-to-ground transition, which has an energy of 465 keV, is not fed in the ^{166}Tm decay due to the low spin of the ^{166}Tm parent. This transition is in coincidence with all four pure-E2 ground-band transitions in the ^{166m}Ho decay. Two other mixed multipolarity transitions in the ^{166m}Ho decay feed the 465-keV gamma ray with sufficient strength to enable us to find a δ value. The eight applicable angular correlation fits are presented in Table 6-18.

Table 6-18: Summary of angular correlation fits for the coincidences used to determine $\delta(465)$. See Table 6-2 for table notation.

Source	$E(\gamma_U)$	J_i to J_f	$E(\gamma_L)$	J_i to J_f	A_{22}		A_{44}		Cascade
Ho	465	7^+ to 8^+	81	2^+ to 0^+	0.033	*50*	0.020	*67*	Direct
Ho	465	7^+ to 8^+	184	4^+ to 2^+	-0.036	*18*	-0.106	*22*	Direct
Ho	465	7^+ to 8^+	280	6^+ to 4^+	0.009	*18*	-0.120	*22*	Direct
Ho	465	7^+ to 8^+	366	8^+ to 6^+	-0.020	*15*	-0.088	*19*	Direct
Ho	411	6^- to 7^+	465	7^+ to 8^+	0.051	*19*	0.010	*25*	Direct
Ho	452	6^- to 7^+	465	7^+ to 8^+	0.010	*34*	0.011	*45*	Direct
Ho	411	6^- to 7^+	301	7^+ to 5^+	-0.100	*11*	0.002	*12*	Direct
Ho	452	6^- to 7^+	301	7^+ to 5^+	-0.085	*16*	-0.025	*20*	Direct

The 301-keV pure-E2 7^+ to 5^+ intra-gamma transition is used to find the mixing ratios of the 411 and 452-keV transitions. See the previous section for the mixing ratios determined for these two transitions. The data for the 465-81-keV angular correlation were too poor to use to find a δ value. The δ(E2/M1) values produced by the remaining five angular correlations were not sufficient to rule out a positive value for $\delta(465)$, but

we can place the limits that $\delta(465) > 275$ or $\delta(465) < -46$. The $\delta(465)$ values are presented in Table 6-19, along with their weighted average.

Table 6-19: Summary of $\delta(465)$ values. See Table 6-3 for notation.

Source	Method	$E(\gamma_C)$	J_i to J_f	δ	+	-	$1/\delta$	+	-
Ho	χ2	184	4^+ to 2^+	48	∞	26	0.0209	0.0239	0.0239
Ho	χ2	280	6^+ to 4^+	-27	11	53	-0.0366	0.0241	0.0245
Ho	χ2	366	8^+ to 6^+	-165	128	∞	-0.0061	0.0205	0.0207
Ho	χ2(411)	411	6^- to 7^+	-46	32	∞	-0.0219	0.0639	0.0521
Ho	χ2(452)	452	6^- to 7^+	-8	4	117	-0.1221	0.1141	0.1099
		Weighted Average		-110	64	∞	**-0.0091**	**0.0127**	**-0.0127**

6.2.10. The 8^+ gamma to 8^+ ground transition (645 keV)

The 8^+ to 8^+ gamma-to-ground transition, which has an energy of 645 keV, is not fed in the ^{166}Tm decay due to the low spin of the ^{166}Tm parent. This transition is in coincidence with all four pure-E2 ground-band transitions in the ^{166m}Ho decay. However, Compton backscattering problems were such that the 645-81-keV and 645-184-keV angular correlations were not measurable. No other gamma rays feed the 8^+ level of the gamma band. The two remaining angular correlation fits are presented in Table 6-20.

Table 6-20: Summary of angular correlation fits for the coincidences used to determine $\delta(645)$. See Table 6-2 for table notation.

Source	$E(\gamma_U)$	J_i to J_f	$E(\gamma_L)$	J_i to J_f	A_{22}		A_{44}		Cascade
Ho	645	8^+ to 8^+	280	6^+ to 4^+	-0.178	*49*	0.080	*65*	Direct
Ho	645	8^+ to 8^+	366	8^+ to 6^+	-0.116	*42*	0.029	*56*	Direct

The δ(E2/M1) values produced by these two angular correlations do not individually rule out a large negative value. However, their weighted average does bring the uncertainty limits down to the degree that their weighted average does not allow a negative value. Conservative limits of uncertainty are quoted in an effort to reflect the tentative nature of the averaged value. The values are presented in Table 6-21, along with their weighted average.

Table 6-21: Summary of $\delta(645)$ values. See Table 6-3 for notation.

Source	Method	$E(\gamma_C)$	J_i to J_f	δ	+	-	$1/\delta$	+	-
Ho	$\chi 2$	280	6^+ to 4^+	4.1	∞	2.2	0.2432	0.2938	0.2732
Ho	$\chi 2$	366	8^+ to 6^+	1.8	∞	0.6	0.5483	0.2697	0.6643
		Weighted Average		2.4	26	0.9	**0.4088**	**0.2527**	**-0.3742**

6.3. Intra-gamma band δ(E2/M1) mixing ratios

As discussed in Chapter 3 the properties of the intra-gamma transitions are also of interest in testing various theories of deformed nuclei. In this work we were able to measure the mixing ratios of three intra-gamma transitions, two of which have not previously been measured. These three transitions are not fed very strongly in the ^{166}Tm decay and thus the measurements presented here are only from the ^{166m}Ho decay. Presented in Table 6-22 for convenience are the final values for the mixing ratios of all three intra-gamma transitions determined in this work. Note that since these δ values are

not nearly as large as those of the gamma-to-ground transitions, only three decimal places are quoted for $1/\delta$.

Table 6-22: Summary of intra-gamma mixing ratios. For those transitions where δ overlaps infinity see the text for limiting values.

$E(\gamma)$	J_i to J_f	δ	+	-	$1/\delta$	+	-
119	**5^+ to 4^+**	2.45	0.93	0.53	**0.408**	**0.112**	**0.112**
141	**6^+ to 5^+**	1.15	1.04	0.62	**0.872**	**1.014**	**0.416**
160	**7^+ to 6^+**	1.65	0.93	1.16	**0.607**	**1.449**	**0.219**

6.3.1. The 5^+ to 4^+ intra-gamma band transition (119 keV)

The 5^+ to 4^+ intra-gamma transition, which has an energy of 119 keV, is in coincidence with two strong gamma-to-ground transitions that follow it and two strong gamma rays that precede it. The correlation fits for these four coincidences are presented in Table 6-23.

Table 6-23: Summary of angular correlation fits for the coincidences used to determine $\delta(119)$. See Table 6-2 for table notation.

Source	$E(\gamma_U)$	J_i to J_f	$E(\gamma_L)$	J_i to J_f	A_{22}		A_{44}		Cascade
Ho	119	5^+ to 4^+	875	4^+ to 2^+	0.131	*55*	-0.191	*74*	Direct
Ho	119	5^+ to 4^+	691	4^+ to 4^+	-0.068	*48*	-0.031	*63*	Direct
Ho	712	6^- to 5^+	119	5^+ to 4^+	-0.261	*90*	0.10	*12*	Direct
Ho	753	6^- to 5^+	119	5^+ to 4^+	-0.40	*18*	0.34	*24*	Direct

For the 691-keV mixed gamma-to-ground transition the final δ value given in Section 6.2.4 was used to find $\delta(119)$ using the chi-squared with a mixed transition

method. The mixing ratios for 712 and 752-keV transitions are given in Section 6.2.5. The $\delta(119)$ values determined using these four coincidences are presented in Table 6-24, along with their weighted average.

Table 6-24: Summary of $\delta(119)$ values. See Table 6-3 for notation.

Source	Method	$E(\gamma_C)$	J_i to J_f	δ	+	-	$1/\delta$	+	-
Ho	$\chi 2$	875	4^+ to 2^+	+2.54	0.89	0.63	+0.393	0.129	0.102
Ho	$\chi 2$(691)	691	4^+ to 4^+	+2.64	1.63	1.03	+0.379	0.241	0.145
Ho	$\chi 2$(712)	712	6^- to 5^+	+1.17	1.26	0.57	+0.854	0.798	0.442
Ho	$\chi 2$(753)	753	6^- to 5^+	+1.17	2.62	0.73	+0.854	1.423	0.590
		Weighted Average		+2.45	0.61	0.53	**+0.408**	**0.112**	**0.081**

6.3.2. The 6^+ to 5^+ intra-gamma band transition (141 keV)

The 6^+ to 5^+ intra-gamma transition, which has an energy of 141 keV, is in coincidence with two strong gamma-to-ground transitions that follow it and two strong gamma rays that precede it. The correlation fits for these four coincidences are presented in Table 6-25.

Table 6-25: Summary of angular correlation fits for the coincidences used to determine $\delta(141)$. See Table 6-2 for table notation.

Source	$E(\gamma_U)$	J_i to J_f	$E(\gamma_L)$	J_i to J_f	A_{22}		A_{44}		Cascade
Ho	141	6^+ to 5^+	810	5^+ to 4^+	0.31	*34*	0.40	*47*	Direct
Ho	141	6^+ to 5^+	530	5^+ to 6^+	0.66	*35*	-0.60	*48*	Direct
Ho	571	6^- to 6^+	141	6^+ to 5^+	0.33	*11*	0.34	*15*	Direct
Ho	612	6^- to 6^+	141	6^+ to 5^+	0.41	*25*	0.45	*34*	Direct

The experimental uncertainty for both $\delta(810)$ and $\delta(529)$ is enough to make those coincidences useless in determining $\delta(141)$. Therefore only two values could be used to get an average for this transition. Fortunately the two values agree remarkably well. The mixing ratios for the 571 and 612-keV transitions are given in Section 6.2.7. The $\delta(141)$ values determined using these two coincidences are presented in Table 6-26, along with their weighted average.

Table 6-26: Summary of $\delta(119)$ values. See Table 6-3 for notation.

Source	Method	$E(\gamma_C)$	J_i to J_f	δ	+	-	$1/\delta$	+	-
Ho	χ2(712)	571	6^- to 6^+	+1.15	1.88	0.67	+0.873	1.215	0.543
Ho	χ2(753)	612	6^- to 6^+	+1.15	3.30	0.78	+0.872	1.840	0.647
		Weighted Average		+1.15	1.04	0.62	**+0.872**	**1.014**	**0.416**

6.3.3. The 7^+ to 6^+ intra-gamma band transition (160 keV)

The 7^+ to 6^+ intra-gamma transition, which has an energy of 160 keV, is in coincidence with two strong gamma-to-ground transitions that follow it and two strong gamma rays that precede it. The correlation fits for these four coincidences are presented in Table 6-27.

The experimental uncertainty for $\delta(671)$ and $\delta(452)$ is enough to make those coincidences useless in determining $\delta(160)$. Therefore only two values could be used to get an average for this transition. Again, the two values agree favorably. The mixing ratios for the 411-keV transition is given in Section 6.2.8. The $\delta(160)$ values determined

using these two coincidences are presented in Table 6-28, along with their weighted average.

Table 6-27: Summary of angular correlation fits for the coincidences used to determine $\delta(160)$. See Table 6-2 for table notation.

Source	$E(\gamma_U)$	J_i to J_f	$E(\gamma_L)$	J_i to J_f	A_{22}	A_{44}	Cascade
Ho	160	7^+ to 6^+	951	6^+ to 4^+	0.20 *12*	-0.24 *17*	Direct
Ho	160	7^+ to 6^+	671	6^+ to 6^+	-0.053 *99*	0.02 *13*	Direct
Ho	411	6^- to 6^+	160	7^+ to 6^+	-0.188 *71*	0.014 *94*	Direct
Ho	452	6^- to 6^+	160	7^+ to 6^+	0.19 *16*	-0.09 *22*	Direct

Table 6-28: Summary of $\delta(160)$ values. See Table 6-3 for notation.

Source	Method	$E(\gamma_C)$	J_i to J_f	δ	+	-	$1/\delta$	+	-
Ho	$\chi 2$	951	6^+ to 4^+	+1.9	2.0	1.6	+0.517	2.973	0.262
Ho	$\chi 2(411)$	411	6^- to 6^+	+1.5	2.0	1.0	+0.687	1.659	0.399
		Weighted Average		+1.65	0.93	1.16	**+0.607**	**1.449**	**0.219**

6.4. Band-mixing analysis of gamma-to-ground intensities

In addition to these angular correlation results, data from these experiments reveal spectroscopic information about the intensities of the gamma rays emitted in the decays. These intensities can be used to investigate the effects of mixing between the gamma and ground bands and the E2 transition strengths [48]. Presented here is a brief treatment of the preliminary results of this analysis, which will assist us in comparing our results to the band-mixing theory in Chapter 7.

As discussed in Section 3.8, the following equation should describe the effects of first order band mixing on the value of the $B(\mathrm{E2}; J_i, K=2 \rightarrow J_f, K=0)$ reduced transition probabilities (reproduced here for convenience)

$$B(\mathrm{E2}; J_i, K=2 \rightarrow J_f, K=0) = 2\left\langle J_i, 2, 2, -2 \middle| J_f, 0 \right\rangle^2 \left| M_1 + M_2 \left(X_f - X_i \right) \right|^2 \quad (3\text{-}25)$$

We recast this equation so that a linear plot can be described by

$$\frac{\sqrt{B(\mathrm{E2}; J_i, K=2 \rightarrow J_f, K=0)}}{\sqrt{2}\left\langle J_i, 2, 2, -2 \middle| J_f, 0 \right\rangle} = M_1 + M_2 \left(X_f - X_i \right) \quad (6\text{-}1)$$

and the parameters M_1 and M_2 can be calculated by a least-squares regression. The Mikhailov plot generated with this data is shown in Figure 6-8. The uncertainty limits of each data point are of the size of the marker circle or smaller. A linear fit to the data gives the results $M_1 = 0.4243 \pm 0.0025$ and $M_2 = 0.00778 \pm 0.00016$.

These values for M_1 and M_2 produce the common band-mixing parameter $z_2 = 0.0396 \pm 0.0009$ which compares very well with recent previous measurements $z_2 = 0.0393 \pm 0.0013$ by Adam [29], the original measurement $z_2 = 0.041 \pm 0.002$ by Reich and Cline [13], as well as others [20,21,32].

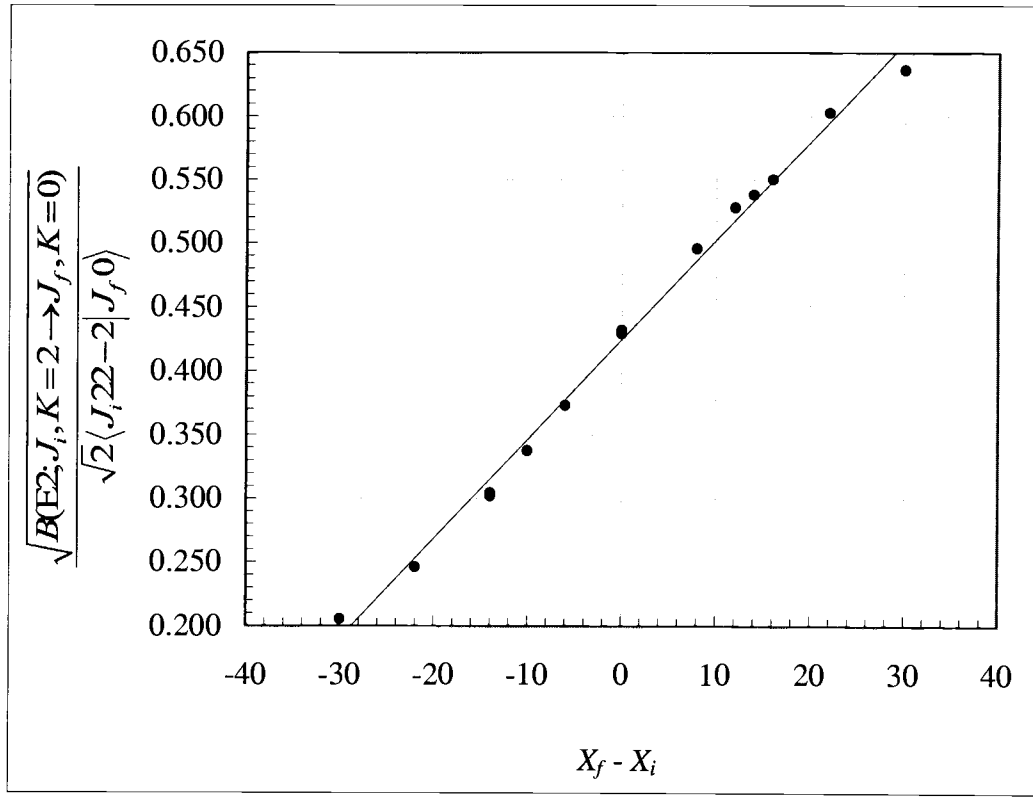

Figure 6-8: Mikhailov plot for ^{166}Er. The error bars on each data point are the size of the marker circle or smaller.

The precision in this diagram is considerably improved over previous such analyses [13]. As such the forthcoming analysis of this data is perhaps the first time that strong evidence for a non-linear shape to this data has been observed. In Figure 6-8 it can be seen with the naked eye that there is a slightly cubic shape to the otherwise very linear data. Figure 6-9 shows the same data now fitted by a 3rd-order polynomial.

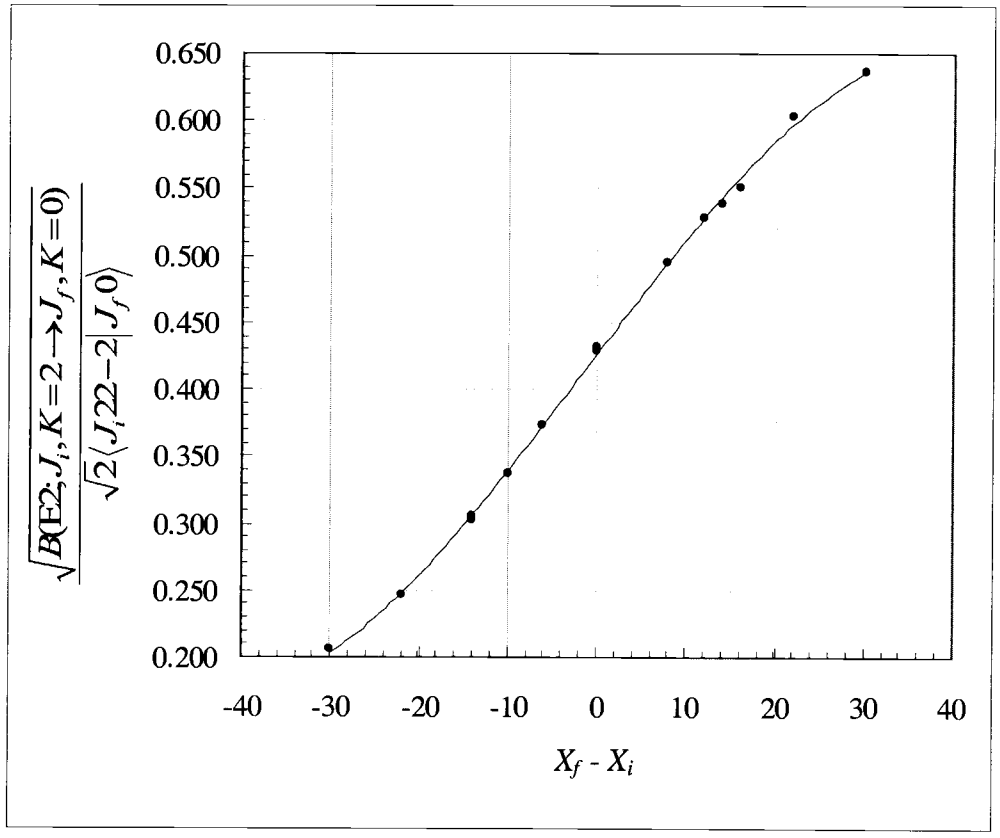

Figure 6-9: Mikhailov plot for ^{166}Er fitted to a 3rd-order polynomial. The error bars on each data point are the size of the marker circle or smaller.

It can be seen that the data is reproduced quite well by this cubic fit. The four fit parameters are $M_1 = 0.4264 \pm 0.0013$, $M_2 = 0.00883 \pm 0.00014$, $M_3 = -(7.6 \pm 3.5) \times 10^{-6}$ and $M_4 = -(18.0 \pm 2.1) \times 10^{-7}$. The ramifications for this cubic shape are still under investigation by this research group.

7. Discussion

Having established our experimental results, we now turn to the questions of how our values compare with those measured in other experiments and whether our values can be faithfully reproduced by any of the available theories.

7.1. Gamma-to-ground mixing ratios compared to previous experiments

As described in Chapter 4, mixing ratios of the ten mixed-multipolarity gamma-to-ground transitions of ^{166}Er have been measured in many previous studies. In Table 7-1 our results are presented in comparison with those in previous studies

Note that West [40] gives two values for $\delta(671)$ and $\delta(645)$, and Domingos [39] gives two values for $\delta(705)$. In Table 7-1 the values which show the best agreement with other works are presented.

A discussion of each previous measurement would not be productive. However, there are a few previous studies worth comment. The work by Hamilton [30] is the only other work in which chi-squared minimization was used to extract mixing ratio values, and thus their work offers the most direct comparison. Generally speaking, our values agree with the general size and sign of Hamilton's values. A notable exception would be the 594 keV 3^+ to 4^+ transition, for which Hamilton's value is significantly larger than other previous measurements, while ours agrees with other works. In most other cases widening the uncertainty limits to 1.5 standard deviations brings the two values into

Table 7-1: Comparison of gamma-to-ground mixing ratios with previous experiments. Gamma rays are listed in keV. Results are presented starting with the most recent. If no sign is presented for the mixing ratio it indicates that the original paper only measured $|\delta|$. A "*" indicates that the chi-squared minimization method was used for finding δ. For some values that include infinity (marked bold in the "By" column) the notation has been altered to fit the space available. In one case (underlined in the "By" column) a sign has been changed to correct what we believe was a typo in the original paper.

	705	**779**	**594**	**691**	**810**	**530**	**671**	**831**	**465**	**645**
By	2^+-2^+	3^+-2^+	3^+-4^+	4^+-4^+	5^+-4^+	5^+-6^+	6^+-6^+	7^+-6^+	7^+-8^+	8^+-8^+
A*	$-128^{+83}_{-\infty}$	$-21.5^{+1.6}_{-1.8}$	$-7.64^{+0.38}_{-0.42}$	-41^{+15}_{-50}	$-25.3^{+3.5}_{-4.9}$	$-33.7^{+1.8}_{-2.0}$	$+9.2^{+3.7}_{-4.2}$	$-15.4^{+2.0}_{-2.7}$	$-110^{+64}_{-\infty}$	$+2.4^{+26.4}_{-0.9}$
B	$\lvert\delta\rvert > 50$	-67^{+30}_{-44}	-23^{+7}_{-120}	$\lvert\delta\rvert > 50$	-27^{+4}_{-6}	-21^{+5}_{-111}	$+16^{+\infty}_{-5}$	-34^{+14}_{-51}		
C*		$-44.6^{+8}_{-12.6}$	$-35.7^{+11.4}_{-32}$	$+566^{+\infty}_{-616}$	$-21.2^{+1.8}_{-2.1}$	$-42.9^{+5.4}_{-7.3}$	$+25.0^{+17.4}_{-7.0}$	$-17.3^{+1.3}_{-1.5}$	-238^{+153}_{-320}	$+4.9^{+2.3}_{-1.1}$
D	$-5^{+1.4}_{-3}$	$+15^{+2.6}_{-6}$	$+5.5^{+7.4}_{-2.2}$	$\lvert\delta\rvert < 8$						
E					-36^{+7}_{-11}			-18^{+2}_{-3}	-63^{+12}_{-19}	
F				$3.8^{+3.4}_{-1.2}$	$24.0^{+54.0}_{-9.8}$	$160^{+\infty}_{-130}$	$76^{+\infty}_{-71}$	$63^{+\infty}_{-44}$	$11.0^{+\infty}_{-6.6}$	
G		-18^{+5}_{-8}	-8^{+3}_{-15}	$-16^{+10}_{-\infty}$	-15^{+1}_{-1}	-60^{+19}_{-45}	$+9.4^{+2.9}_{-1.6}$	$-17.0^{+1.5}_{-1.8}$	-13^{+5}_{-15}	$\lvert\delta\rvert > 1$
G		-20^{+2}_{-4}	-12^{+5}_{-29}	$+16^{+9}_{-\infty}$	-21^{+2}_{-2}	-62^{+17}_{-40}	$+10^{+1.6}_{-1.2}$	-23^{+4}_{-4}	$-51^{+21}_{-\infty}$	
H		$-19^{+10}_{-\infty}$	$-9^{+5}_{-\infty}$	-16^{+4}_{-27}	-20^{+3}_{-4}	-25^{+4}_{-5}	-20^{+9}_{-90}	-22^{+5}_{-7}	-32^{+14}_{-98}	$\lvert\delta\rvert > 1$
I	-22^{+7}_{-13}	$+8.4^{+0.7}_{-0.7}$	$+58^{+\infty}_{-27}$	$-3.7^{+0.5}_{-0.5}$	$\delta \le -17$		$\delta < -0.01$			
J		$-20^{+13}_{-\infty}$			$-84^{+57}_{-\infty}$	$-5.0^{+2.5}_{-2.5}$	$+6.3^{+\infty}_{-2.9}$	$-37^{+17}_{-\infty}$	$-3.1^{+0.9}_{-1.5}$	$+1.6^{+1.0}_{-0.55}$
K		$-18^{+9}_{-\infty}$	-9^{+5}_{-319}	-10^{+4}_{-27}	-20^{+4}_{-4}	-25^{+3}_{-3}	-20^{+9}_{-90}	-22^{+5}_{-7}	$\lvert\delta\rvert > 30$	$\lvert\delta\rvert > 2$
L	-19^{+38}_{-9}			$-3.3^{+3.0}_{-1.2}$						
M					-37^{+7}_{-16}	$-85^{+45}_{-\infty}$		-70^{+30}_{-260}		

A. Current work B. Berendakov [42] C. Hamilton [30] D. Kracikova [38]
E. Alzner [28] F. Kato [16] G. Krane [25] H. Lange [26]
I. Budzynski [37] J. West [40] K. Baker [24] L. Domingos [39]
M. Reich & Cline [15]

agreement. The mixing ratio for the 691 keV 4^+ to 4^+ transition is large and thus can cast doubt on its sign. Because Hamilton's value includes infinity we feel comfortable saying that his value is consistent with ours.

All other measurements were analyzed using the quadratic relationship between δ and the angular correlation coefficients and thus we feel that their uncertainty limits may be smaller than they should be. Regardless, with only a few exceptions we find good agreement between our work and previous measurements and we have generally tightened the uncertainty limits on these values.

In an attempt to address the question of whether finding δ from the A_{22} coefficient produces smaller error bars than the chi-squared minimization method we have performed both analyses on one of our most accurately measured values. Table 7-2 shows a comparison between the results of the chi-squared minimization method and the results of the quadratic method when applied to both δ and $1/\delta$ for the 810-184 keV 5^+-4^+-2^+ angular correlation. We can immediately see the value in solving for $1/\delta$ directly, as it more readily reproduces the asymmetric uncertainty limits that are characteristic of mixing ratios.

This comparison does not show that the quadratic method produces smaller uncertainty limits than the chi-squared minimization method, though we feel that finding such an example somewhere in our data set would not be difficult. However, even in this case the symmetriziation of the uncertainty limits that occurs when solving for δ directly could result in a finite uncertainty limit for a value that should include infinity.

Table 7-2: Comparison of δ values produced by different methods. The table represents data from the 810-184 keV angular correlation from the ^{166m}Ho decay. Note that solving for δ directly produces symmetric uncertainty limits, thus underestimating the uncertainty in one direction and overestimating it in the other.

Method	δ	+	-
Chi-Squared ($1/\delta$)	-22.4	3.7	5.4
Quadratic ($1/\delta$)	-21.9	4.7	8.3
Quadratic (δ)	-21.9	6.0	6.0

7.2. Theoretical analysis of gamma-to-ground mixing ratios

As described in Chapter 3, M1 transitions are forbidden in the basic rotor model approximations. One way to introduce the possibility of M1 transitions between the gamma and ground bands is through first-order band-mixing. Recall from Section 3.9 our formula for predicting the mixing ratio from band-mixing theory (reproduced here for convenience).

$$\delta \cong E\frac{-AQ_0}{z_2(g_K - g_R)} \tag{3-28}$$

Calculations of the constant A were performed by Krane in 1973 [49]. In this paper Krane calculates relative values of the constant A for the first four mixed-multipolarity gamma-to-ground transitions. Our calculations, using the same relative units are displayed with Krane's in Table 7-3.

Table 7-3: Comparison of values for the constant A in Equation (3-28) between current calculations and those of Krane [49]. Note the disagreement in both sign and magnitude for the 594 keV 3^+ to 4^+ transition, and the systematic sign change whenever $J_f > J_i$.

	705	**779**	**594**	**691**	**810**	**530**	**671**	**831**	**465**	**645**
By	2^+-2^+	3^+-2^+	3^+-4^+	4^+-4^+	5^+-4^+	5^+-6^+	6^+-6^+	7^+-6^+	7^+-8^+	8^+-8^+
A	0.177	0.331	-0.040	0.092	0.064	-0.020	0.063	0.027	-0.012	0.048
B	0.176	0.330	0.048	0.092						

A. Current work
B. Krane [49]

Despite many re-calculations for the 594 keV 3^+ to 4^+ transition we are forced to conclude that Krane's value for this transition is incorrect in both magnitude and sign. In particular, since Krane did not calculate values for the other transitions in which $J_f > J_i$ (530 and 465 keV) he may have not noticed the systematic deviation of the sign of these values.

When comparing these relative values for the mixing ratio to our experimental values we will normalize their magnitudes to the 810 keV 3^+ to 4^+ transition, which we believe has the best agreement with previous experiments.

Table 7-4 displays our experimental values for the gamma-to-ground transitions along with the theoretical predictions from several sources (including our own calculations, described above).

We can immediately tell from our calculations that the basic band mixing model does not do well reproducing the sign or magnitude of gamma-to-ground mixing ratios.

Table 7-4: Gamma-to-ground mixing ratios compared to theoretical predictions. Relative values (indicated by an underline mark in the "By" column) are normalized to the 810-keV transition. Some literature sources (marked bold in the "By" column) quote the "reduced" mixing ratio (δ / E), from which we have calculated δ.

	705	**779**	**594**	**691**	**810**	**530**	**671**	**831**	**465**	**645**
By	2^+-2^+	3^+-2^+	3^+-4^+	4^+-4^+	5^+-4^+	5^+-6^+	6^+-6^+	7^+-6^+	7^+-8^+	8^+-8^+
A	$-128^{+83}_{-\infty}$	$-21.5^{+1.6}_{-1.8}$	$-7.64^{+0.38}_{-0.42}$	-41^{+15}_{-50}	$-25.3^{+3.5}_{-4.9}$	$-33.7^{+1.8}_{-2.0}$	$+9.2^{+3.7}_{-4.2}$	$-15.4^{+2.0}_{-2.7}$	$-110^{+64}_{-\infty}$	$+2.4^{+26.4}_{-0.9}$
B	-70.3	-131.5	+16.0	-36.7	-25.3	+7.9	-25.1	-10.7	+4.7	-19.1
C	-11	-49	-35	+4.4	-48	-48	+2.9	-319	+91	+2.5
D	-16.8	-9.5	-17.1	-13.4	-4.4	-15.4	-38.5	-2.6	-17.9	+9.4
E	-13	-11	-6.4	-5.3	-5.2		-3.3			

A. Current experimental values
B. Current calculations (relative, normalized to 810-keV transition)
C. Hamilton [30] (Dynamic Deformation Model)
D. Lipas [44] (2^{nd}-order IBA-1)
E. Wagner [31] (IBA-2 using calculations done by Van Isacker [50])

Thus, while the Mikhailov analysis given in Section 6.4 shows that the E2 strengths of the gamma to ground transitions are quite consistent with first-order band-mixing theory, the same cannot be said of the M1 strengths of those same transitions. Since our values are relative ones, we cannot draw conclusions regarding whether band-mixing is

including too-much or too little M1 strength in these transitions, only that the systematics of the M1s – especially in sign – are not well reproduced by the band-mixing model.

The dynamic deformation model (DDM) proposed by Hamilton in 1990 [30] is successful in predicting the sign of the mixing ratio in every case except the 691 keV 4^+ to 4^+ and 465 keV 7^+ to 8^+ transitions. Though experimental values for these two mixing ratio have often included infinity (and therefore some uncertainty in the sign of the mixing ratio) a survey of the experimental results indicates that the negative sign is favored in nearly all measurements. Hamilton's DDM model does not have as much success in predicting the magnitude of the mixing ratios, even on a relative basis.

The calculations by Lipas in 1987 [44] are done by including higher order terms in the M1 operator under the IBA-1 model (first order IBA-1 does not allow M1 transitions between rotational bands). These calculations are somewhat successful in predicting the signs of the mixing ratio, only failing for the 671 keV 6^+ to 6^+ transition, but again they do not reproduce the magnitudes of the mixing ratios.

Wagner [31] uses IBA-2 calculations for M1 transition matrix elements produced by Van Isacker [50] to predict the mixing ratios of both gamma-to-ground and intra-gamma transitions using the IBA-2 model. Only a few calculations are presented and they are generally far too small and uniform in magnitude to describe our experimental results well. They also show no signs of a mechanism for the changing sign of delta that is experimentally observed.

7.3. Intra-gamma mixing ratios compared to previous experiment

Due to their significantly smaller intensities the intra-gamma-band transitions are much more difficult to study than the gamma-to-ground transitions. The mixing ratio for the 119 keV 5^+ to 4^+ transition has been directly measured once previously, but our work represents the first direct (model independent) measurements of the mixing ratios for the 141 keV 6^+ to 5^+ and 160 keV 7^+ to 6^+ intra-gamma-band transitions. In Table 7-5 our values for these three transitions are presented along with the previous measurements.

Table 7-5: Comparison of intra-gamma-band mixing ratios with previous experiments. Gamma rays are listed in keV. The source of the measured values are given in the first column. The Method column indicates how the mixing ratios were measured (see the text for descriptions). If no sign is given for a value, the sign was not measured.

		97	**119**	**141**	**160**
By	Method	4^+-3^+	5^+-4^+	6^+-5^+	7^+-6^+
Current exp.	$\chi 2$		$+2.45^{+0.93}_{-0.53}$	$+1.15^{+1.04}_{-0.62}$	$+1.65^{+0.93}_{-1.16}$
Alfter [33]	Quad.		$+1.94^{+0.23}_{-0.21}$		
Current calc.*	C.-C.O.	$1.99^{+0.39}_{-0.39}$	$1.83^{+0.11}_{-0.11}$	$1.52^{+0.13}_{-0.13}$	$1.50^{+0.15}_{-0.15}$

* Calculations are based on intensities from the Nuclear Data Sheets [12].

Only one of the previous measurements (Alfter [33]) was done directly, using angular correlations and the quadratic relationship to extract δ from the angular correlation coefficients. The other measurement is based on our calculations using the cascade-to-crossover formalism developed in Section 3.7 and the intensities listed in the Nuclear Data Sheets [12]. Several other groups have previously done similar calculations

using the best intensities available at that time [31,45]. The model dependence of this calculation may introduce systematic errors that are not accounted for in the quoted uncertainties, which should be considered when comparing the values.

There is acceptable agreement between our value for the 119-keV transition and that of Alfter. However, as noted in Chapter 4 it appears from the Alfter article that this group did not account for the presence of the 121-keV gamma ray in their angular correlation measurement. The effects of this nearby peak could have altered their value for the mixing ratio, and at the very least we can say that their uncertainty limits should be considered as minimum estimates.

The model dependent measurements show a trend of decreasing mixing ratios with increasing spin, which has been seen in previous calculations as well. However, due to the size of the uncertainty limits on our values we can neither argue for, nor rule out any systematic trends. That said, we seem to be in good agreement in both sign and magnitude with the cascade-to-crossover calculations.

7.4. Theoretical analysis of intra-gamma mixing ratios

Despite the lack of experimental values for the intra-gamma-band mixing ratios, there are several theoretical predictions to compare our values to. Table 7-6 shows our experimental values along with theoretical calculations based on IBA-1 and IBA-2 models.

Table 7-6: Comparison of intra-gamma band mixing ratios with theoretical predictions.

		97	**119**	**141**	**160**
By	Method	4^+-3^+	5^+-4^+	6^+-5^+	7^+-6^+
A	Exp.		$+2.45^{+0.93}_{-0.53}$	$+1.15^{+1.04}_{-0.62}$	$+1.65^{+0.93}_{-1.16}$
B	IBA-2	1.5	1.3	1.2	1.1
C	IBA-1	0.23	0.23	0.22	0.20

A. Current work
B. Wagner [31]
C. Lipas [44]

As mentioned in regards to the gamma-to-ground transitions, Wagner [31] calculates IBA-2 values for these mixing ratios using M1 transition matrix elements calculated Van Isacker [50]. Unlike the gamma-to-ground transitions for which the IBA-2 predictions are arguably the least successful, here IBA-2 seems to reproduce the correct order of magnitude.

In contrast, the 2nd-order IBA-1 calculations give by Lipas [44] give values for delta that are much too small, indicating that his model does not allow for strong enough M1 contributions in the intra-gamma-band transitions.

Again we see that both IBA-1 and IBA-2 theories predict a decrease of the mixing ratio as the spin increases, in agreement with the cascade-to-crossover analysis presented in the previous section.

Another calculation that may be performed using our experimental values for the mixing ratio of the intra-gamma-band transitions is to extract a value of $(g_K - g_R)$ for the

emitting state. We can relate the mixing ratio of an intra-band transition to the quantity $Q_0/(g_K - g_R)$ using Equation (3-12) (reproduced here for convenience)

$$\delta = \sqrt{\frac{3}{5}} \frac{e}{4\mu_N \hbar c} E \frac{1}{\sqrt{(J_i+1)(J_i-1)}} \frac{Q_0}{(g_K - g_R)} \tag{3-12}$$

Given the energy of the gamma ray, the spin of the emitting level, and a value for the intrinsic electric quadrupole moment of that band, Q_0, we can extract a value for the gyromagnetic ratio of that state. In these calculations we have assumed Q_0 = 7.67 electron-barns [51]. Table 7-7 shows the values of $(g_K - g_R)$ determined from the measured mixing ratios of the intra-gamma-band transitions.

Table 7-7: Deduced values of $(g_K - g_R)$ for intra-gamma-band transitions. $(g_K - g_R)$ is measured in nuclear magnetons.

$E(\gamma)$	J_i to J_f	$(g_K - g_R)$	+	-
119	5^+-4^+	0.348	0.075	0.132
141	6^+-5^+	0.880	0.473	0.801
160	7^+-6^+	0.697	0.491	0.393

Due to the large limits of uncertainty on our values for the mixing ratios, our values for $(g_K - g_R)$ do not contribute significantly to previous measurements by other methods. However, previous measurements, such as that by Brandolini [43] deduced a value of g_R for the states of the ground band that hovers around a value of 0.28, and a value of 0.37 for $(g_K - g_R)$ of the 2^+ state of the gamma band. Our values are in

agreement with these previous measurements and this serves to further validate our measurements of the intra-gamma-band mixing ratios.

8. Conclusions

There are three separate but intertwined subjects presented in this work. Primarily we have presented measurement and analysis of the mixed-multipolarity gamma-to-ground transitions. We have also measured intra-gamma-band mixing ratios, some for the first time. Band-mixing analysis has also been presented. A summary of each of these topics as well as a brief discussion about methodology and future work is presented in this chapter.

8.1. Band-mixing analysis

The band mixing analysis presented in this work is notable in two respects. The first-order analysis agrees remarkably well with previous measurements, and current measurements are of sufficient precision to see a third-order shape the Mikhailov plot. This shape has not previously been observed and the theoretical interpretation of this new information will be of some interest.

8.2. Gamma-to-ground mixing ratios

For the ten mixed-multipolarity gamma-to-ground transitions that are fed in the decays of ^{166m}Ho and ^{166}Tm our measurements agree with previous measurements in most cases. The signs of our results are consistent with previous measurements but in some instances the uncertainty limits must be extended to 1.5 standard deviations before there is overlap between magnitudes.

First order band-mixing calculations do not reproduce relative values of these gamma-to-ground mixing ratios, especially in regards to sign. The dynamic deformation model and 2^{nd}-order IBA-1 calculations are moderately successful in predicting the signs and magnitudes of the gamma-to-ground mixing ratios, but neither model proves to be entirely accurate. In particular the behavior of the $J_i = J_f$ transitions seems to defy explanation in these theories. IBA-2 calculations do not well reproduce the experimental values.

8.3. Intra-gamma-band mixing ratios

Measurements of three intra-gamma-band mixing ratios have been presented. Two of these have been measured for the first time, while the third is in good agreement with the one prior measurement, despite a potential problem with this previous value.

Calculations of the intra-gamma-band mixing ratios, based on current literature intensities and the simple rotational model, show good agreement with experimental values. IBA-1 and IBA-2 models are not as successful, though the IBA-2 predictions are of the right order of magnitude. IBA-1 gives results that are too small by an order of magnitude.

Our experimental values are not precise enough to discern whether the predicted decrease in the mixing ratio with increasing spin is occurring.

Values for the g-factors of the gamma-vibrational-band, based on the rotational model, are consistent with previous measurements. This offers some validation that our measurements of the intra-gamma-band mixing ratios are correct.

8.4. Experimental methods

We have presented an argument that in cases where the mixing ratio is expected to be large, solving for $1/\delta$ rather than δ offers a clearer experimental result and allows for more effective communication and averaging.

We also believe there is growing evidence that solving for the mixing ratio using a chi-squared minimization method is preferable to the quadratic approach, when possible.

Finally, in terms of methodology we have shown the impressive power of large detector arrays. Despite years of study of both decays, and the ^{166m}Ho decay in particular, we were able to produce more precise measurements and extend the limits of measurability to a significant extent. The flexibility of instruments such as the 8π gives an impressive glimpse at the tools of modern gamma-ray spectroscopy.

8.5. Future work

While this work has concentrated on the nuclear structure aspects of the ^{166}Er nucleus, a significant amount of spectroscopic information on this nucleus remains to be mined from our data. In addition, information regarding E3/M2/E1 multipole-mixing may be accessible from some of the high lying negative parity states in this nucleus.

Though it might offer an interesting perspective on competing nuclear structure theories, we feel that it is unlikely further experiments seeking to measure the intra-gamma-band mixing ratios will be productive. Given that this experiment represents hundred of hours of data collection on a 20-detector array it would require unprecedented counting times to improve on the statistical accuracy of these measurements. Due to the extreme weakness of the intra-gamma-band transitions it is unclear there will ever be a method for measuring these mixing ratios with any greater accuracy.

Both in experiment and in theoretical models we would like to see further pursuit of the cubic shape to the Mikhailov data presented here. Several questions present themselves: Does this shape arise in other highly deformed nuclei? Does the presence of the cubic shape indicate any processes that might lead to a better theoretical explanation of the gamma-to-ground mixing ratios?

There are only a few cases in which further study of the gamma-to-ground mixing ratios in ^{166}Er could be fruitful. The mixing ratio for the 2^+ to 2^+ gamma-to-ground transition remains difficult to measure, mostly due to its very large value and lack of feeding in the ^{166m}Ho decay. However, it is unlikely that more will be learned by further study of the majority of the gamma-to-ground transitions in ^{166}Er.

More theoretical work addressing the large variances in the measured mixing ratios for gamma-to-ground transitions in ^{166}Er does seem warranted by our data. In particular, the mixing ratios of transitions with $J_i = J_f$ exhibit anomalous properties relative to the rest of the transitions.

BIBLIOGRAPHY

[1] J.D. Jackson, *Classical Electrodynamics* 3rd ed. (New York: John Wiley & Sons, Inc., 1999).

[2] K.S. Krane, *Introductory Nuclear Physics* (New York: John Wiley & Sons, Inc., 1988).

[3] M.A. Preston and R.K. Bhaduri, *Structure of the Nucleus* (Reading MA: Addison-Wesley Publishing Company, Inc., 1975).

[4] K.S. Krane, *Table of Coefficients for Analysis of Angular Distribution of Gamma Radiation from Oriented Nuclei*, Lost Alamos Report LA-4677, 1971.

[5] R.M. Steffen and K. Alder in *The Electromagnetic Interaction in Nuclear Spectroscopy*, edited by W.D. Hamilton (Amsterdam, Holland: North-Holland Publishing Company, 1975, Ch. 12).

[6] P.D. Schmelzenbach, *The Study of ^{150}Sm Through the Beta Decay of ^{150}Pm, ^{150m}Eu and ^{150g}Eu*, Doctoral Thesis: Oregon Sate University (2003).

[7] M.G. Mayer and J.H.D. Jensen, *Elementary Theory of Nuclear Shell Structure* (New York: John Wiley & Sons, Inc., 1955).

[8] P.E. Garrett et al., Journal of Physics G **27**, R1 (2001).

[9] A. Bohr and B. Mottelson, *Nuclear Structure Volume I: Single Particle Motion* (River Edge NJ: World Scientific, 1998).

[10] A. Bohr and B. Mottelson, *Nuclear Structure Volume II: Nuclear Deformations* (River Edge NJ: World Scientific, 1998).

[11] K.S. Krane and R.M. Steffen, Physical Review C, **2**, 724 (1970).

[12] E.N. Shurshikov and N.V. Timofeeva, *Nuclear Data Sheets* **65**, 365 (1992).

[13] C.W. Reich and J.E. Cline, Nuclear Physics A **159**, 181 (1970).

[14] J.E. Cline and C.W. Reich, Physical Review **129**, 2152 (1963).

[15] C.W. Reich and J.E. Cline, Physical Review **137**, 1424 (1965).

BIBLIOGRAPHY (Continued)

[16] K. Kato et al., Journal of the Physical Society of Japan **50**, 2810 (1981).

[17] T.E. Sampson, Nuclear Instruments and Methods **150**, 361 (1978)

[18] V.N. Danilenko et al., Appl. Radiat. Isot. **40**, 789 (1989)

[19] J. Morel et al., Appl. Radiat. Isot. **47**, 529 (1996)

[20] C. Gunther and R. Parsignault, Physical Review **153**, 1297 (1967).

[21] S.B. Burson et al, Physical Review **158**, 1161 (1967).

[22] A.W. Sunyar, Physical Review **186**, 1227 (1969).

[23] G. Carlsson et al., Physica Scripta **6**, 247 (1972).

[24] K.R. Baker et al., Physics Letters **57B**, 441 (1975).

[25] K.S. Krane and J.D. Moses, Physical Review C, **24**, 654 (1981).

[26] J. Lange et al., Z. Physics A **303**, 321 (1981).

[27] H. Marshak and C.H. Speigelman, Nuclear Instruments and Methods in Physics Research A **234**, 455 (1985).

[28] A. Alzner et al., Z. Physics A **322**, 467 (1985).

[29] J. Adam et al., Bull. Acad. Sci. USSR, Phys. Ser. **52**, 17 (1988).

[30] W.D. Hamilton et al., Journal of Physics G **16**, 219 (1990).

[31] W. Wagner, Bulletin of the Russian Academy of Sciences **56**, 675 (1992).

[32] C. Ardisson et al., Il Nuovo Cimento **105**, 215 (1992).

[33] I. Alfter et al., Z. Physics A **355**, 277 (1996).

[34] J. Żylicz et al., Nuclear Physics **81**, 88 (1966).

[35] J. Adam et al., Czech Journal of Physics B **29**, 997 (1979).

BIBLIOGRAPHY (Continued)

[36] J. Adam et al., Seriya Fizicheskaya **53**, 875 (1989).

[37] M. Buzynski et al., Isv. Acad. Nauk USSR (Ser. Fiz.) **44**, 1831 (1980)

[38] T.I. Kracíková et al., Hyperfine Interactions **34**, 127 (1987).

[39] J.M. Domingos, Nuclear Physics A **180**, 600 (1972).

[40] R.L. West et al., Nuclear Physics A **270**, 300 (1976).

[41] S.A. Berendakov and A.M. Demidov, Soviet Journal of Nuclear Physics **52**, 179 (1991).

[42] S.A. Berendakov and A.M. Demidov, Bulletin of the Russian Academy of Sciences **56**, 74 (1992).

[43] F. Brandolini et al., Nuclear Physics A **600**, 272 (1996).

[44] P.O. Lipas et al., Nuclear Physics A **469**, 348 (1987).

[45] H.S. Binarh et al., Journal of the Physical Society of Japan **59**, 2359 (1990).

[46] H.R. Andrews at al., Technical Report No. AECL-8329 (unpublished).

[47] D.C. Radford, Radware, http://radware.phy.ornl.gov/, 2002.

[48] W.D. Kulp et al., to be published.

[49] K.S. Krane, Physical Review C, **4**, 1494 (1973).

[50] P. Van Isacker, Nuclear Physics A **476**, 301 (1987).

[51] V. Rieckert, *Quadrupole Moments and g-Factors of Low-Lying Bands in Odd-A-Nuclei (150 < A < 190),* Masters Thesis: Oregon Sate University (1987).